NAVAL POSTGRADUATE SCHOOL

MONTEREY, CALIFORNIA

THESIS

CHARACTERIZATION OF AMBIENT NOISE RECORDED IN THE NORWEGIAN SEA

by

Christopher M. Griggs

March 2023

Thesis Advisor: Kay L. Gemba
Co-Advisor: Daniel Brooker,
Naval Research Laboratory

This project was funded in part by the NPS Naval Research Program.

THIS PAGE INTENTIONALLY LEFT BLANK

REPORT DOCUMENTATION PAGE	*Form Approved OMB No. 0704-0188*

1. AGENCY USE ONLY *(Leave blank)*	**2. REPORT DATE** March 2023	**3. REPORT TYPE AND DATES COVERED** Master's thesis

4. TITLE AND SUBTITLE CHARACTERIZATION OF AMBIENT NOISE RECORDED IN THE NORWEGIAN SEA	**5. FUNDING NUMBERS** N00014-22-WX-0-1713; NPS-23-N069-A
6. AUTHOR(S) Christopher M. Griggs	
7. PERFORMING ORGANIZATION NAME(S) AND ADDRESS(ES) Naval Postgraduate School Monterey, CA 93943-5000	**8. PERFORMING ORGANIZATION REPORT NUMBER**
9. SPONSORING / MONITORING AGENCY NAME(S) AND ADDRESS(ES) Office of Naval Research, 875 Randolph St., Arlington, VA, 22217	**10. SPONSORING / MONITORING AGENCY REPORT NUMBER**

11. SUPPLEMENTARY NOTES The views expressed in this thesis are those of the author and do not reflect the official policy or position of the Department of Defense or the U.S. Government. This project was funded in part by the NPS Naval Research Program.

12a. DISTRIBUTION / AVAILABILITY STATEMENT Approved for public release. Distribution is unlimited.	**12b. DISTRIBUTION CODE** A

13. ABSTRACT (maximum 200 words)

This thesis characterizes mid-frequency (1–9 kHz) ambient noise collected with an acoustic array over a two-week period in the Norwegian Sea. Noise characterization is an important prerequisite for many applications, including department of defense applications, environmental and biological research. The basic methodology consists of calibrating single hydrophone data for power spectral density (PSD) in dB re 1 μPa^2/Hz. We present omni-directional ambient noise statistics over time, including percentiles and standard deviation for a variety of temporal averages, ranging from 1 to 60 min. These results compare well to historic observations. Wenz suggests spectrum level of approximately 45 (dB re 1 μPa^2/Hz) for a sea state 2, while the result from this thesis finds spectrum level of approximately 43 (dB re 1 μPa2/Hz). Furthermore, results are compared to a wind-based ambient noise model. The model prediction tracks with the data presented relatively well with a slight offset. The slight offset is further explored and gives details of the prevailing sea state. As predicted, the model slightly overestimates the PSD level of the data at sea state 2. This misfit is explored for different sea states and wind speeds.

14. SUBJECT TERMS physics, acoustics, array, ambient noise, hydrophone, sonar, underwater noise	**15. NUMBER OF PAGES** 161
	16. PRICE CODE

17. SECURITY CLASSIFICATION OF REPORT	**18. SECURITY CLASSIFICATION OF THIS PAGE**	**19. SECURITY CLASSIFICATION OF ABSTRACT**	**20. LIMITATION OF ABSTRACT**
Unclassified	Unclassified	Unclassified	UU

NSN 7540-01-280-5500

Standard Form 298 (Rev. 2-89)
Prescribed by ANSI Std. 239-18

THIS PAGE INTENTIONALLY LEFT BLANK

Approved for public release. Distribution is unlimited.

CHARACTERIZATION OF AMBIENT NOISE RECORDED IN THE NORWEGIAN SEA

Christopher M. Griggs
Lieutenant, United States Navy
BS, United States Naval Academy, 2015

Submitted in partial fulfillment of the
requirements for the degree of

MASTER OF SCIENCE IN APPLIED PHYSICS

from the

NAVAL POSTGRADUATE SCHOOL
March 2023

Approved by: Kay L. Gemba
Advisor

Daniel Brooker
Co-Advisor

Frank A. Narducci
Chair, Department of Physics

THIS PAGE INTENTIONALLY LEFT BLANK

ABSTRACT

This thesis characterizes mid-frequency (1–9 kHz) ambient noise collected with an acoustic array over a two-week period in the Norwegian Sea. Noise characterization is an important prerequisite for many applications, including department of defense applications, environmental and biological research. The basic methodology consists of calibrating single hydrophone data for power spectral density (PSD) in dB re 1 μPa^2/Hz. We present omni-directional ambient noise statistics over time, including percentiles and standard deviation for a variety of temporal averages, ranging from 1 to 60 min. These results compare well to historic observations. Wenz suggests spectrum level of approximately 45 (dB re 1 μPa^2/Hz) for a sea state 2, while the result from this thesis finds spectrum level of approximately 43 (dB re 1 μPa2/Hz). Furthermore, results are compared to a wind-based ambient noise model. The model prediction tracks with the data presented relatively well with a slight offset. The slight offset is further explored and gives details of the prevailing sea state. As predicted, the model slightly overestimates the PSD level of the data at sea state 2. This misfit is explored for different sea states and wind speeds.

THIS PAGE INTENTIONALLY LEFT BLANK

Table of Contents

List of Figures

List of Tables

THIS PAGE INTENTIONALLY LEFT BLANK

List of Acronyms and Abbreviations

ADCP	Acoustic Doppler Current Profiler
AIS	Automatic Identification System
APL-UW	Applied Physics Lab–University of Washington
CTD	An instrument used to measure conductivity, temperature and depth.
ENBW	Equivalent Noise Bandwidth
FFT	Fast Fourier Transform
GPS	Global Positioning System
NCEP	National Center for Environmental Prediction
OASIS	Ocean Ambient Sound Instrument System
PSD	Power Spectral Density
R/V	Research Vessel
SIO	Serial Input/Output

THIS PAGE INTENTIONALLY LEFT BLANK

Acknowledgements

We are grateful to the Marine Physical Laboratory of the Scripps Institution of Oceanography, University of California-San Diego and the Office of Naval Research for sharing the Mid-Frequency Array Norwegian Sea data set.

This research is supported under Naval Research Program (NRP) Topic NPS-23-N069-A and ONR Grant No. N00014-22-WX-0-1713.

This thesis is dedicated to my daughter, Colette.

THIS PAGE INTENTIONALLY LEFT BLANK

CHAPTER 1:
Underwater Acoustic Noise

The historic study of noise can be traced back to Einstein and his study of Brownian motion in his famous 1905 paper: "On the Movement of Small Particles Suspended in a Stationary Liquid Demanded by the Molecular-Kinetic Theory of Heat" [1]. From the early studies of this phenomenon, noise has been intensely studied and can be seen in a broad spectrum of fields. The study of underwater acoustic noise did not escalate until after World War II during which researchers recognized its importance to improve the technological edge held in submarine and mine warfare [2]. The United States Navy spurred more research in the 1960s as the interest in passive arrays became a necessity to maintain technological advantages [2]. Classification and measurement of noise in the underwater domain is important to military applications, marine biology, oceanography and other subjects.

This thesis aims to characterize and measure underwater ambient noise measured from a 2D hydrophone array deployed for approximately 7 days in the Norwegian Sea during the summer of 2018 [3]. This thesis presents omni-directional noise levels from a single hydrophone and compares these calculated levels to the parametric output of a wind model.

1.1 Ambient Noise

There is no widely accepted definition of ambient noise in underwater acoustics [4]. Generally, ambient noise depends on the context. For the context of this thesis, the definition of ambient noise will follow the *Good Practice Guide for Underwater Noise Measurement* [4]. That definition is "in the absence of a specific signal, the ambient noise is defined as all sound except that resulting from the deployment, operation or recovery of the recording" [4]. This definition will be important as the data set analyzed in this thesis aims to exclude anthropogenic noise purposefully injected into the wave guide by an active source used in the testing of the array, noise of the R/V Neil Armstrong, and close range shipping (far range shipping potentially is included but is expected to contribute insignificantly to the results).

1.2 Sources of Ambient Noise

Ambient noise can come from multiple sources. These sources include tides, hydrostatic effects of waves, seismic disturbances, Arctic ice, oceanic turbulence, ship traffic, surface waves, thermal noise and biological noises [5]. Sources of ambient noise vary widely across the frequency spectrum. In a deep sea environment (similar to the Norwegian Sea), it has been observed that ambient noise is frequency dependent [5]. Figure 1.1 shows ambient noise spectrum level as a function of frequency. For frequencies from 1 to 10 Hz, ambient spectrum level will have a slope of -8 to -10 dB/octave [5]. For frequencies from 20–500 Hz, the spectrum level slope will be small with slight changes [5]. For frequencies from 500–50,000 Hz, a slope of -5 to -6 dB/octave is observed. Above 50,000 Hz, the spectral slope will be approximately +6 dB/octave [5]. These differences in magnitude and slopes conclude that different sources dominate at different frequencies. It is important to understand, however, that those grossly averaged results are based on data from the 1960s. 1–9 kHz is the frequency range analyzed for this thesis.

With rising populations and increasing global trade, research shows an increase in ambient noise in the ocean [6]. Ambient noise level has increased in the ocean by up to 9 dB for frequencies greater than 200 Hz [6]. Much of this increase in ambient noise can be attributed to the growth in number of merchant ships and their physical size. From 1980 to 2020 the world's fleet increased from around 500 million dead-wight tons to over 2000 million dead weight tons [7]. In 2005, Donald Ross found that low-frequency ambient noise rose at a rate of about 0.5 dB per year [8]. Propeller blade cavitation is the largest contribution of noise from ships [9]. Cavitation occurs when the local pressure around the blade lowers below the boiling point and bubbles are formed and collapsed. This creates broadband noise at low frequencies (approximately 10–1,000 Hz), while other rotational ship machinery can create tonal noise at the source frequency and its harmonic frequencies [9]. If the source of change in ambient noise level is due to the rise of ambient noise levels from shipping, then it could be argued that early noise models would still prove accurate for predicting ambient noise levels in the mid-frequency (1–9 kHz) because shipping noise contributes mostly in the lower frequency spectrum. This will be explored in Chapter 4.

The hydrophone array used to collect data for this thesis is designed for mid-frequencies (1–9 kHz) [3]. At this frequency range a major source of ambient noise is due to surface

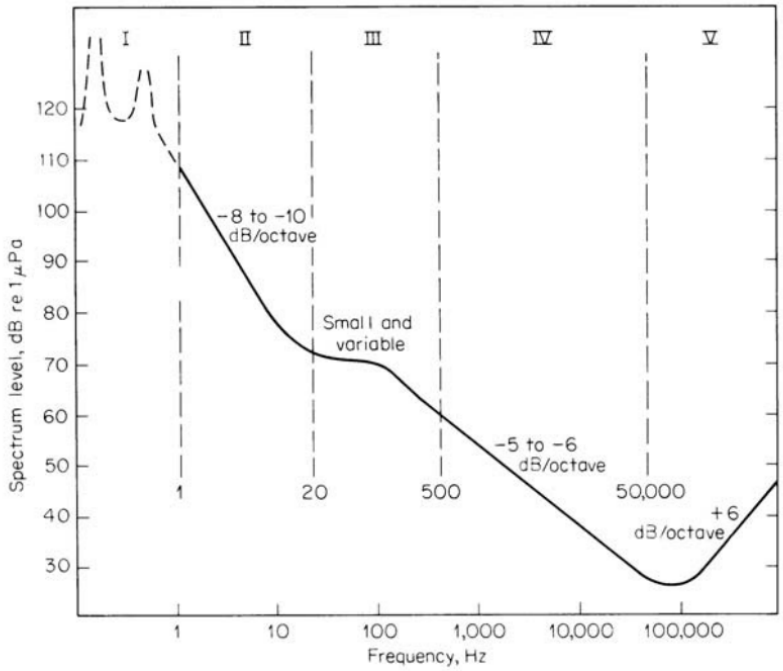

Figure 1.1. "Sample spectrum of deep-sea noise showing five frequency bands of differing spectral slopes. The slopes are given in decibels per octave of frequency. In frequencies from 1 to 10 Hz, ambient spectrum level will have a slope of -8 to -10 dB/octave. In frequencies from 20 to 500 Hz the spectrum level slope will be small with slight changes. In frequencies from 500 to 50,000 Hz, a slope of -5 to -6 dB/octave is seen. Above 50,000 Hz, the spectral slope will be approximately +6 dB/octave." Source: [5].

generated noise. Surface generated noise includes rain, wind, breaking of waves due to sea state and other environmental factors.

Knudsen was an early pioneer in measuring and predicting ambient noise levels due to sea state. Knudsen developed a series of curves that predicted ambient noise as a function of sea state [10]. These curves can be summarized in Equation 1.1:

$$NL = 56 + 19 \log SS - 17 \log f \tag{1.1}$$

where NL is the ambient noise level in dB re 1 μPa/√Hz; f is frequency (valid for 1 to 25

kHz); SS is the sea state. The sea state is a scale from 0 to 8 based on the height of waves (crest to trough) in feet. Table 1.1 defines the various sea states. Similarly to wave height, wind speed is also typically measured on a scale from 0-8, sometimes referred to as the Beaufort Scale [11].

Table 1.1. Meteorologic scales of sea state based on the height of wave in feet as measured from the crest of the wave to the trough and wind speed measured in meters per second. Adapted from [10], [11].

Sea State/Beaufort Scale	Description	Height of Wave (ft.)	Wind Speed (m/s)
0	Calm	0	<0.5
1	Smooth	<1	0.5-1.7
2	Slight	1-3	1.8-3.3
3	Moderate	3-5	3.4-5.4
4	Rough	5-8	5.5-8.4
5	Very Rough	8-12	8.5-11.1
6	High	12-20	11.2-14.1
7	Very High	20-40	14.2-17.2
8	Precipitous	>40	17.3-20.8

Contribution to ambient noise levels from rain or hail has also been studied [9]. As rain droplets impact the water surface, a distinct pressure pulse is formed along with secondary pulsations of gas bubbles. These pressure pulses produce ambient noise from 0.5–10 kHz [9].

Furthermore, biological sounds are a major contribution of low and mid frequency ambient noise [12]. From shellfish, such as snapping shrimp to marine mammals such as whales or dolphins, noise sources from marine life differs widely in the type, duration and frequency [5], [9].

1.3 Ambient Noise Research

Many studies have been performed on ambient noise research. This section reviews research of ambient noise levels throughout the world and is used for comparison in Chapter 4.

1.3.1 Wenz

Gordon Wenz's 1962 paper in the Journal of the Acoustical Society of America was a significant contribution in discussing the predominant components of ambient noise in the ocean on a broad scale as opposed to the characteristics of noise in localized areas. Wenz took various data sets from different locations and compiled his results to come up with curves that predicted ambient sound pressure spectrum level [11]. Figure 1.2 shows the Wenz curves in an updated format by [12]. Wenz found that at frequencies from 100 Hz to 1 kHz the sound pressure spectrum level had a slope of -6 dB per octave at frequencies with a strong dependence on wind, bubbles and spray from surface agitation [11]. Above 20 kHz, this source of noise falls off and thermal noise characterized by a +6 dB per octave slope dominates [11]. This is similar to results compiled in [5]. Wenz excluded biologic sources in his research so his predictions may not be accurate depending on location, the time of year, and the frequency band analyzed.

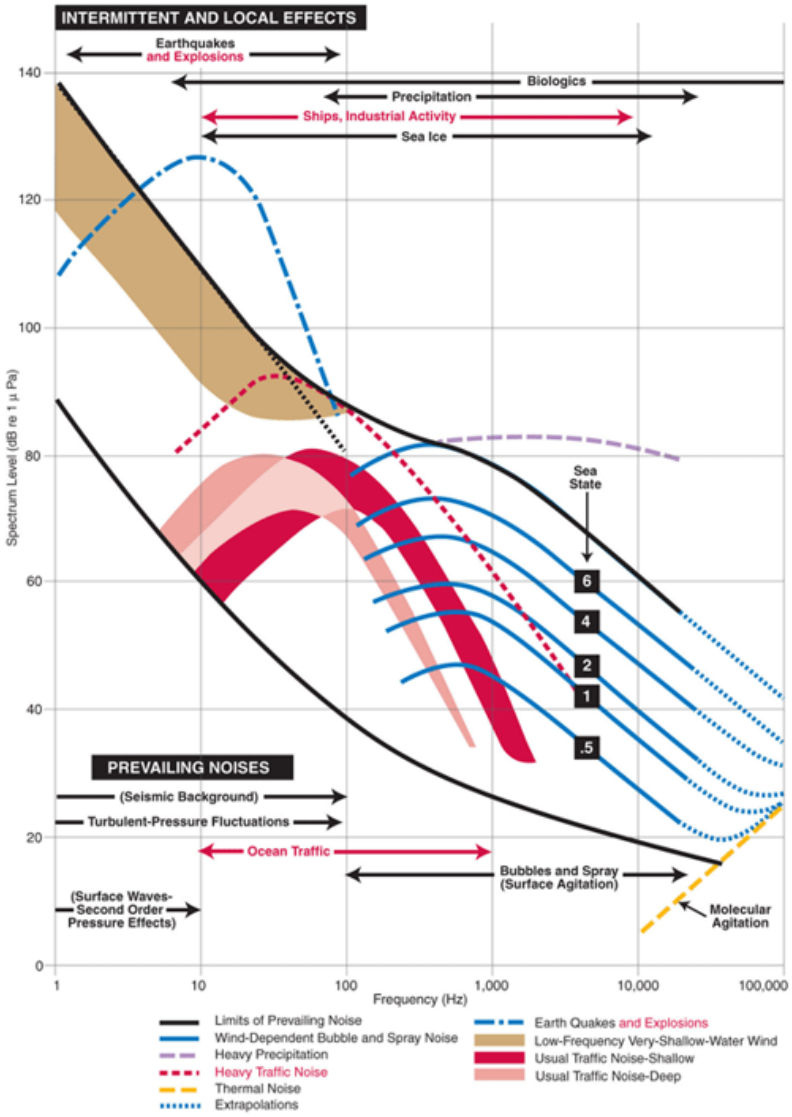

Figure 1.2. "Spectra and frequency distribution of ocean sound sources based on the Wenz Curves." Source: [12]

1.3.2 Pacific Ocean

In the Western Pacific, researchers studied the depth-dependence of ambient noise level for mid-frequencies (1–4 kHz). Figure 1.3 plots results of mean noise level as a function of depth at frequencies from 20 to 4064 Hz. The results varied from around 60 dB re

$1\mu Pa^2Hz^{-1}$ to around 50 dB re $1\mu Pa^2Hz^{-1}$ for frequencies between 1–4 kHz at depths greater than 1200 meters with maximum mean noise level occurring at the sound channel axis with an approximate 15 dB peak at 800 meters [13]. They also found that the mean standard deviations for frequencies higher than 1kHz to remain consistent around 6.3 dB [13]. This study found that ambient noise in the South China Sea was higher in the morning than the afternoon.

In a more comprehensive study, researchers studied ambient noise over the course of two decades (1999-2022) in 6 different locations in the Pacific Ocean [14]. The researchers focused on the effects of wind speed on ambient noise spectrum level [14]. The results are plotted in Figure 1.4. Figure 1.4 is discussed in greater detail in conjunction with the results of this thesis in Chapter 4.

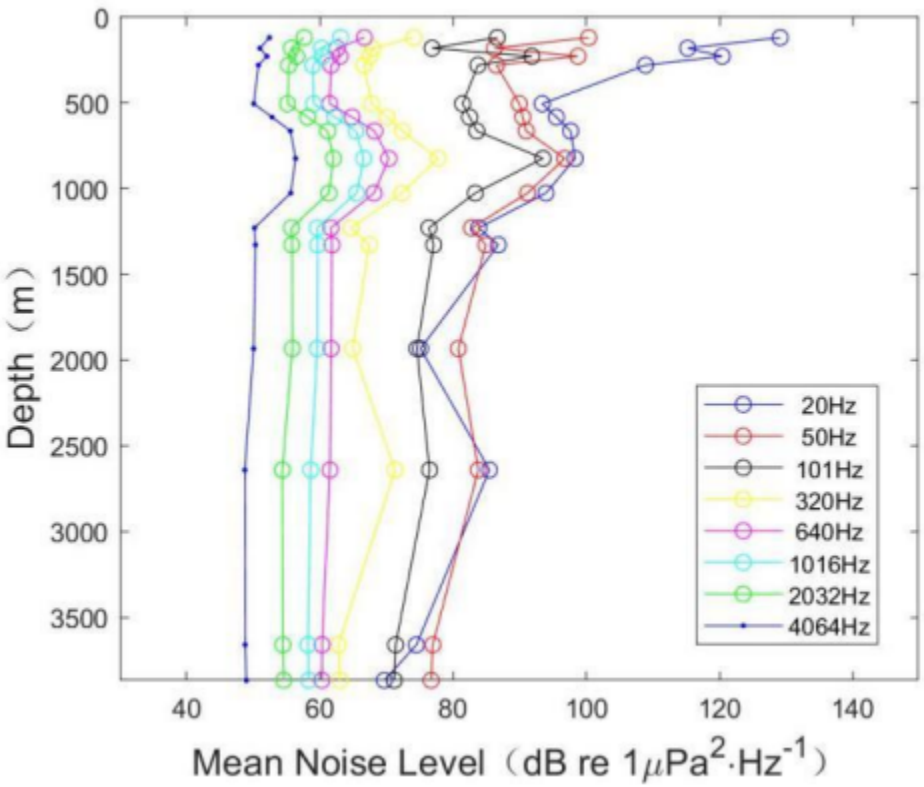

Figure 1.3. Noise level as a measure of depth at various frequencies. The highest mean ambient noise across all frequencies occurs at the sound channel axis in which mean sound velocity is minimum. Noise level is steady at depths beyond the sound channel axis. Noise level decreases as frequency is increased. Data recorded in fall of 2020. Source: [13].

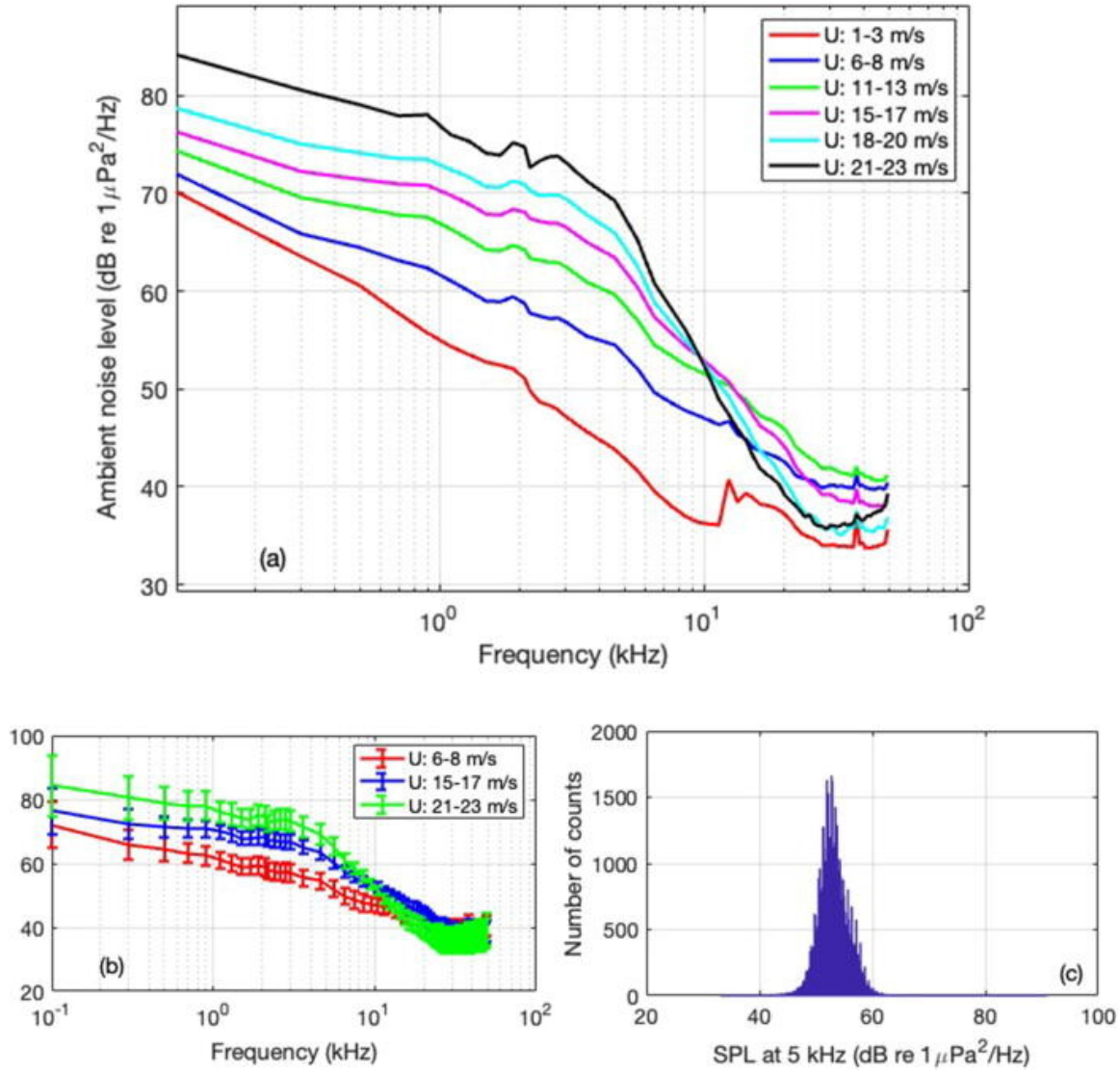

Figure 1.4. (a) "Solid curves: averaged ambient noise spectra recorded by a PAL in the wind speed ranges of 1–3, 6–8, 11–13, 15–17, 18–20, and 21–23 m/s. (b) Mean ambient noise spectra in the wind speed ranges of 6–8, 15–17, and 21–23 m/s with respective standard deviations. The three wind speed ranges have 300 000, 10 000, and 1600 data samples, respectively. (c) Histogram of 6–8 m/s wind speed ambient noise level at 5 kHz [using data in red in (b)] with a well-defined peak centered near 53 dB". Source: [14]

1.3.3 North Atlantic

In the North Atlantic, Perrone found that wind speed and wave height were strongly correlated to mid-frequency noise (0.5 kHz to approximately 2 kHz) with his measurements of omni-directional ambient noise being recorded near the bottom of the Atlantic floor [15]. Figure 1.5 plots their results of spectrum level versus frequency. Specifically, Perrone found that spectrum level varied from approximately -60 dB re 1μbar^2 to -33 dB re 1μbar^2 for wind speeds from 0–2.5 knots up to 47.5–52.5 knots [15].

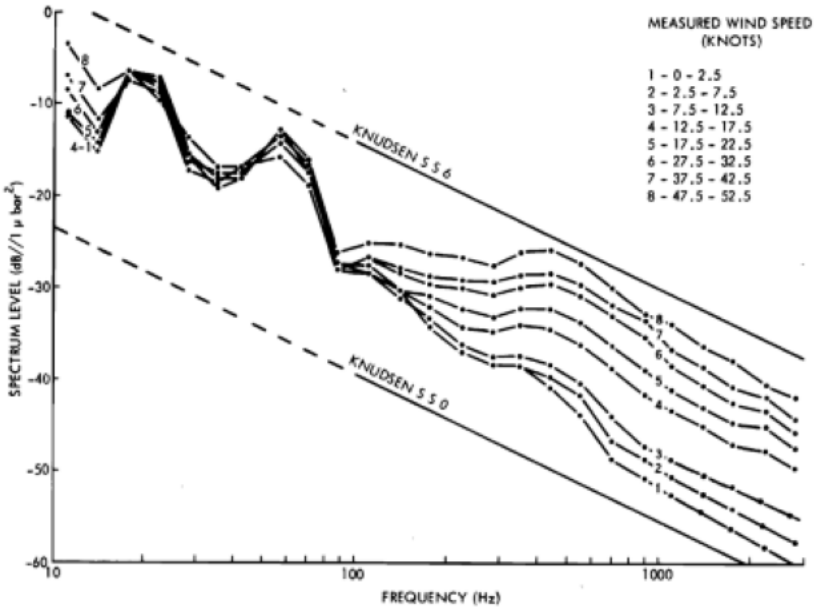

Figure 1.5. Ambient noise spectrum level for frequencies greater than 1 kHz depends greatly upon wind speed in the North Atlantic. Results were measured using an omni-directional hydrophone suspended 400 ft above the sea floor (depth of 14,400 feet). Wind speed and wave height were obtained from an anemometer and a wave staff located on fixed platform 30 miles northwest of the hydrophone. Source: [15].

1.3.4 Canadian Arctic

A study published in the *Marine Pollution Bulletin* took underwater ambient noise measurements from 39 unique data sets over a 6 year period [16]. The study found that the sound pressure level for the 50–1000 Hz band had typical values of about 90-100 dB re 1

μPa across all sites [16]. They found that the noise was heavily dependent upon wind speed, weather and shipping density [16]. The purpose of this study was to create a baseline for underwater noise in the Canadian Arctic for future study of human impact as climate change melts ice bergs and opens new shipping routes for world trade [16].

1.3.5 Baltic Sea

Studies in the Baltic Sea represent similar weather patterns to the data obtained in the Norwegian Sea. The Baltic sea, however, has higher shipping densities and shallower depths compared to the Norwegian Sea [17]. Mid-frequency ambient noise levels in the Baltic are strongly wind dependent, as predicted by [11]. Ambient noise level for 4 kHz was approximately 45–52 dB re 1μPa for wind speeds from 3–6 m/s [17]. A 2014 study measured sound for an extended period of time at numerous locations in the Baltic Sea and found that ice coverage has a profound impact on sound pressure level (dB re 1μPa) with ambient noise dropping 10 dB for 2 kHz one-third octave band [18]. This study also found that median sound pressure level for 2 kHz one-third octave band varied from approximately 80 dB re 1μPa to approximately 95 dB re 1μPa among the various monitoring locations [18]. It should be noted that the monitoring locations where mostly coastal in nature and depths of less than 100 meters [18], which is much shallower than the Norwegian Sea data set analyzed in this thesis.

1.3.6 Norwegian Sea

The data set analyzed in this thesis is recorded in the Norwegian Sea [3]. Helen Walkinshaw published results of ambient noise spectra in the Norwegian Sea and in 1957–1961 [19]. Walkinshaw's research used omni-directional hydrophones, bottomed in 240–350 fathoms (438–640 meters) with samples taken every 20 minutes during daytime hours [19]. This research measured amplitude levels of selected frequencies from 30 Hz to 1 kHz [19]. Figure 1.6 shows the sound pressure spectrum level (dB re 1 μb) versus various frequencies ranging from 30 Hz to 1 kHz. Comparing these results to [10], it can be seen that this particular area of the South Norwegian Sea has ambient noise levels (for frequencies greater than 100 Hz) about 7 to 10 dB higher [19]. Walkinshaw found that ambient noise in the South Norwegian Sea does not match well with the Knudsen curves, but that it most closely resembles the Knudsen curves in sea-state 3 in frequency ranges of 200 to 400 Hz [19]. Walkinshaw

assessed that the higher noise levels are most likely attributed to higher commercial fishing activity, much higher wind speeds and sea states [19].

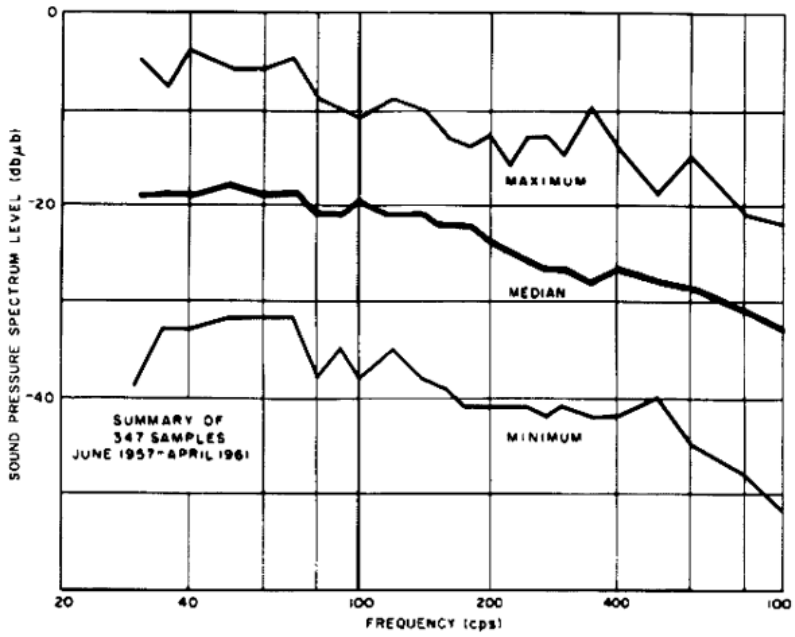

Figure 1.6. Median, minimum, maximum sea noise spectrum for the south Norwegian Sea. Data is taken over four years. The maximum and minimum values have a difference of about 25 dB throughout the range of frequencies. Below 100 Hz, sound pressure spectrum is the highest with a value of approximately -20 dB re 1 μb and remains flat up to 100 Hz. From 400 Hz to 1 kHz, the median sound pressure density dropped by about 15 dB and has a slope of about -3.5 dB per octave. Source: [19].

A second study in the Norwegian Sea attempted to determine wind speed and direction from underwater acoustic noise [20]. The results are shown in Figure 1.7. The study found ambient noise level (measured at wind speeds of 3 m/s) ranged from approximately 57 dB re $1\mu Pa^2Hz^{-1}$ at 1 Hz to approximately 35 dB re $1\mu Pa^2Hz^{-1}$ at 100 Hz [20]. The level dropped at a rate of 20 dB $decade^{-1}$ for the first decade then leveled off from 10–100 Hz [20]. For wind speeds of 7 m/s and 15 m/s they found a consistent decreasing rate of 20 db $decade^{-1}$ from 1 to 100 Hz [20]. Sound level ranged from 35 to 60 dB (re 1μPa at 1-m depth) for 8 kHz [20]. Furthermore, this data was measured from the Ocean Ambient Sound Instrument System

(OASIS) comprising of conventional Acoustic Doppler Current Profilers (ADCPs). The OASIS was surface facing which would imply higher levels. The average water depth in this area is 2000 m compared to 3146 m from the region analyzed in this data set [20].

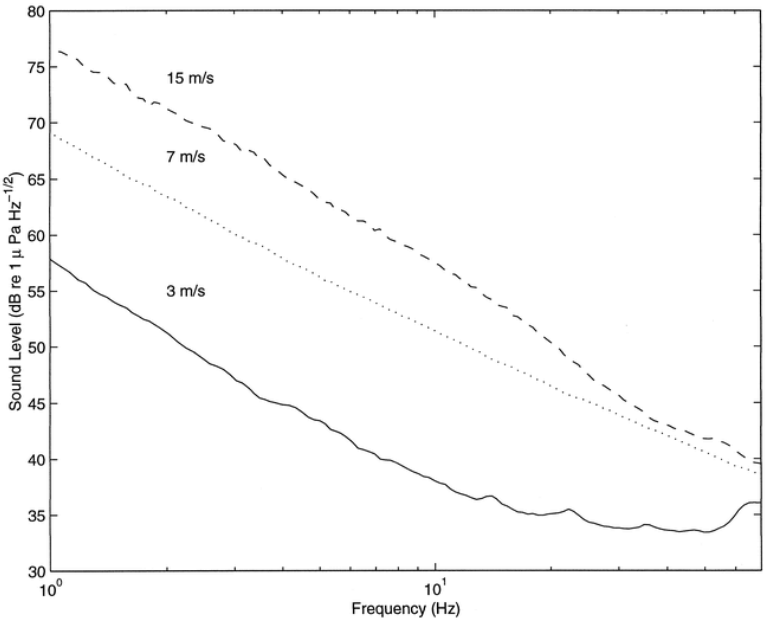

Figure 1.7. Ambient sound level for wind speeds of 3, 7 and 5 m/s at frequencies from 1 to 100 Hz. The data plotted is the average at the respective wind speeds and has greater than 8 hours of data. Of note, this sound level is calibrated and corrected to a receiver depth of 1 meter. For 3 m/s sound level dropped by 20 dB decade^{-1} from 1 to 10 Hz and then leveled off around 35 dB for 10 to 100 Hz. 7 m/s show a steady drop of about 15 dB decade^{-1}from 1 to 100 Hz. 15 m/s wind speed shows a relatively steady drop with about a 17 dB decade^{-1}. Source: [20].

Figure 1.8 shows the locations of studies [19] and [20] in comparison to the data recorded in 2018 that is analyzed in this thesis. The data analyzed in this thesis is labeled as "Mid-Freq Array 2018" and is in a similar location to the data recorded in [20]. The data recorded in [19] is in a much different location with different traffic patterns and bathymetric features.

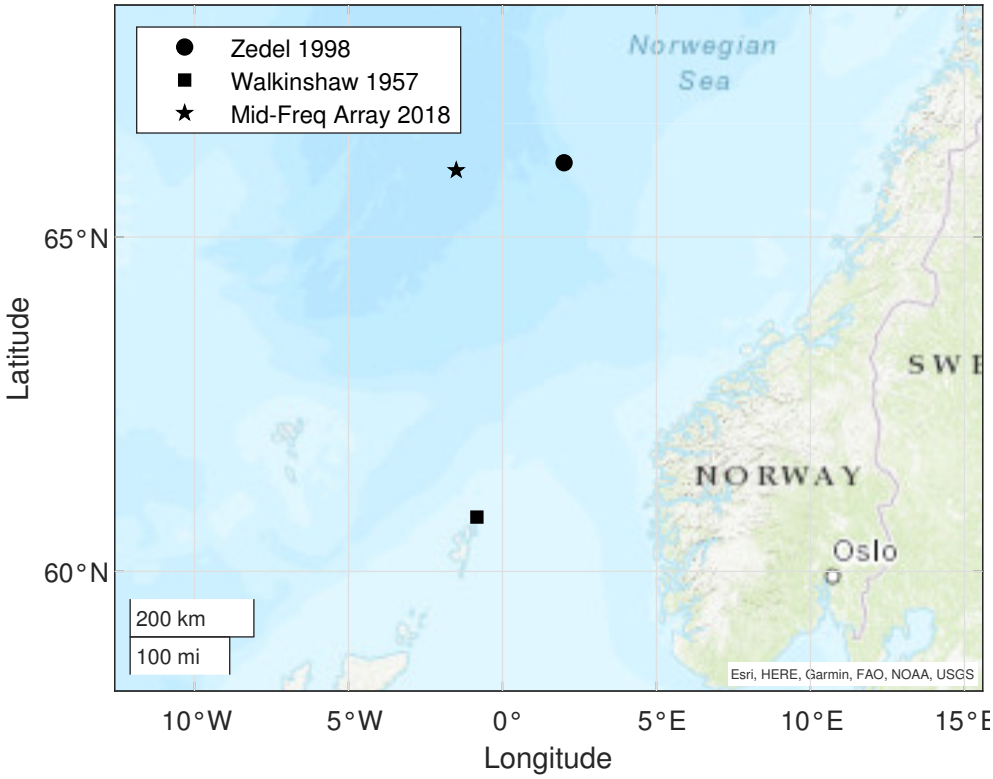

Figure 1.8. The locations of the three studies that measured ambient noise in the Norwegian Sea.

The sparse studies in the Norwegian Sea highlight the need for updated research in the area. Both the Walkinshaw and Zedel research were conducted decades prior to the data analyzed in this thesis. Additionally, Walkinshaw only published low-frequency spectrum levels, while Zedel only published qualitative results for ambient noise sound levels above 100 Hz [19], [20].

This thesis compares results and expands the frequencies analyzed to better lay the groundwork for understanding the ambient noise in an important geographical region.

1.4 Applications for Ambient Noise Research

Measuring and understanding ambient noise in the ocean has a diverse range of applications. Studies measured ambient noise levels to examine its effect on marine life [21]. Researchers

used ambient noise levels to study macro-climate changes by estimating ice melt rates within tidewater glacier fjords and sub ice shelf cavities in the Arctic [22]. Military applications include anti-submarine warfare and mine warfare. Understanding the specifics and characteristics of ambient noise is vital for sonar array performance on submarines and is a key component of the sonar equations.

The sonar equations allow us to predict performance of various sonar arrays [5]. The passive-sonar equation most applicable to sonar arrays found on submarines is $TL = SL - NL + DI - DT$; where TL is the transmission loss, NL is noise level, SL is the source level, DI is the receiving directivity index, and DT is the detection threshold. One can see that a thorough and accurate reflection of noise level in the ocean environment can affect sonar performance and effectiveness of submarines. In addition to the passive sonar equation, ambient noise level has an effect on the active sonar equation.

The active sonar equation is $DT = SL - 2TL + TS - (NL - DI)$, where DT is the detection threshold, SL is the source level, TL is the transmission loss, NL is the noise level and DI is the directivity index. Unlike in the passive case, the active sonar equation accounts for transmission losses both from the source to the target and from the target back to the source. Active sonar has an incredible range in applications. Submarine applications include but are not limited to torpedo homing, fathometer operations, and localized target detection. Fathometer operations are also used widely by commercial and surface ships to prevent groundings. Additionally, fishing vessels use a special type of active sonar to locate schools of fish.

Understanding the cause and effects of ambient noise for various geographic regions allows better modeling for sound propagation and sonar performance.

THIS PAGE INTENTIONALLY LEFT BLANK

CHAPTER 2:
Methodology and Signal Processing

Chapter 2 covers the methodology of calculating the results. Sections include details of the data acquisition system, calculation of power spectral density, data calibration, statistics and model prediction methodology.

2.1 Data Acquisition and Hardware

The single hydrophone data is subset of a 512 element 2D array deployed to an approximate depth of 150 meters [3]. The nominal acoustic array design frequency is 6 kHz. The array uses a communications buoy that includes 900 MHz, 2.4 GHz radio modems, iridium x1202 modem, equipped with Global Positioning System (GPS), Automatic Identification System (AIS) transponder, and 3 alkaline battery packs with several floats. Figure 2.1 shows a diagram of the array used to collect the data. The array is deployed from the Research Vessel (R/V) Neil Armstrong. Analyzed 16–bit data of 1–hour duration are demeaned and converted into units of volts. The demeaning process centers the discrete counts around zero by subtracting the mean from the data value and then converting them to volts with a 5 V range (-2.5V to +2.5V). Serial input/output (SIO) data files are saved for each individual element. For this thesis, the omni-directional data from element 276 is used. This element is chosen because it is centrally located in the hydrophone array. The SIO data is converted from counts to volts at a sampling rate f_s = 25,000 samples per second allowing analysis from 1–9 kHz in this thesis. Above ~9 kHz the data levels roll off due to the anti-aliasing filter. There is a high pass filter at 500 Hz. Therefore only frequencies from 1–9 kHz are presented.

2.2 Power Spectral Density

The SIO data is converted into .mat files (Section 2.1) of 1–hour duration. A MATLAB script extracts snapshots of 32768 (2^{15}) samples (1.311 seconds of data) with 50% overlap. This is also referred to as FFT length ($FFTL$). A Kaiser windowing function with a Beta value of 2.5π, shown in Figure 2.2, windows snapshots temporally before conversion into the

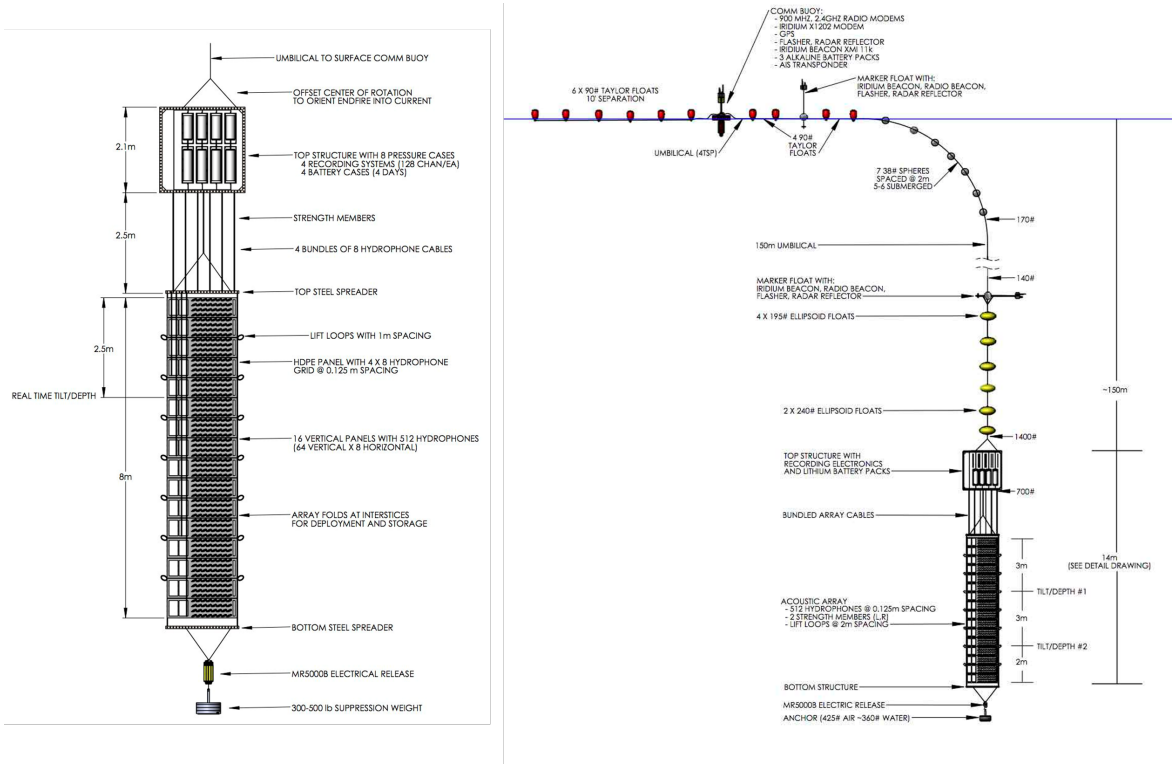

Figure 2.1. 512 element mid-frequency noise array used to collect the acoustic data in the Norwegian Sea.Element 276 (about mid-center of the array) is used for processing.

frequency domain via MATLAB's Fast Fourier Transform (FFT) function. This frequency domain data is adjusted by a normalization constant for power spectral density (PSD).

5492 snapshots are saved per 1–hour data files to be manipulated by other scripts. The dimensions of the FFT output matrix and subsequent .mat files are number of snapshots (5492) by the number of frequency bins (16385).

Snapshots are averaged incoherently for a selected averaging duration (1, 2, 5, 10, 15, 30 and 60 minutes) with 50% overlap before calibration. The single sided PSD is converted to units of dB re $1\mu\text{Pa}^2$/Hz adjusting for the gain of the data acquisition system via a calibration constant (further discussed in Section 2.3) by Equation 2.1:

$$PSD_{dB} = 10\log_{10}(PSD_{uncal}) - \text{Calibration}. \tag{2.1}$$

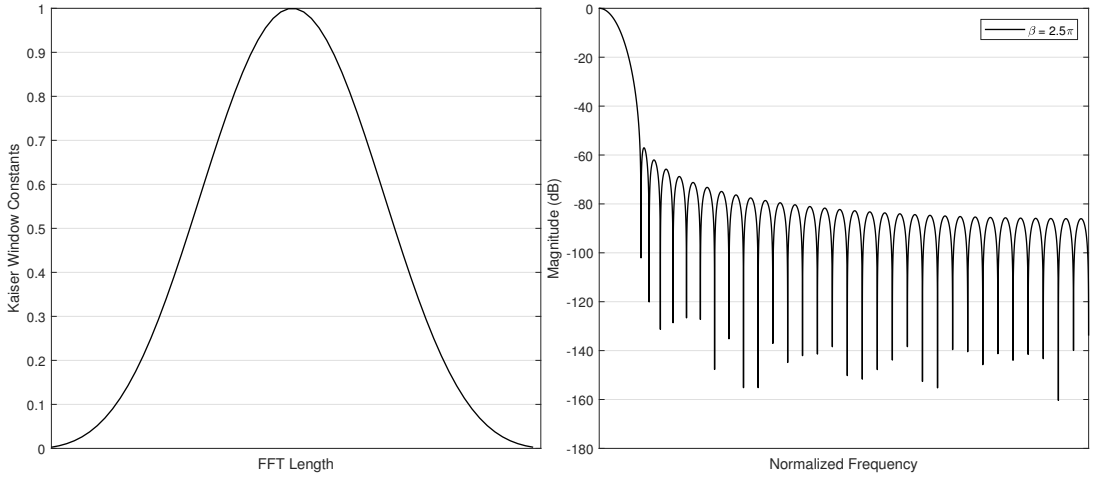

Figure 2.2. Temporal Kaiser window function applied to each snapshot. The left portion of the figure is the time domain window while the right portion is a zoomed–in plot of its magnitude (dB) spectrum.

The frequencies selected for narrowband analysis fall into the range of 1–9 kHz. Presented results use a single frequency bin without averaging over adjacent bias.

Equivalent noise bandwidth (ENBW) is given by Equation 2.2 [23]. In the fraction, the numerator is the sum of the squares while the denominator is the square of the sum of these windowing constants $w[\mathrm{n}]$, where n is a data sample:

$$\mathrm{ENBW} = \mathrm{FFTL} * \frac{\sum_{n=1}^{\mathrm{FFTL}}(w[\mathrm{n}]^2)}{(\sum_{n=1}^{\mathrm{FFTL}} w[\mathrm{n}])^2} = 1.652. \tag{2.2}$$

Using ENBW, PSD can be converted to power P by converting from Hz^{-1} to bin^{-1} for single sided spectra:

$$\begin{aligned} P_{dB} &= PSD_{dB} + 10\log\left(\frac{f_s}{\mathrm{FFTL}}\mathrm{ENBW}\right) \\ &= PSD_{dB} + 1.0. \end{aligned} \tag{2.3}$$

All results in this thesis are calculated in units of PSD (dB re 1 μPa^2/Hz), and Equation 2.3 is for the convenience of the reader for converting to power.

2.3 Data Calibration

For calibration, the mid-frequency array has a phone sensitivity gain of -156 dB re 1V/μPa, a fixed gain of 34 dB and a variable gain default setting of 20 dB. Combining these gains gives a default calibration gain level of –102 dB re 1V/μPa. The variable gain changes off the default (20 dB) four times listed in Table 2.1. The calibration constant (dB re 1V/μPa) in Table 2.1 is used in Equation 2.1.

Table 2.1. Variable Gain (dB) and used Calibration Constant (dB) of the hydrophone at various times of the experiment.

Date	Time (GMT-Z)	Variable Gain (dB)	Calibration Constant (dB re 1V/μPa)
7AUG2018	1650-1900	10	–112
7AUG2018	1900-2107	0	–122
13AUG2018	0821-1249	0	–122
13AUG2018	1700-1820	0	–122
All others	All others	20	–102

2.4 Statistics

10th, 25th, 50th, 75th, 90th and 99th percentiles are calculated using MATLAB's percentile function. These percentiles are computed using individual snapshots on the decibel scale. The standard deviation also is computed over individual snapshots on the decibel scale.

2.5 Wind Speed Model

An ambient noise model developed at the Applied Physics Lab at the University of Washington (APL-UW) predicts ambient noise level at the surface based on wind speed [24].

The methodology of the model is detailed below.

From Equation 46 on page II-35 in [24], the total noise level is given by Equation 2.4 where PSD_r is the total received power spectral density [μPa^2/Hz], PSD_s is the surface noise power spectral density [μPa^2/Hz], and PSD_t is the thermal power spectral density [μPa^2/Hz]:

$$PSD_r = PSD_s + PSD_t \approx PSD_s. \tag{2.4}$$

PSD_t contributes a small amount toward overall ambient noise spectrum level for the frequency range analyzed (1–9 kHz) thus Equation 2.4 reduces to $PSD_r \approx PSD_s$. This approximation is justified in Figure 1.2, where thermal noise only becomes a noticeable source of ambient noise above 10 kHz.

Equation 2.5 (Eq. 53 in Ref [24]) calculates surface noise power spectral density for an omni-directional hydrophone under isovelocity conditions, where A is a scale factor or noise source level at the air/sea interface at the vertical incidence [μPa^2/Hz/steradian], α is chemical absorption coefficient [dB/km], D is receiver depth [km] and β_v is the depth-integrated total extinction cross section for a near surface bubble layer. Equation 2.5 can be reduced to the simplified expression πA_f with small errors in instances when the argument of E_3 is less than 0.06:

$$PSD_s = 2\pi A E_3(0.23\alpha D + \beta_v) \approx \pi A_f. \tag{2.5}$$

The empirical model in [24] for A_f is expressed in Equations 2.6 and 2.7. A_{20} is the scale factor level based on 20 kHz, and A_f is the scale factor level for a given frequency f in kHz. Values are based on the wind speed [m/s] at a height of 10 m above the surface of the sea assuming $T_{air} - T_{surf} \leq 1^{\circ}$C and $v_{wind} \geq 1$m/s.

$$10 \log A_{20} = 20.5 + 22.4 \log v_{wind} \tag{2.6}$$

$$10 \log A_f = 10 \log A_{20} + 20.7 - 15.9 \log f \tag{2.7}$$

Combining Eq. 2.6 and Eq. 2.7 yields Eq. 2.8:

$$10 \log A_f = 41.2 + 22.4 \log v_{wind} - 15.9 \log f. \tag{2.8}$$

Combining Eq. 2.5 with 2.8, the predicted noise PSD [dB re 1 μPa^2/Hz] at the surface is:

$$\begin{aligned} PSD_s\,[\text{dB}] &= 10 \log \pi + 10 \log A_f && (2.9) \\ &= 10 \log \pi + 41.2 + 22.4 \log v_{wind} - 15.9 \log f. && (2.10) \end{aligned}$$

The APL-UW model is compared to the data collected in this thesis in Section 4.4 using wind speed collected with two sensors mounted on the R/V Neil Armstrong.

CHAPTER 3:
Norwegian Sea Environment

Chapter 3 provides an overview of the environmental conditions encountered during the experiment. Sections discuss wind, temperature, sound speed profile and sound propagation. For the purposes of this thesis, the "first deployment" refers to the data collected from 1650Z on August 7th, 2018 through 0820Z on August 11th, 2018. The "second deployment" refers to the data collected from 1200Z on August 12th, 2018 through 1820Z on August 13th, 2018.

3.1 Wind

As discussed in Section 1.2, wind profoundly impacts ambient noise level. Wind speed (m/s) is measured from two sensors attached to the R/V Neil Armstrong. The two sensors are located on the port and starboard sides of the ship at a height of 18.1 meters. Figure 3.1 shows the wind speed (m/s) over the course of two weeks. Figure 3.2 shows the wind speed with a 10 minute sliding average for the raw data at height of 18.1 m and an equivalent wind speed converted to a height of 10 m. The wind speed conversion changes the original wind speed by <1 m/s at all times. The height conversion from 18.1 m to 10 m is done via Equation 3.1:

$$v_{10m} = v_{18m} \frac{\log\left(\frac{10}{Z_0}\right)}{\log\left(\frac{18.1}{Z_0}\right)}, \tag{3.1}$$

where $Z_0 = 0.0002$ m. The height conversion is necessary since Eq. 2.6 requires wind speed input at 10 m. Henceforth, wind speed will refer to the converted equivalent wind speed at 10 m. Note that the calculated change in wind speed from 18.1m to 10 m is small, and that results are very similar when compared to approaches including a Charnock parameter.

During the first deployment of the array, wind speed (averaged between port and starboard sensor) has a maximum of 14.74 m/s with a mean of 4.63 m/s. The standard deviation for

wind speed during the first deployment is 2.49 m/s. During the second deployment, wind speed peaks to 10.19 m/s. The mean wind speed during the second deployment is 4.10 m/s. The standard deviation of wind speed during the second deployment of the array is 2.34 m/s. Of note, these wind speeds are not always near location of the array. Figure 3.3 shows the range (km) of the R/V Neil Armstrong between the hydrophone array during the first deployment.

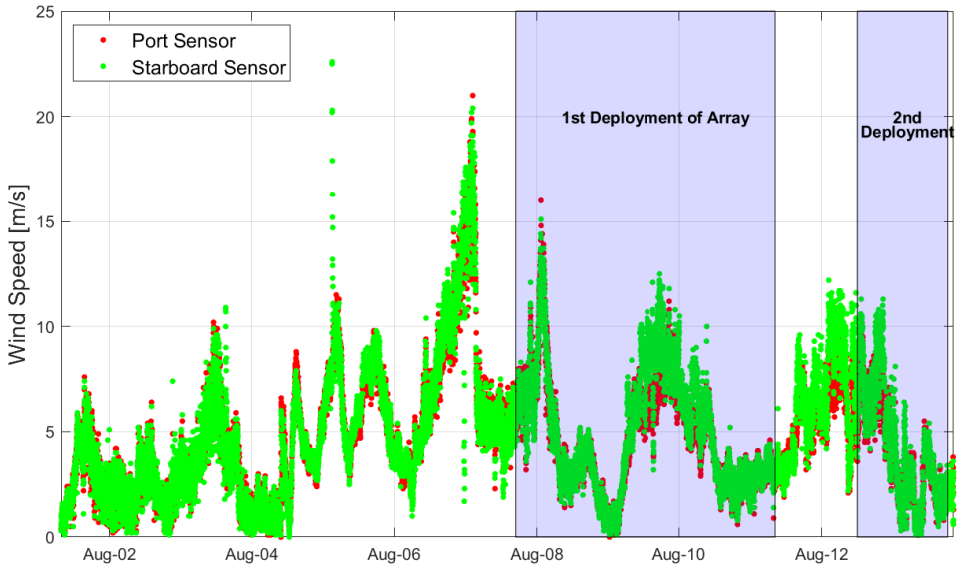

Figure 3.1. Wind speed obtained from two sensors located on the port (red) and starboard (green) sides of the R/V Neil Armstrong. The shaded regions include data obtained while the array was deployed in the water and collecting data (7AUG2018 16:50Z to 11AUG18 08:20Z and 12AUG18 12:00Z to 13AUG18 18:20Z).

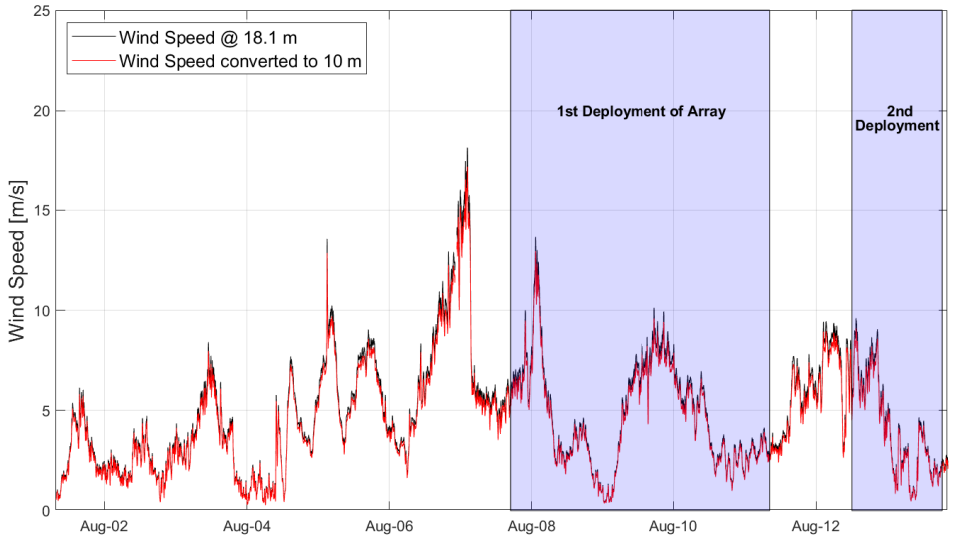

Figure 3.2. Wind speed [m/s] at a height of 18.1 m and at a converted height of 10 m. A 10 minute sliding average is applied to both wind speeds.

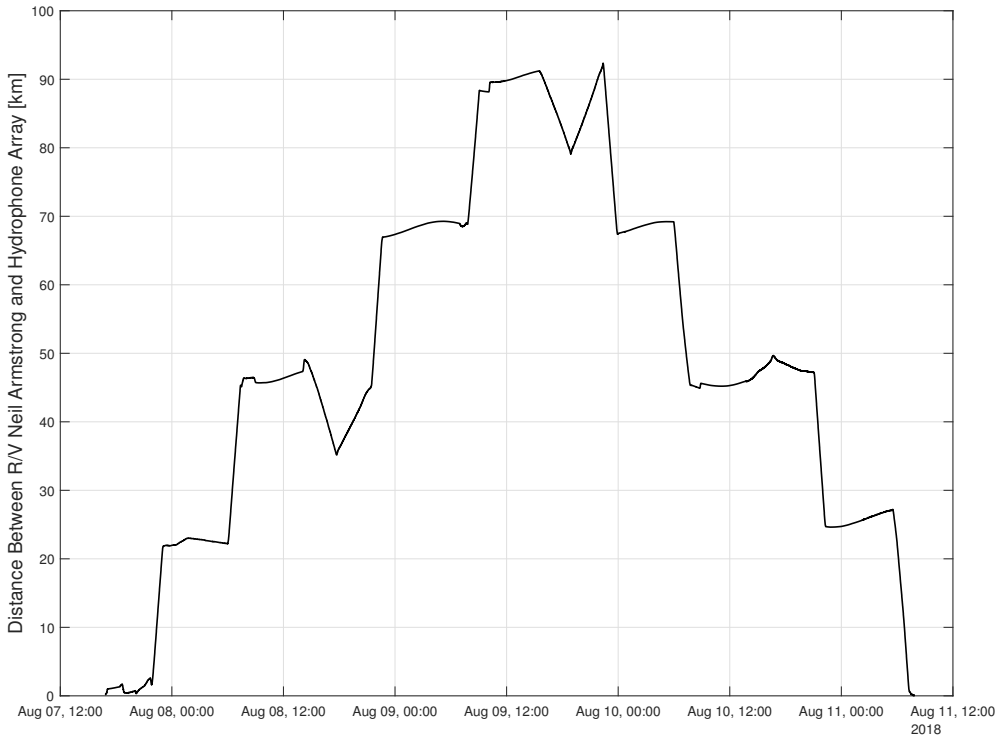

Figure 3.3. Range (km) between the R/V Neil Armstrong and the Mid-Frequency Array during the first deployment of the array.

3.2 Sea State

Figure 3.4 shows the array movement during the first deployment of the array. The cyclical nature of the drift is due to the Coriolis effect from the earth's rotation. The array drift to the north can be attributed to the sea state and prevailing northerly current in the Norwegian Sea. While not directly measured, sea state can be implied based on wind speed from Table 1.1. Based on this Table, sea state varied from a Beaufort Scale of 0 (around 0000Z August 9th) to as high as a 7 (around 1700Z August 8th).

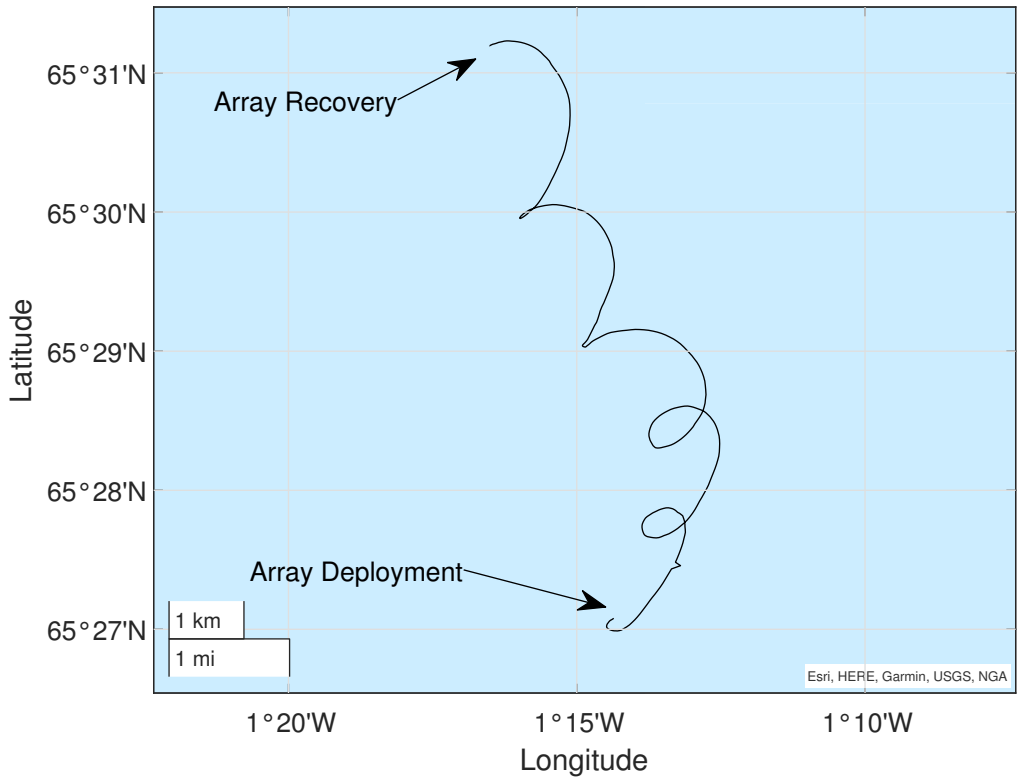

Figure 3.4. Array drift during the first deployment due to wind, current and sea state. The cyclical nature of the drift in the array is due to the Coriolis effect.

3.3 Temperature

Temperature is measured using an instrument that records conductivity, temperature and depth (CTD). A CTD deployed from R/V Armstrong 10 times over the course of the experiment to a depth of 3000 and 1000 meters (once to 3000 m, nine to 1000 m). Figure 3.5 shows the mean temperature (˚C) from all 10 CTD deployments as a function of depth. Data beyond 1000 meters shown is data collected from one CTD deployment and thus not an average. Surface temperature during the experiment averaged 12.3˚C with average temperature decreasing to 5.1˚C at 165 meters (near the nominal depth of the array). Surface temperature varies from the minimum of 11.6˚C and a maximum of 12.6˚C.

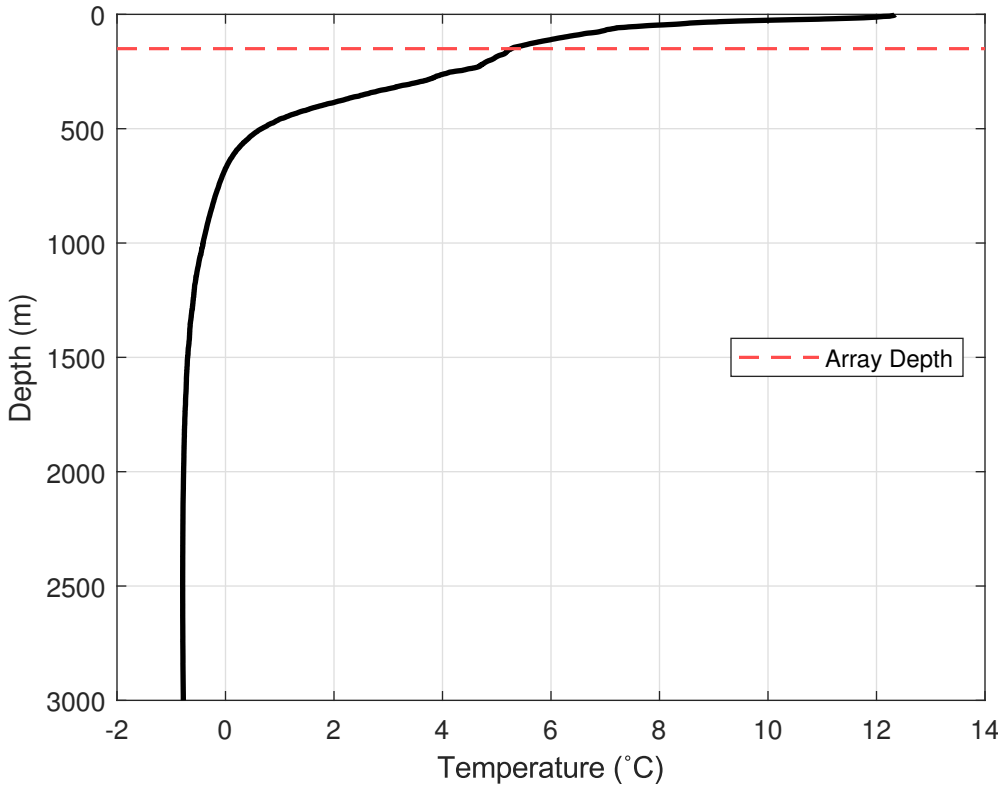

Figure 3.5. The mean temperature from 10 deployments of the CTD as a function of depth. The average temperature for the first 1000 meters was calculated from all 10 CTD deployments. Data beyond 1000 meters shown is data collected from one CTD deployment and thus not an average. Surface temperature averaged 12.3 ° C with ocean temperature decreasing to -0.78 ° C around 3000 meters.

The standard deviation of temperature can help describe where layers in the ocean are as a function of depth. Higher standard deviation of temperature could indicate that there is a possible thermal layer around that depth. Figure 3.6 shows the standard deviation of ocean temperature over depth. Interestingly, the standard deviation of temperature reaches a maximum just under the surface with a sharp decrease at around 50 meters followed by another sharp increase at around 150 meters. This increase is most likely due to CTD deployments 2 and 7. These temperature profiles are taken a significant distance away

(~40 km away) from the array and thus are assumed not to be indicative of the temperature profile at the location of the array. As depth increases beyond 400 meters, the standard deviation drops significantly indicating smaller variance between the locations as expected. The locations of the 10 CTD deployments are shown on Figure 3.10.

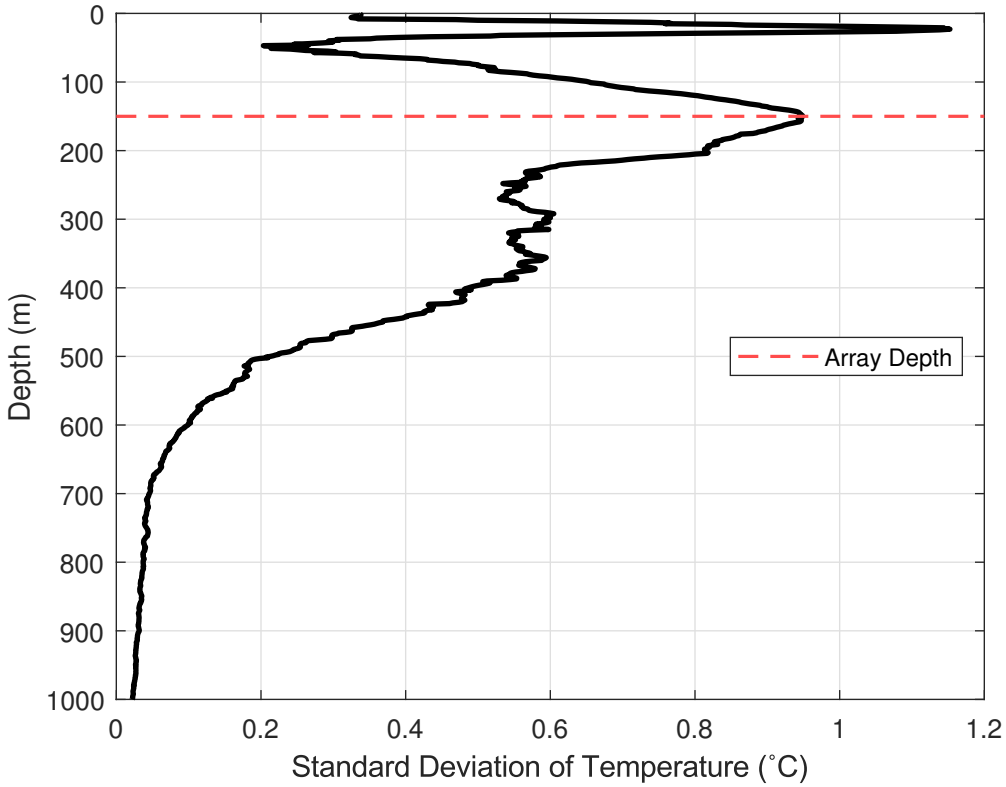

Figure 3.6. Standard deviation of temperature plotted over depth up to 1000 meters. Standard deviation is maximum just under the surface with a sharp decrease at around 50 meters followed by another sharp increase at around 150 meters. This increase is most likely due to CTD deployments 2 and 7. Those temperature profiles were taken a significant distance away (~40 km away) from the array. As depth increases beyond 400 meters, the standard deviation drops significantly indicating smaller temperature variance as expected. Only one CTD deployment was done beyond 1000 meters making standard deviation useless beyond 1000 meters.

3.4 Sound Speed Profile

The sound speed profile is important to understanding and predicting sound propagation through the ocean. Figure 3.7 shows the average sound speed profile from 10 CTD deployments. The sound speed profile found shows a strong negative gradient from the surface down to about 550 meters. This is an important feature because in a negative sound gradient means that sound ray paths from a source would typically bend down toward the minimum sound speed due to Snell's refractive law [25]. The minimum sound speed is about 1460 m/s, with a maximum measured sound speed of about 1495 m/s near the surface and around 3000 meters. It is assumed that below a depth of 3000 meters, the sound speed would continue to linearly increase down to the bottom of the ocean due to the corresponding pressure increase from depth. The average depth of the ocean in this region is 3146 m with a standard deviation of ~10 m [26]. The hydrophone array deployed to a depth of about 150 meters which would put it squarely in the negative sound gradient shown in Figure 3.7. The array aperture is approximately 8 meters in height and therefore would not interact in any significant manner in the deep thermal layer. The higher sound speed at the surface of the ocean can be attributed to the higher surface temperatures due to the warm summer conditions. Colder surface temperature results in slower sound speed and could cause the sound speed gradient becoming positive towards the surface [25]. The deep sound channel axis is at a depth of 600 meters. It should be noted that the various deployments of the CTD did not occur directly next to the array as some occurred as far away as the first and second convergence zone. The average of all 10 deployments depicts a good estimate for the sound speed profile for sound rays at the array. Figure 3.10 shows the CTD deployment locations relative to the array location during the first deployment.

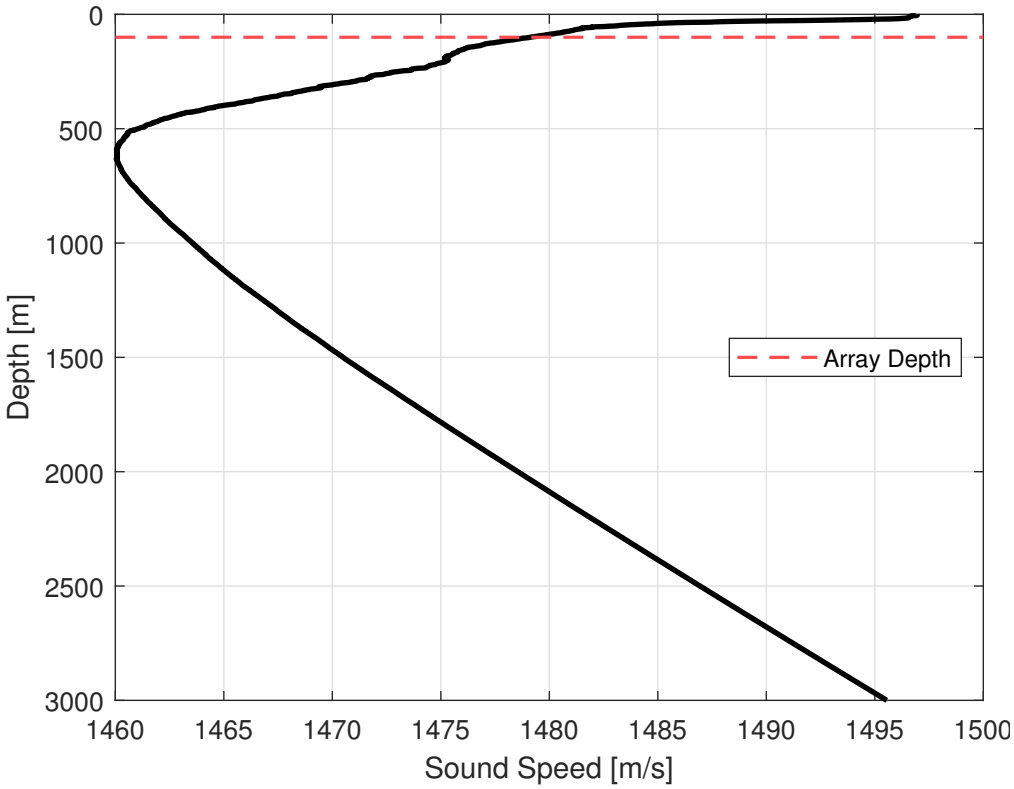

Figure 3.7. Mean sound speed profile of 10 CTD deployments. A CTD deployed 10 times throughout the experiment ranging from both morning and evening deployments. Of note, only the first deployment of the CTD went to 3000 meters, the rest deployed to a depth of 1000 meters.

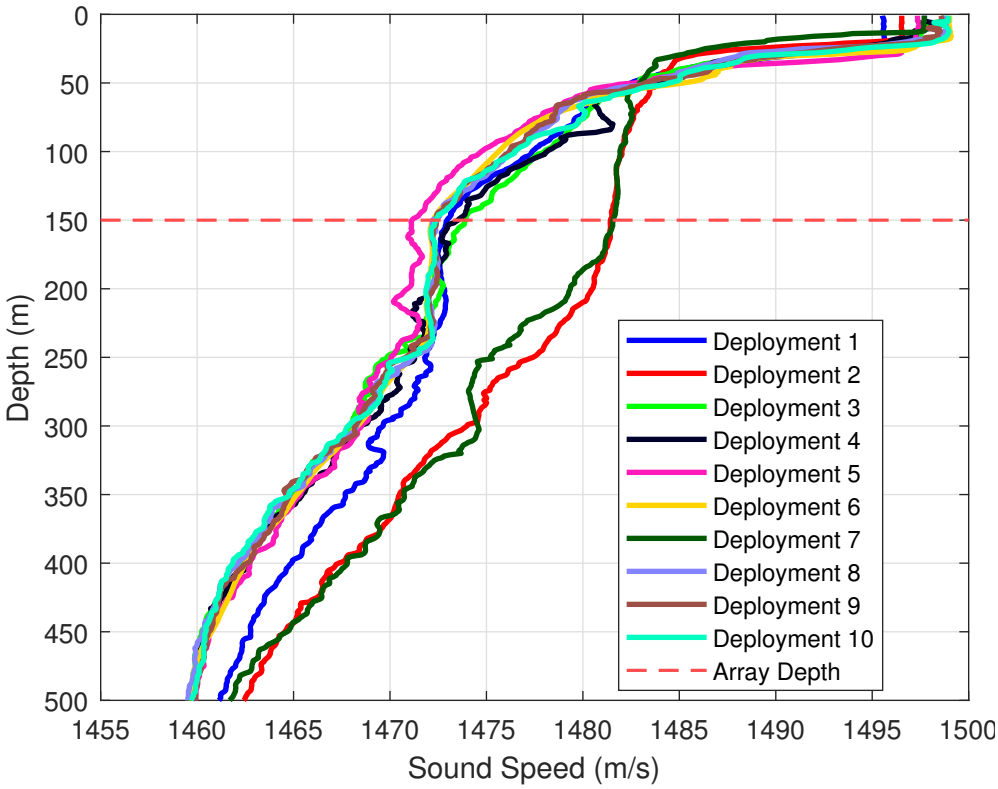

Figure 3.8. Sound Speed Profile of all ten CTD deployments. Through most of the deployments, the sound speed profiles are pretty similar, the two outliers include deployments 2 and 7. Both of those were taken further to the northeast and thus the ship could have crossed a thermal front of some sort. Locations of the CTD deployments are on figure 3.10.

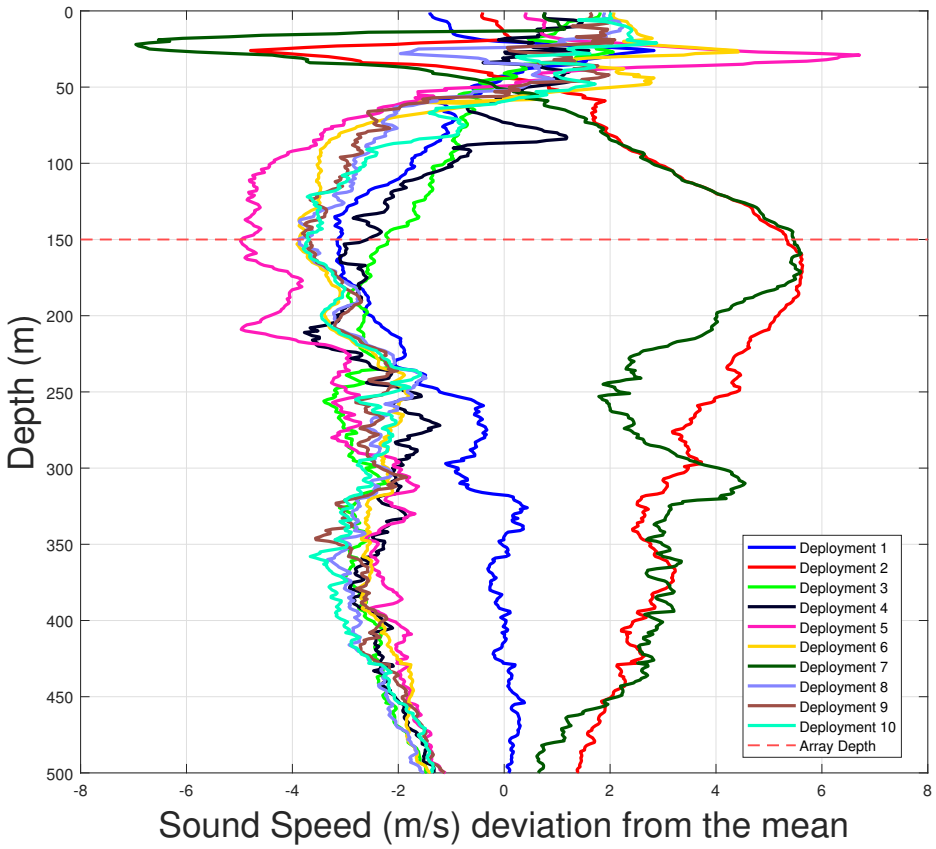

Figure 3.9. Sound speed (m/s) of all 10 CTD deployments subtracted from the mean and plotted over depth in meters. The deviations of both deployments 2 and 7 also show that this area has a significantly different temperature gradient which results in differing sound speed profiles.

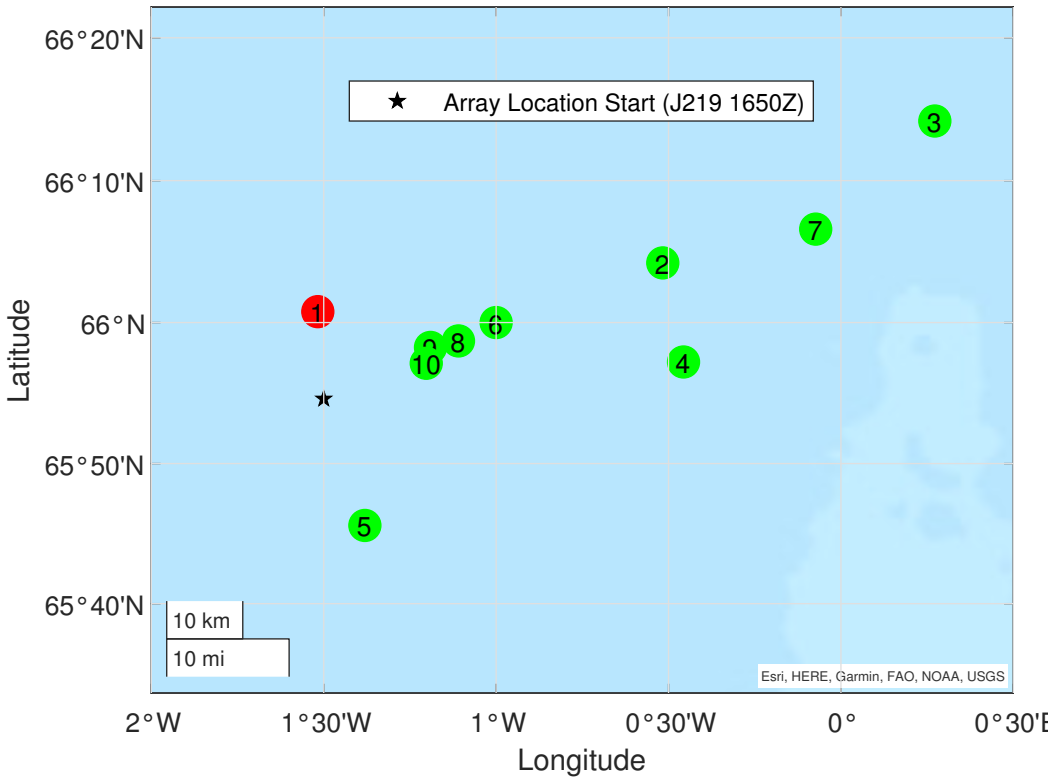

Figure 3.10. CTD deployment locations compared to location of array during first deployment of the array. The CTD deployments are labeled 1-10 in sequential order. The first deployment (red) is the only one deployed to 3000 meters, the rest (green) deployed to 1000 meters. The location of the mid-frequency array is plotted as a black star. The array was retrieved at the same location as CTD deployment number 5.

3.5 Sound Propagation

Figure 3.11 highlights the different propagation paths sound could travel to reach the array. Figure 3.11 uses a source depth of 150 m (array depth) and a frequency of 3 kHz. While Figure 3.11 shows the ray traces emanating from a source, the transmission loss between an omni-source and an omni-receiver are equivalent [27]. The principle of reciprocity, derived by Lord Rayleigh, allows propagation losses to be calculated in one direction (either source to target or target to source) [27]. The details of the sound speed profile on the left panel of Figure 3.11 are discussed in Section 3.4. While there is bottom bounce propagation and

convergence zone propagation, the transmission loss on these ray traces is approximately 70 dB at 3 kHz, not including bottom attenuation. Ambient sound at these distances does not significantly contribute to ambient noise levels at the array considering ambient noise levels measured are approximately 58 dB at 1 kHz decreasing to approximately 45 dB at 9 kHz (Figure 4.1). The observed mid-frequency ambient noise level in this classical, deep water profile is expected to mostly originate from the noise generated by the surface. The first convergence zone range is at 40 km with an annulus of 10 km. This is highlighted in the bottom right panel of Figure 3.11. Using the GEBCO bathymetric database the average bottom depth in the vicinity of the array deployment is 3146 m and a standard deviation of ~10 m [26].

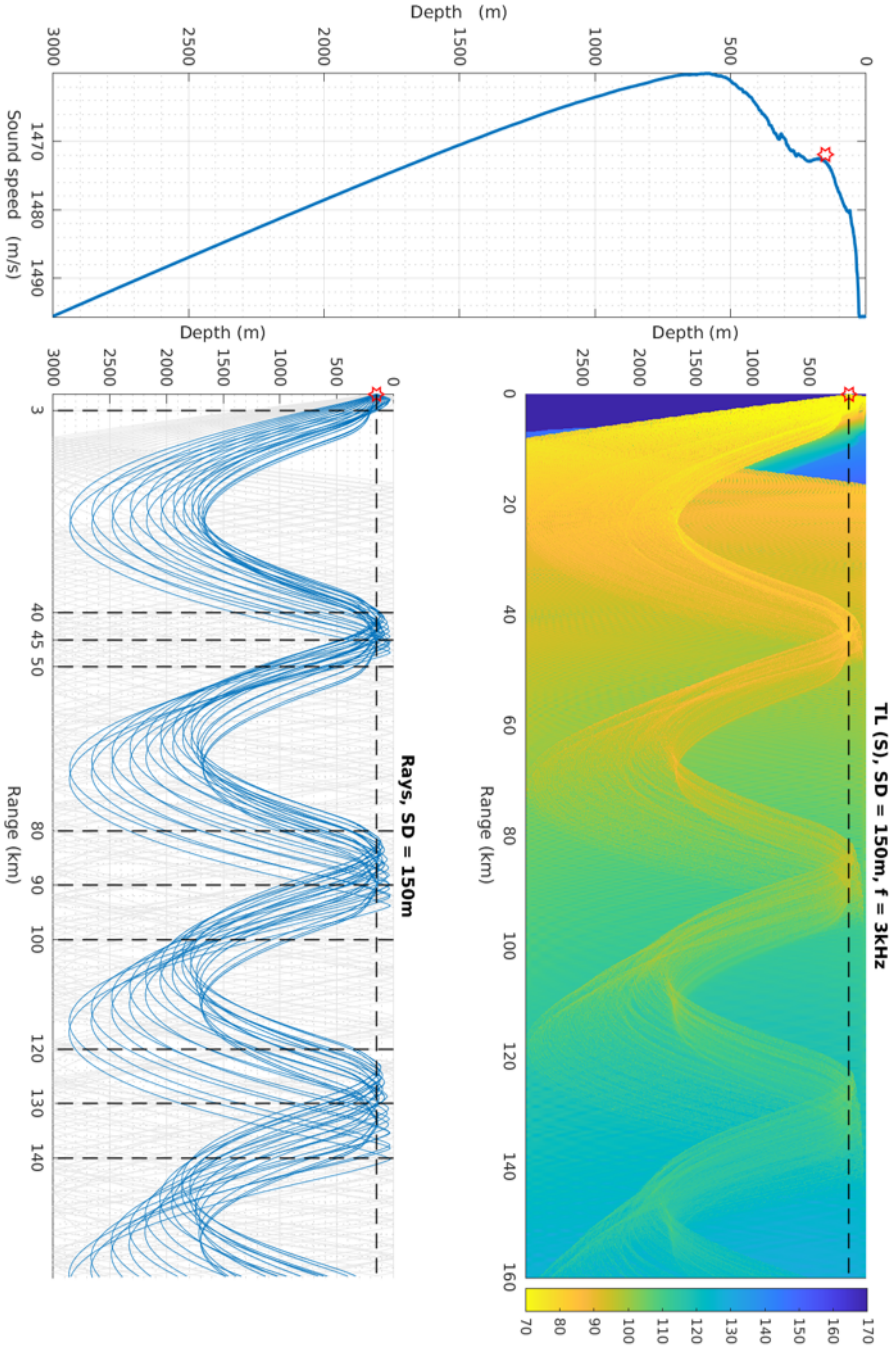

Figure 3.11. Left: Sound speed profile from the first CTD deployment. Top Right: Sound rays for a source at 150 m at a frequency of 3 kHz. Transmission Loss plotted as a function of color from 70 dB to 170 dB. Bottom Right: Selected convergence zone ray traces to highlight the propagation distance of the convergence zone and the annulus of the convergence zone. No surface or bottom loss included. Thorp volume attenuation.

CHAPTER 4:
Results and Discussion

Chapter 4 includes selected broadband and narrowband results analyzed from the data set. Chapter 4 also explores the wind dependence of the data and compares the results to a model. Supplemental figures and results are located in Appendix A. To keep the results in context, there are several times listed in Table 4.1 in which anthropogenic noise is purposefully inserted for testing unrelated to this thesis's objective.

Table 4.1. Anthropogenic noise testing times that skew data results.

Date	Time (Z)	Type of Testing
07AUG18	1859-2122	Short Range Calibration testing.
08AUG18	0916-1347	Source transmissions at first convergence zone (CZ).
08AUG18	1433-1730	Source transmissions at first convergence zone (CZ).
08AUG18	1815-2116	R/V Neil Armstrong own-ship noise near array.
09AUG18	1036-1545	Source tonals (130 dB centered on 2.5, 3.5, 4.5 and 5.5 kHz)
09AUG18	1550-2200	Broadband noise from ~80 km away from array.
10AUG18	0930-1050	Various broadband noise spectrum levels at first CZ (~46 km).
10AUG18	1055-1215	Various broadband noise spectrum levels at first CZ (~46 km).
10AUG18	1225-1735	Various broadband noise spectrum levels at first CZ (~46 km).
12AUG18	1453-1740	Tonals at first CZ (~46 km).
13AUG18	0918-1505	Short range calibration transmissions.
13AUG18	1527-1606	Ship transiting at 9.5 knots towards array at 14 km.

4.1 Broadband Results

Spectrum Level [dB re 1 μPa^2/Hz] versus frequency along with accompanying percentiles and one standard deviation are plotted for three experiment times in Figures 4.1, 4.2, and

4.3. Additional time averages can be found in Appendix A.2. Results in Figure 4.1 are consistent with the levels found in Figures 1.1 and 1.2. Day time results, plotted for 1300Z on 12 August 2018 in Figure 4.3, show spectrum level consistent with night time results found in Figure 4.1 (0000Z on 10 August 2018). The results in Figure 4.2 show about a 7–10 dB drop in spectrum level for all frequencies when compared to the results in Figures 4.1, and 4.3. This can be attributed to a drop in wind speed which is further discussed in Section 4.3. The PSD in Figure 4.2 has higher variability observed across the frequency spectrum analyzed when compared to Figures 4.1 and 4.3. This could indicate the presence of a mid-frequency interfering signal such as a biologic.

The standard deviation for Figures 4.1, 4.2, and 4.3 are within the results found in Figures 1.1 and 1.2. The spectrum level of the ambient noise (PSD, black line) implies a sea state of approximately 3–5. Table 1.1 indicates that this sea state level would have wave heights from 3–12 feet.

The frequency range analyzed (1–9 kHz) falls in Urick's region IV in Figure 1.1. In this region, Urick found spectrum level to drop approximately 5–6 dB/octave [2]. It would be expected to see the spectrum level reduce at a near linear fashion from 1–9 kHz [2]. This slope matches with the results found in Figures 4.1, 4.2 and 4.3. The results in Figures 4.1, and 4.3 show about a -5 dB/octave slope from 2–8 kHz. The results in Figure 4.2 show a slightly steeper slope but is variable from 2–8 kHz (likely an interfering biologic).

The results found in [20] showed spectrum levels were much lower than the results presented in this thesis. However, Zedel's intentions were to predict and calculate wind speed from ambient noise and not necessarily record and publish spectrum levels on a broad frequency spectrum [20]. Furthermore, [20] only presented spectrum levels for frequencies below 1 kHz (Figure 1.7), making the 1 kHz reported in this thesis the only real bench mark to compare results against.

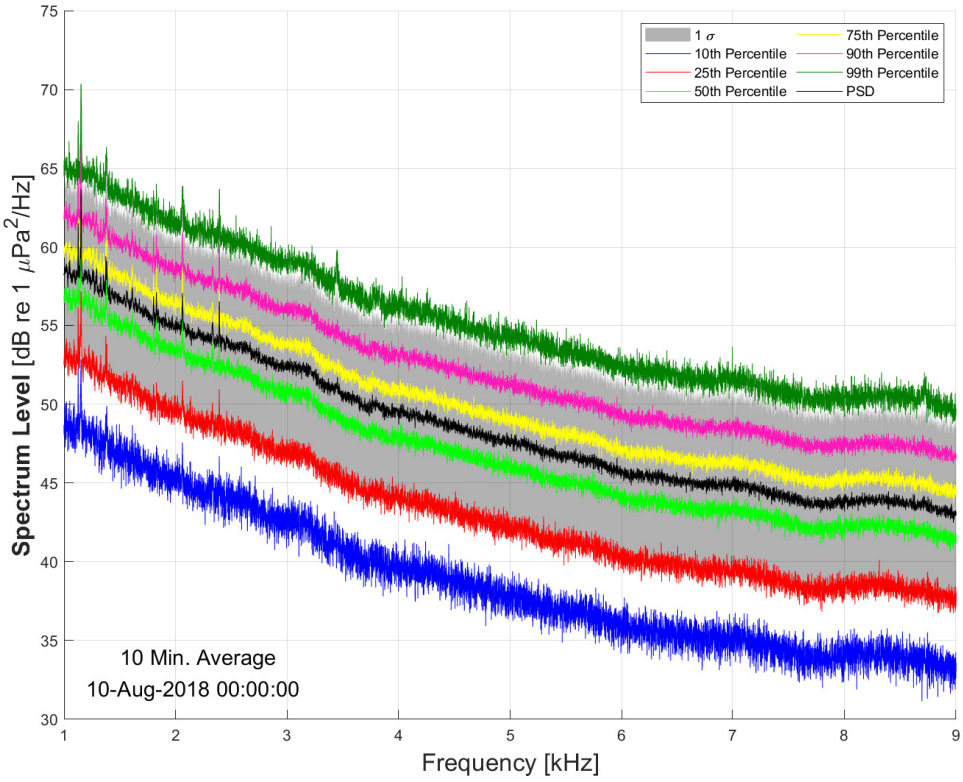

Figure 4.1. Spectrum Level [dB re 1 μPa^2/Hz] versus frequency [kHz] using a 10 minute sliding average. This data is taken from midnight on 10AUG2018. The statistics are described in Section 2.4. See additional time averages in Appendix A.2.

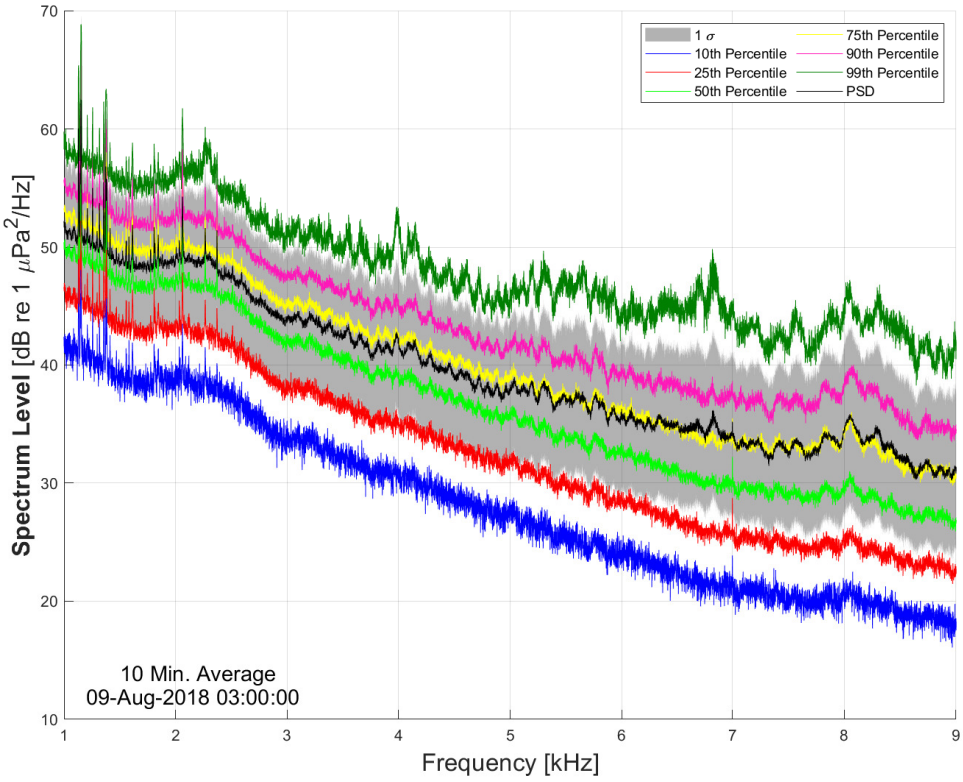

Figure 4.2. Spectrum Level [dB re 1 μPa^2/Hz] versus frequency [kHz] using a 10 minute sliding average. This data is taken from 0300Z on 09AUG2018. The statistics are described in Section 2.4. See additional time averages in Appendix A.2.

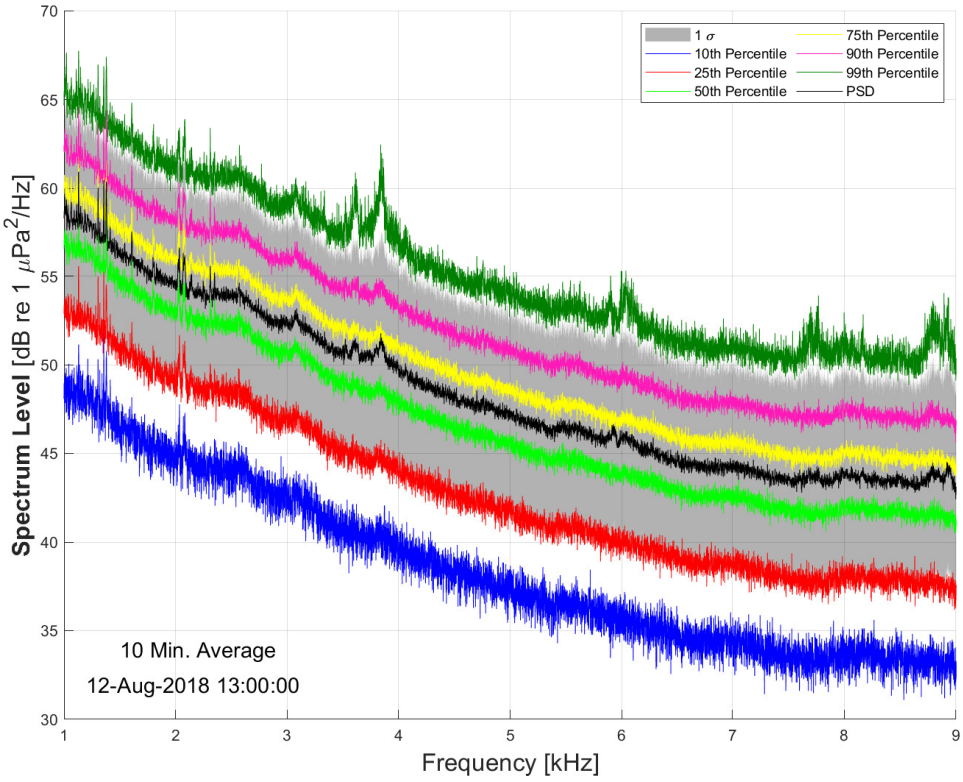

Figure 4.3. Spectrum Level [dB re 1 μPa^2/Hz] versus frequency [kHz] using a 10 minute sliding average. This data is taken from 1300Z on 12AUG2018. The statistics are described in Section 2.4. See additional time averages in Appendix A.2.

4.2 Narrowband Results

Ambient noise spectrum level [dB re 1 μPa^2/Hz] is calculated for 9 selected frequencies (1–9 kHz in increments of 1 kHz) across the first and second deployments in Figures 4.4 through 4.9. For both deployments, a sliding average of 10 minutes is used. Additionally, time averages of 1, 2, 5, 15, 30 and 60 minutes are calculated and can be found in Appendix A.1. Of note, the spike and rapidly changing PSD around 1000 on 13 AUG is due to short range calibration testing unrelated to this thesis. Frequencies of 1–3 kHz have significantly higher PSD values than the frequencies at 4–6 kHz and 7–9 kHz. Table 4.2

lists the approximate PSD minimum and maximum values seen throughout the experiment. As [2] found, as frequency increases the ambient noise spectrum level decreases. The PSD values are also consistent with those found by [11] as displayed in Figure 1.2.

Table 4.2. PSD value range for selected frequencies (1–9 kHz)

Frequency (kHz)	Approximate PSD values (dB re 1 μPa^2/Hz)
1	50 to 60
2	48 to 56
3	42 to 53
4	38 to 52
5	34 to 50
6	30 to 49
7	28 to 48
8	26 to 45
9	24 to 45

Furthermore, the trend of the PSD tends to dip about 10 dB overnight on August 9th for all selected frequencies. This dip between day time and night time PSD values is most likely correlated to the wind values which is discussed in Section 4.3. The spectrum level difference between the 10th percentile and the 99th percentile is approximately 20 dB for 1–9 kHz with the 99th percentile spectrum levels trending closer to the standard deviation than the 10 percentile spectrum levels.

Figure 4.10 illustrates the distribution by comparing the number of occurrences of a specific PSD using a 0.5 dB bin width. Figure 4.10 uses a 1 minute average instead of a 10 minute average to increase the population size available for the bins. This figure highlights how spectrum level drops as frequency increases. Additionally, the ambient noise spectrum level is distributed with a heavy tail biased towards lower spectrum level.

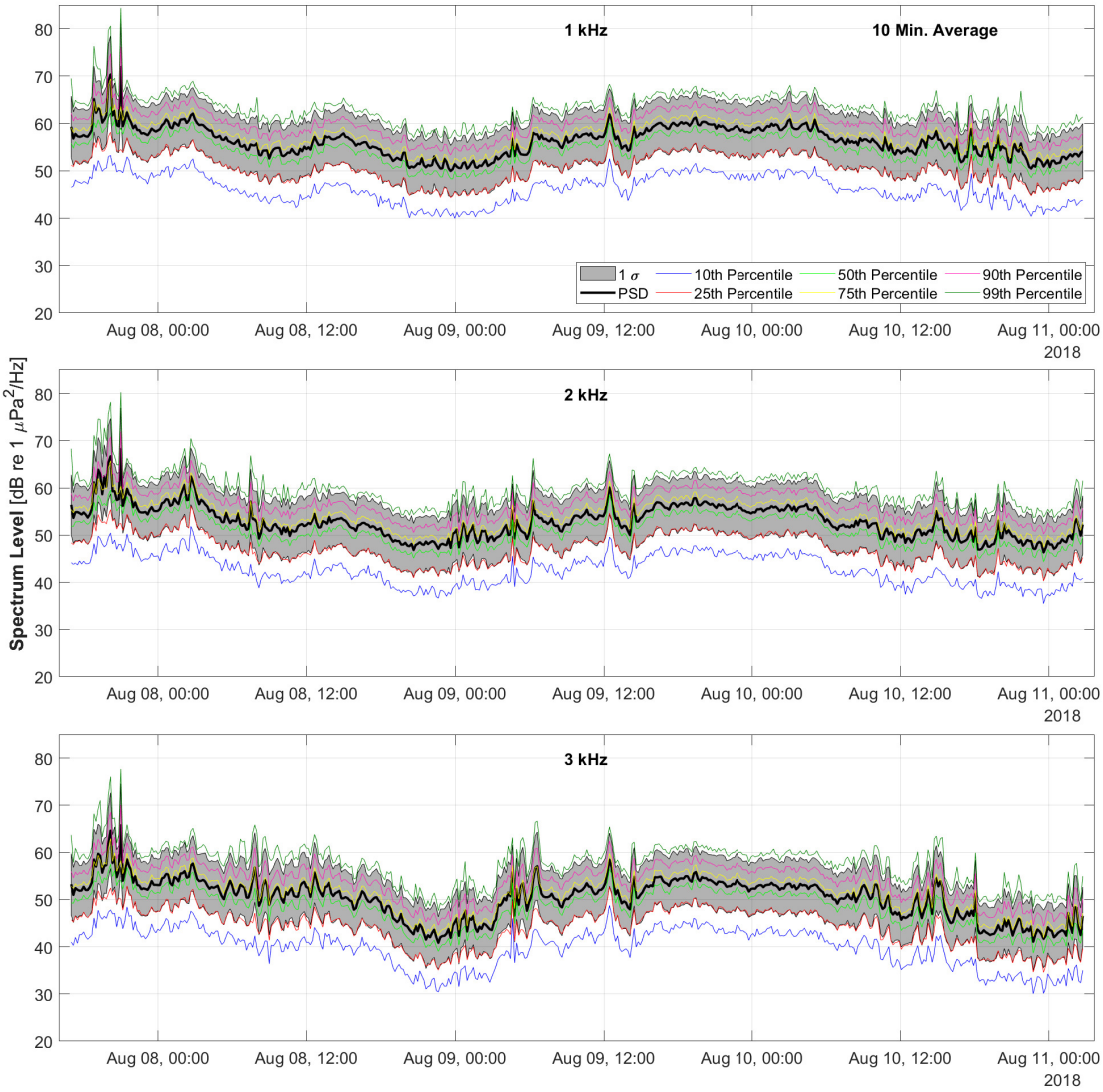

Figure 4.4. Spectrum Level [dB re 1 μPa^2/Hz] of frequencies 1, 2, and 3 kHz from 8AUG18 to 11AUG18 using a 10 minute sliding average. The statistics are described in Section 2.4.

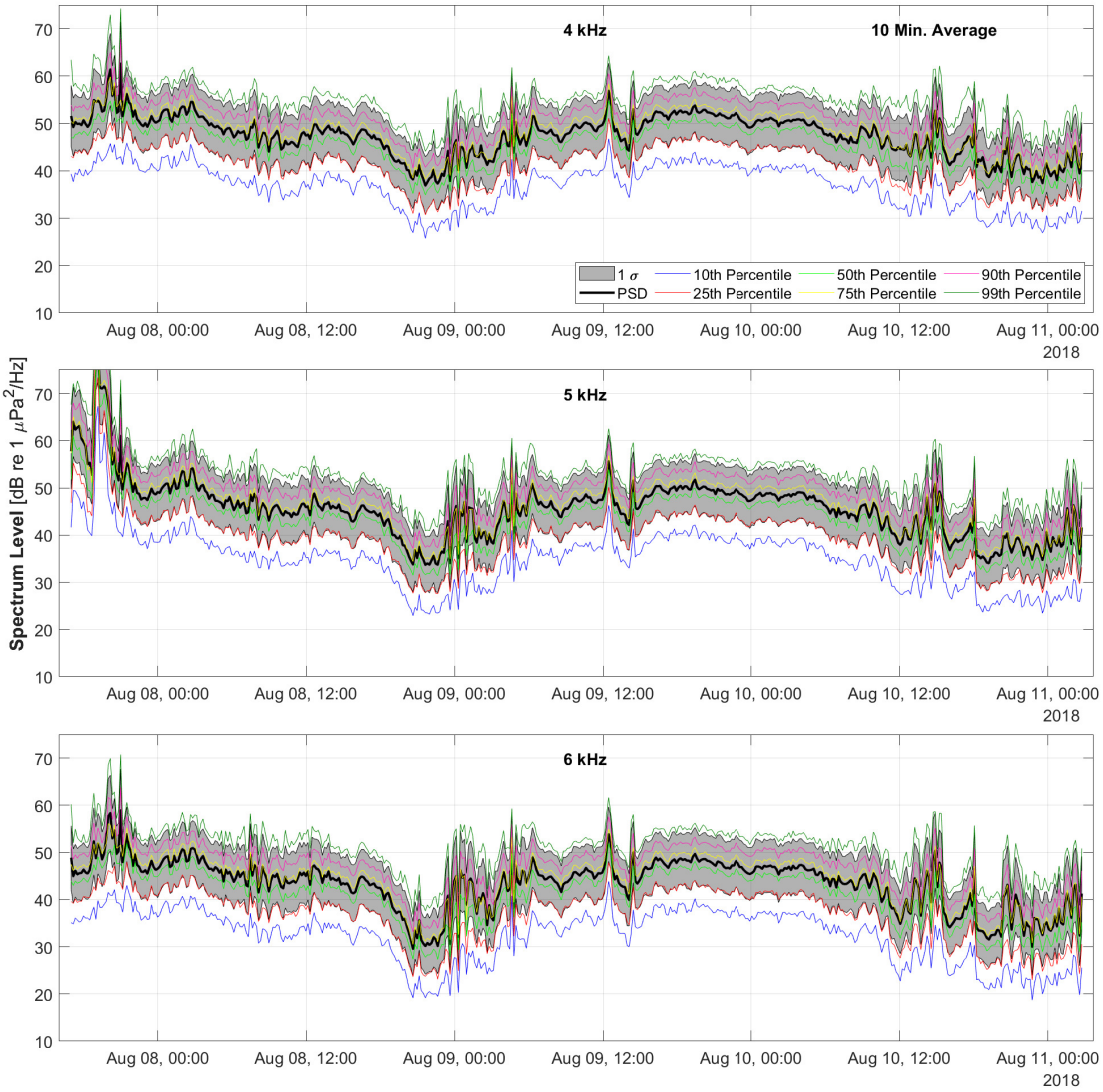

Figure 4.5. Spectrum Level [dB re 1 μPa^2/Hz] of 4, 5 and 6 kHz frequencies plotted in time from 8AUG18 to 11AUG18 using a 10 minute sliding average. The statistics are described in Section 2.4.

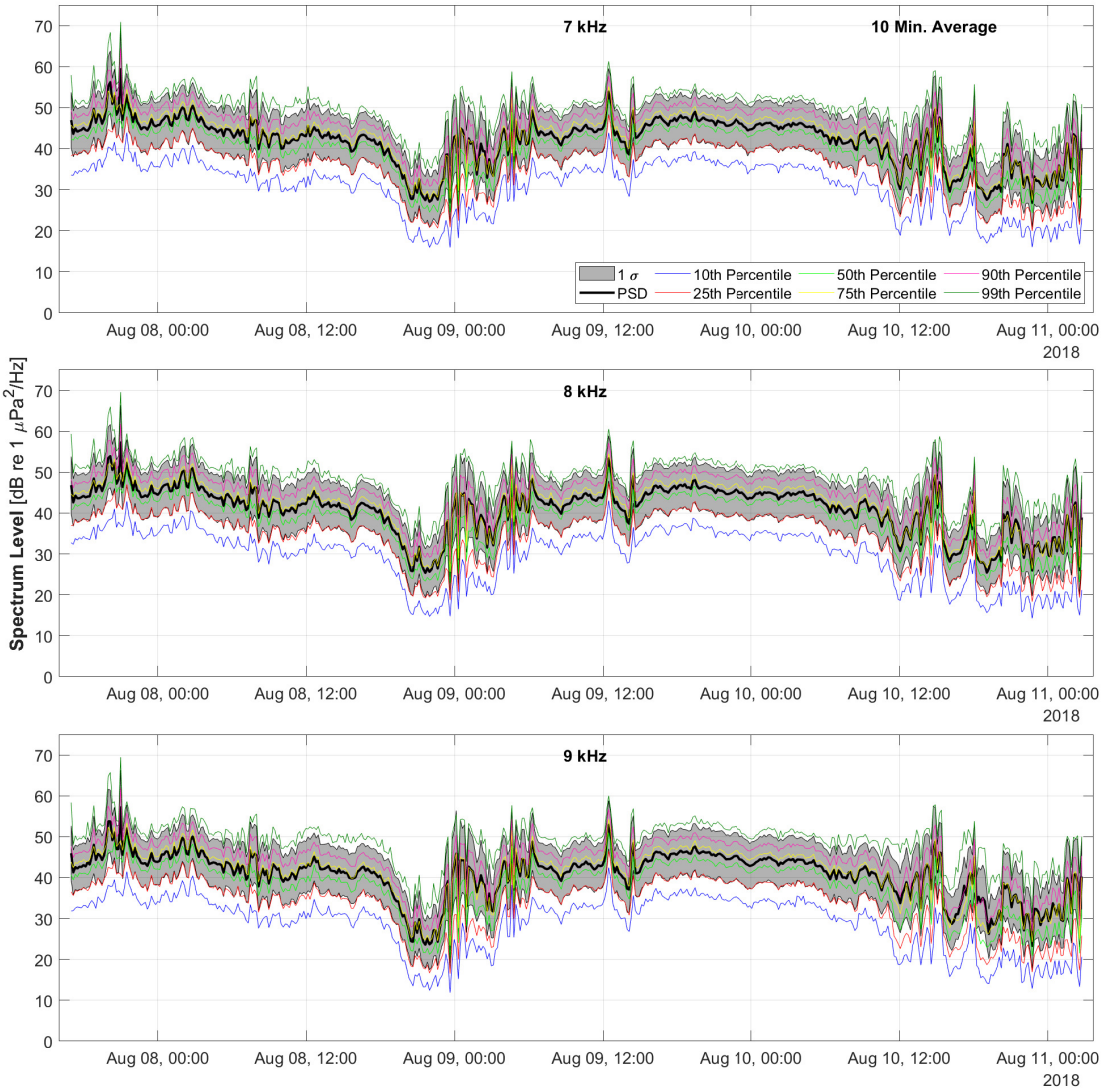

Figure 4.6. Spectrum Level [dB re 1 μPa^2/Hz] of 7, 8, and 9 kHz frequencies from 8AUG18 to 11AUG18 using a 10 minute sliding average. The statistics are described in Section 2.4.

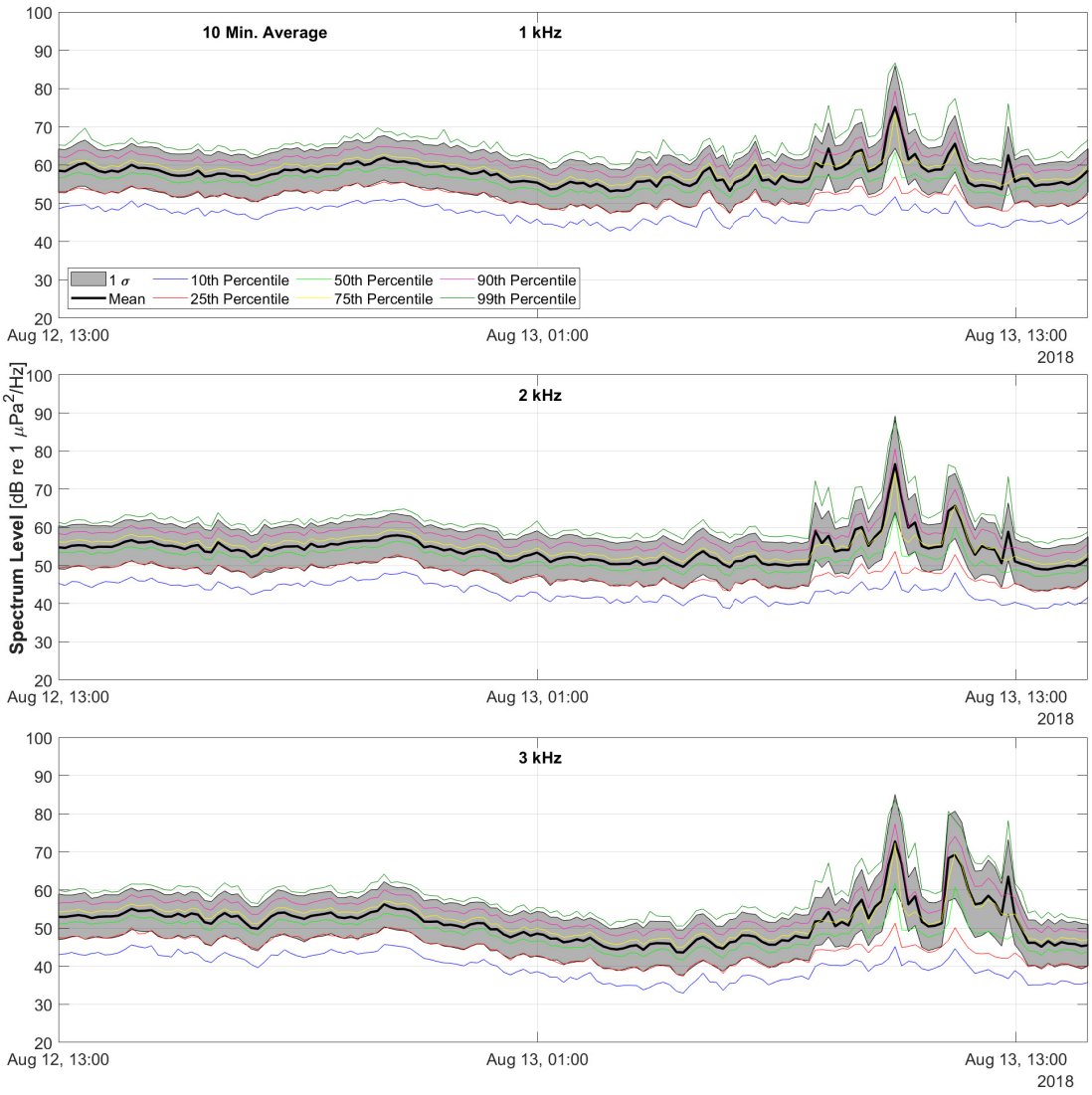

Figure 4.7. Spectrum Level [dB re 1 μPa^2/Hz] of 1, 2, and 3 kHz frequencies from 12AUG18 to 13AUG18 using a 10 minute sliding average. The statistics are described in Section 2.4. Of note, the spike and rapidly changing PSD around 1000 on 13 AUG is due to various noise testing. See Table 4.1.

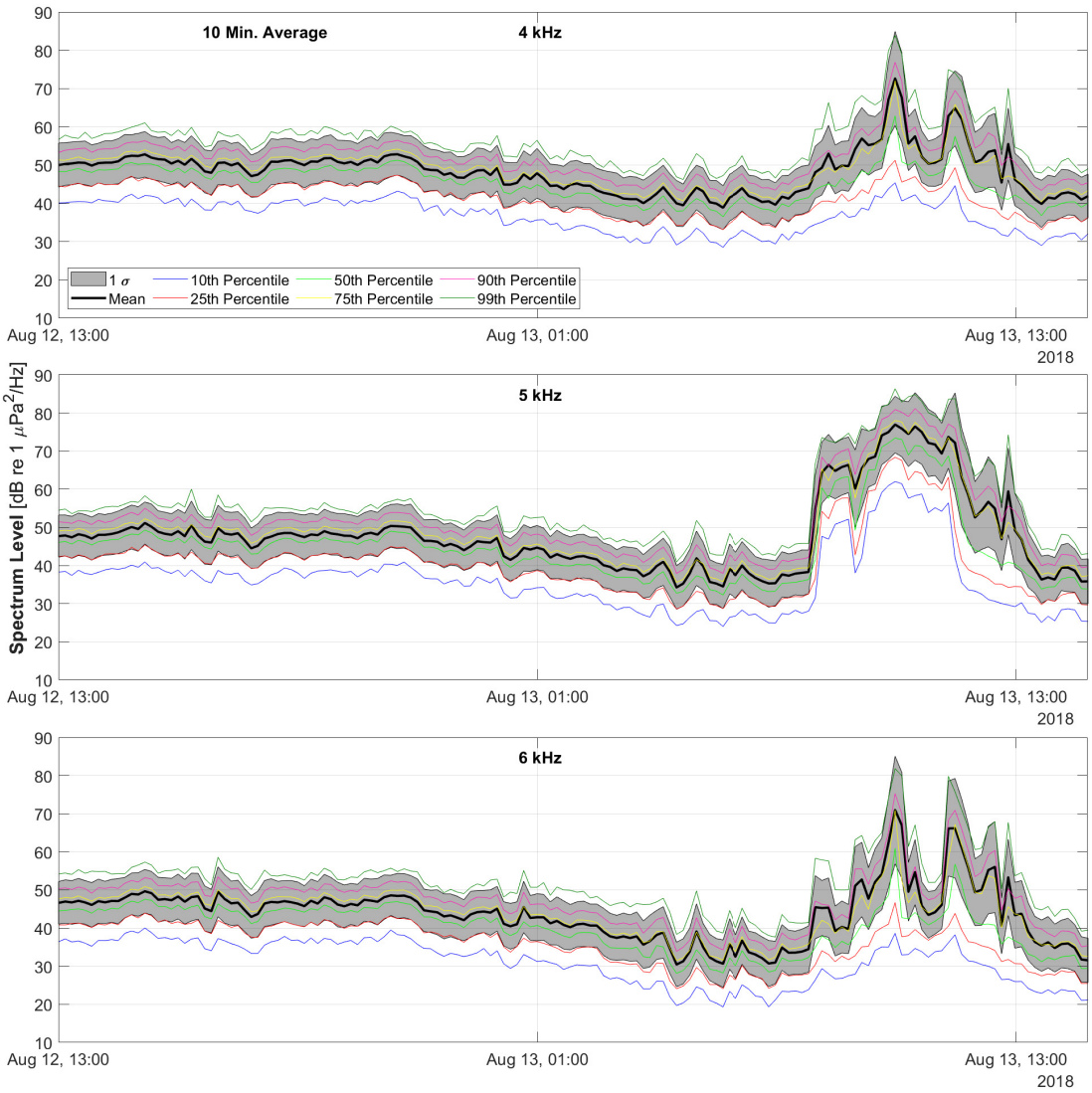

Figure 4.8. Spectrum Level [dB re 1 μPa^2/Hz] of 4, 5, and 6 kHz frequencies from 12AUG18 to 13AUG18 using a 10 minute sliding average. The statistics are described in Section 2.4. Of note, the spike and rapidly changing PSD around 1000 on 13 AUG is due to various noise testing. See Table 4.1.

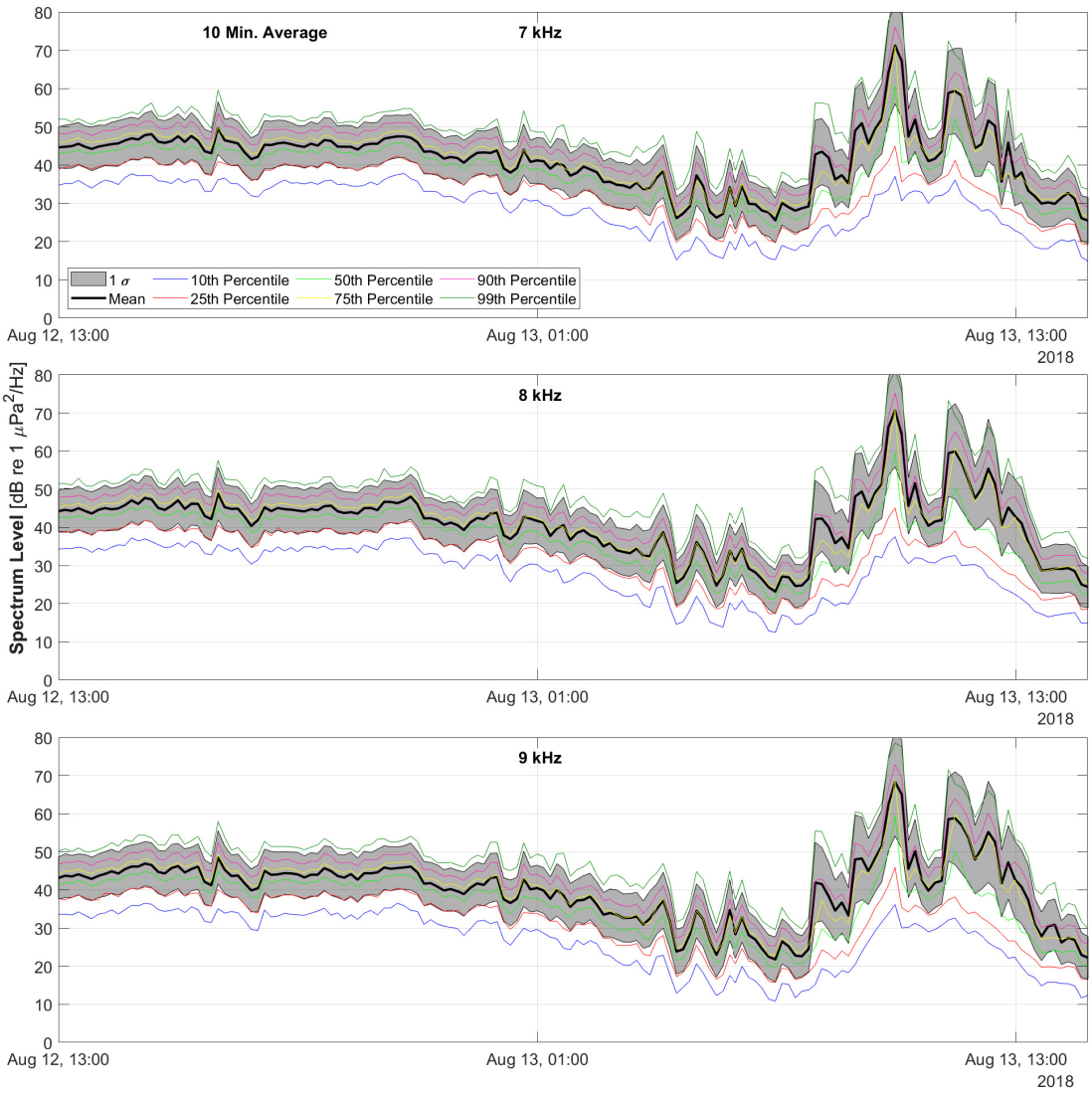

Figure 4.9. Spectrum Level [dB re 1 μPa^2/Hz] of 7, 8, and 9 kHz frequencies from 12AUG18 to 13AUG18 using a 10 minute sliding average. The statistics are described in Section 2.4. Of note, the spike and rapidly changing PSD around 1000 on 13 AUG is due to various noise testing. See Table 4.1.

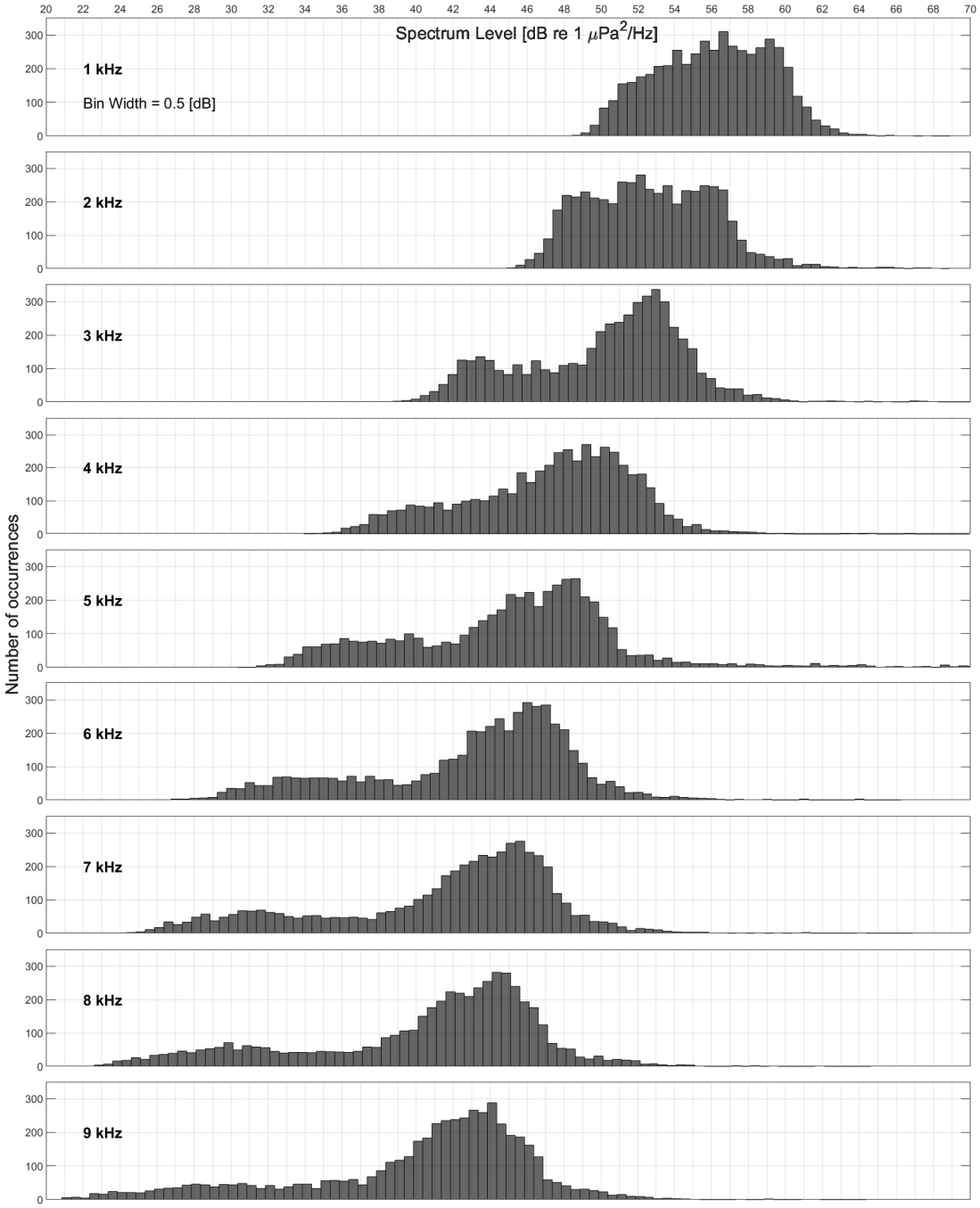

Figure 4.10. Histogram plots separately comparing the number of occurrences for a specific spectrum level bin for 1–9 kHz during the first deployment. One minute sliding average and a bin width of 0.5 dB are used.

4.3 Data-Wind Speed Comparison

The spectrum level of the measured ambient noise is heavily influenced by wind speed. Below 2 kHz, ambient noise spectrum level is less impacted by the wind speed versus higher frequency ambient noise. Figure 4.11 shows a plot of wind speed from two different sources (R/V Neil Armstrong and National Centers for Environmental Prediction (NCEP) Forecast system) compared to spectrum levels for 1, 4, and 7 kHz for the first deployment of the array. The NCEP Forecast system uses a complex wind speed model, while the wind speed from the R/V Neil Armstrong is an average of the two sensors located on the ship (see Figure 3.3 for distance of ship from the hydrophone array) [28]. The distance between the ship and hydrophone array may induce an offset in time. Figures 4.13 and 4.14 show wind speed and spectrum level for 4 kHz plotted on one single plot for both the first and second deployments. Figures 4.13 and 4.14 illustrate that ambient noise spectrum level correlates well with wind speed. Higher frequency (such as 7 kHz) ambient noise spectrum levels are more strongly correlated to wind speed than lower frequency ambient noise spectrum levels such as 1 kHz. Figures 4.13 and 4.14 use a ten minute sliding average for both spectrum level and wind speed data respectively. This strong correlation between wind speed and ambient noise spectrum level is in line with results found by [11]. Figures 4.13 and Figures 4.14 show a time shift between the spectrum level and the wind speed. This is most likely due to the distance between the R/V Neil Armstrong (wind sensor) and the array. If one was shifted in time, the spectrum level and wind speed would most likely produce an even higher correlation.

Figure 4.15 shows a histogram plot spectrum level [dB re 1 μPa^2/Hz] compared to wind speed [m/s] for 1–9 kHz frequencies. The results on Figure 4.15 is in line with results in Figure 4.16 found by [29]. Spectrum level decrease from 1 kHz to 9 kHz for wind speeds 2–4, 4–6, 6–8 shown in Figure 4.15 is closely correlated to the slope calculated using a linear regression in Figure 4.16 by [29]. Ma et al. [29] found a uniform slope of -15.7 dB/decade for 1–50 kHz valid for wind speeds up to 14 m/s. The slope is similar to the APL-UW model slope used (-15.9 dB/decade) found in Section 2.5.

Spectrum level [dB re 1 μPa^2/Hz] versus frequency [kHz] for sea states 1–5 is plotted in Figure 4.17. Figure 4.17 shows data from the first deployment only and uses a one minute incoherent average of spectrum level. Sea states on Figure 4.17 are determined from wind

speed using the Beaufort Scale (see Table 1.1). The distinct tonals in spectrum level are from the active source testing conducted as all signals are included (see Table 4.1). Sea state 1 (wind speeds 0.5–1.7 m/s) spectrum level is approximately 53 dB re 1 μPa^2/Hz at 1 kHz and drops to approximately 37 dB re 1 μPa^2/Hz at 9 kHz. Sea state 5 (wind speeds 8.5–11.1 m/s) spectrum level is approximately 60 dB re 1 μPa^2/Hz at 1 kHz and drops to approximately 47 dB re 1 μPa^2/Hz at 9 kHz. Figure 4.17 results are fairly consistent with results in Figures 1.2, 1.4, and 4.16. For sea state 5, results for this thesis are approximately 10 dB re 1 μPa^2/Hz lower than the Wenz curves at 1 kHz. Additionally, the results on Figure 4.17 for sea state 5 are approximately 6–7 dB re 1 μPa^2/Hz lower at 1 kHz compared to results in Figure 1.4 (sea state 5 would be between the 6–8 and 11–13 m/s curves). However, spectrum level for sea states 2–4 closely match the results in Figure 4.16. The overall slope and shape is similar of the results is similar to Figures 1.2, 1.4, and 4.16.

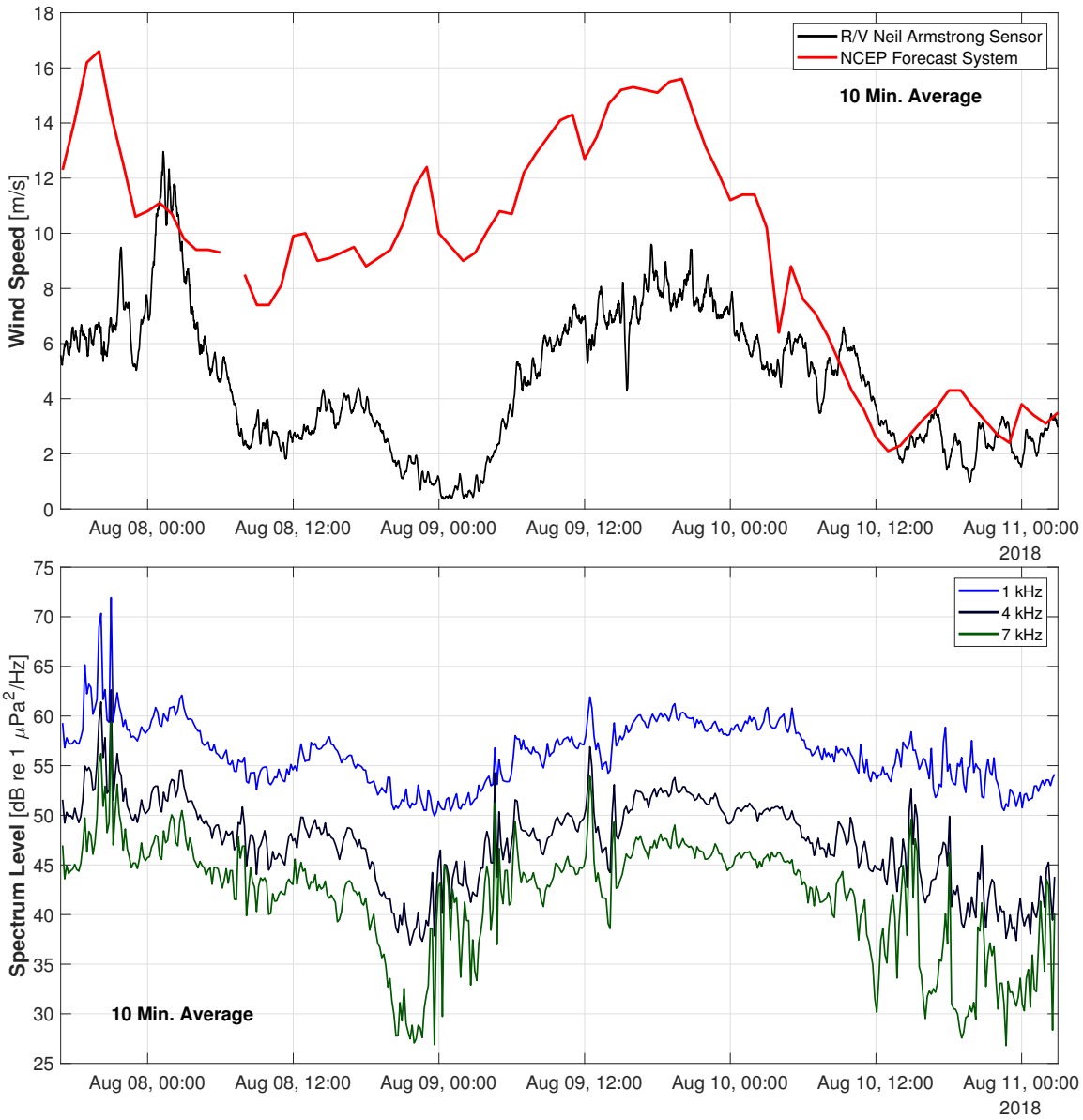

Figure 4.11. Top: Wind Speed [m/s] from two different sources from 08AUG18 to 11AUG18. Bottom: Spectrum Level [dB re 1 $\mu Pa^2/Hz$] from 08AUG18 to 11AUG18. A 10 minute sliding average is used on both the wind data and the frequency data. See Ref. [28] for NCEP forecast system data.

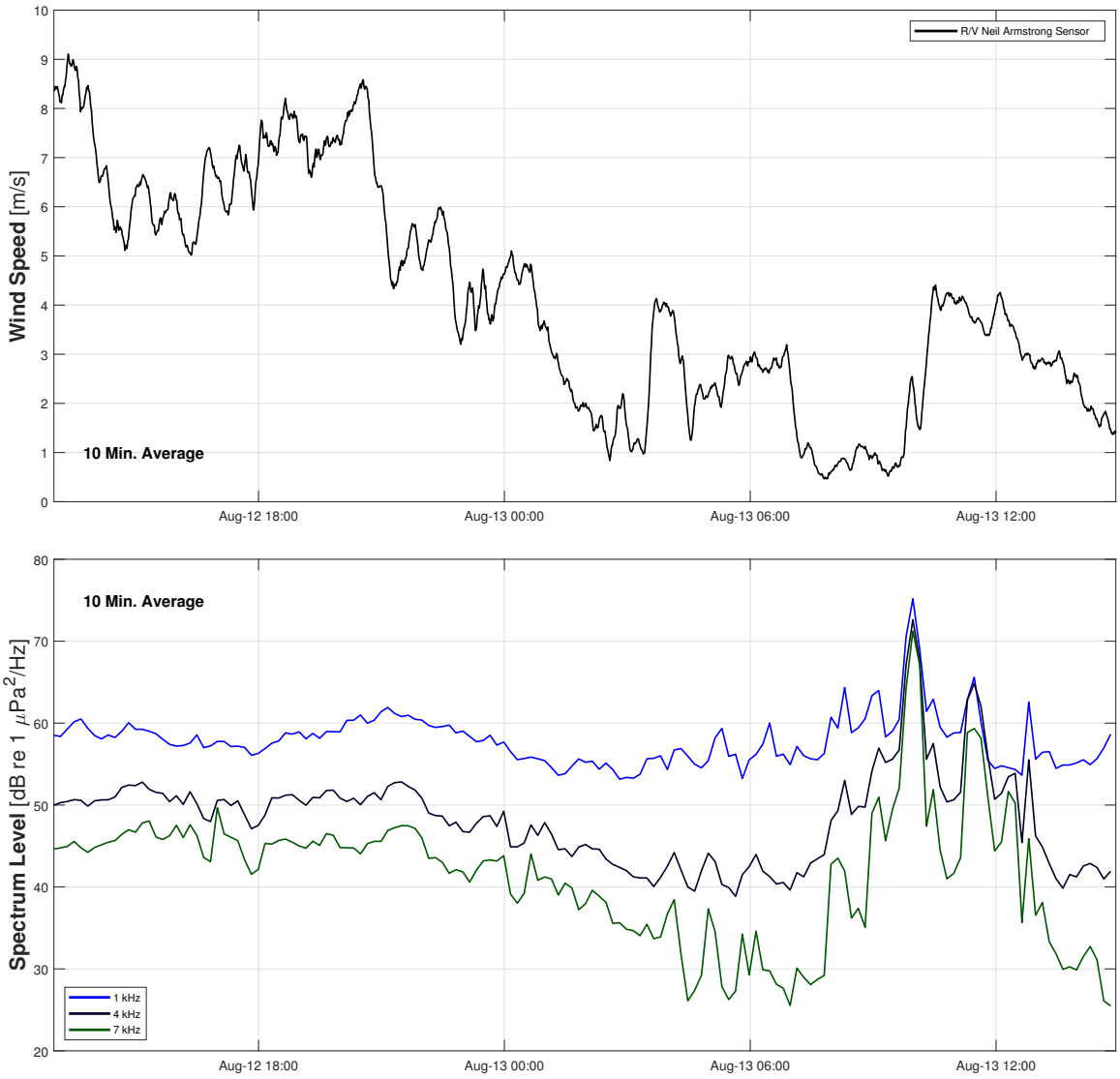

Figure 4.12. Wind Speed [m/s] from sensors located onboard the R/V Neil Armstrong and Spectrum Level [dB re 1 μPa^2/Hz] from 12AUG18 to 13AUG18. A 10 minute sliding average is used on both the wind data and the frequency data.

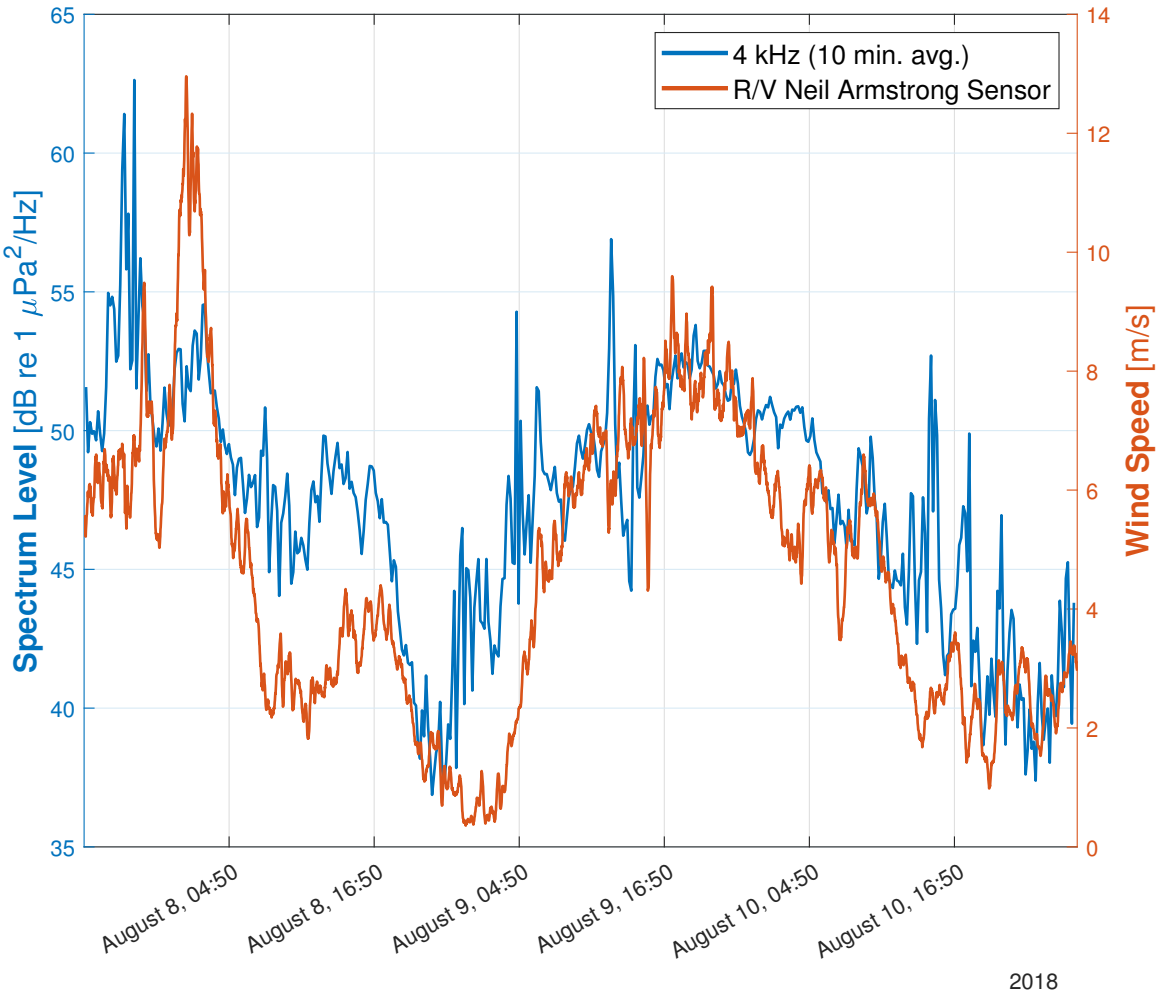

Figure 4.13. Spectrum Level [dB re 1 μPa^2/Hz] of 4 kHz (left) and wind speed (right) from 8AUG18 to 11AUG18. A 10 minute sliding average is used on both the wind data and the frequency data.The wind had a strong effect on the spectrum level of the ambient noise at 4 kHz.

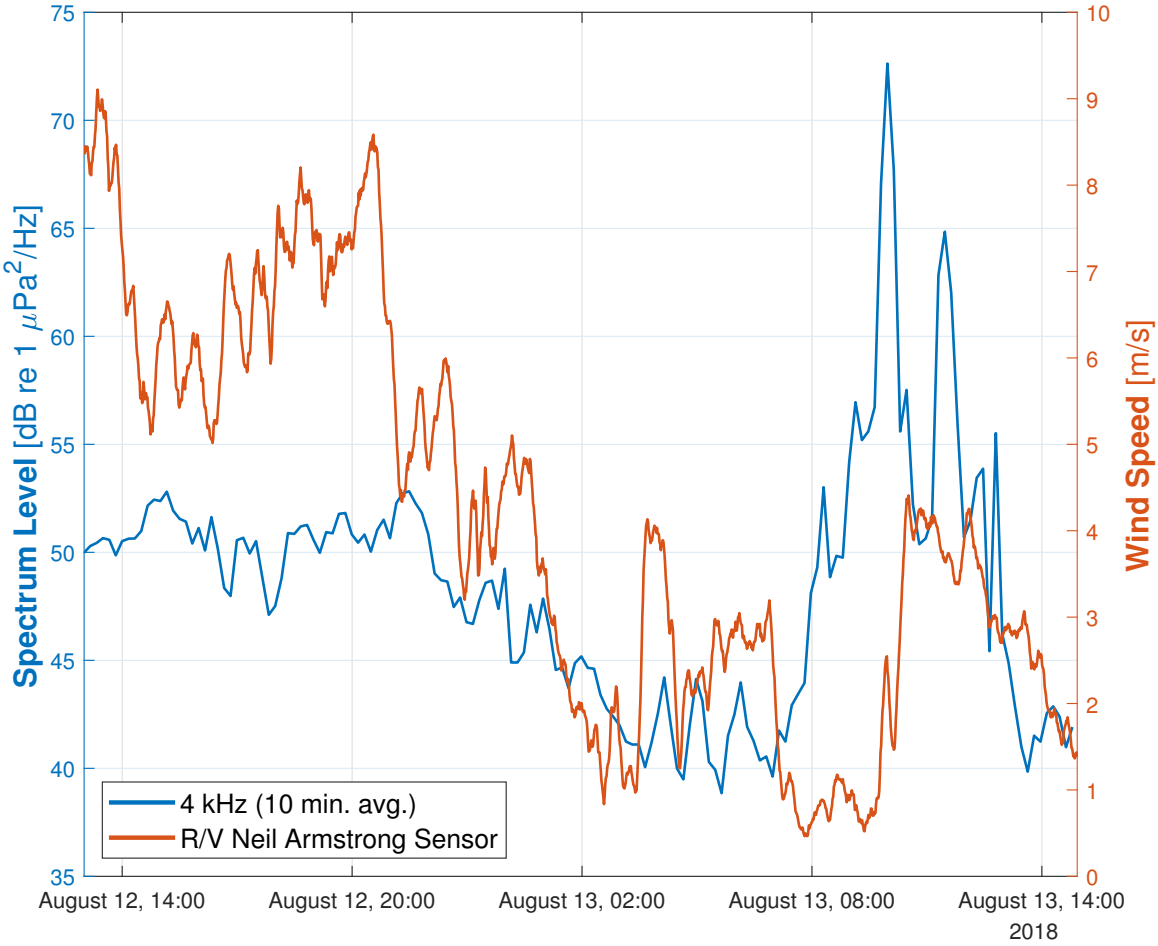

Figure 4.14. Spectrum Level [dB re 1 μPa^2/Hz] of 4 kHz (left) and wind speed (right) from 12AUG18 to 13AUG18. A 10 minute sliding average is used on both the wind data and the frequency data. The wind had a strong effect on the spectrum level of the ambient noise at 4 kHz.

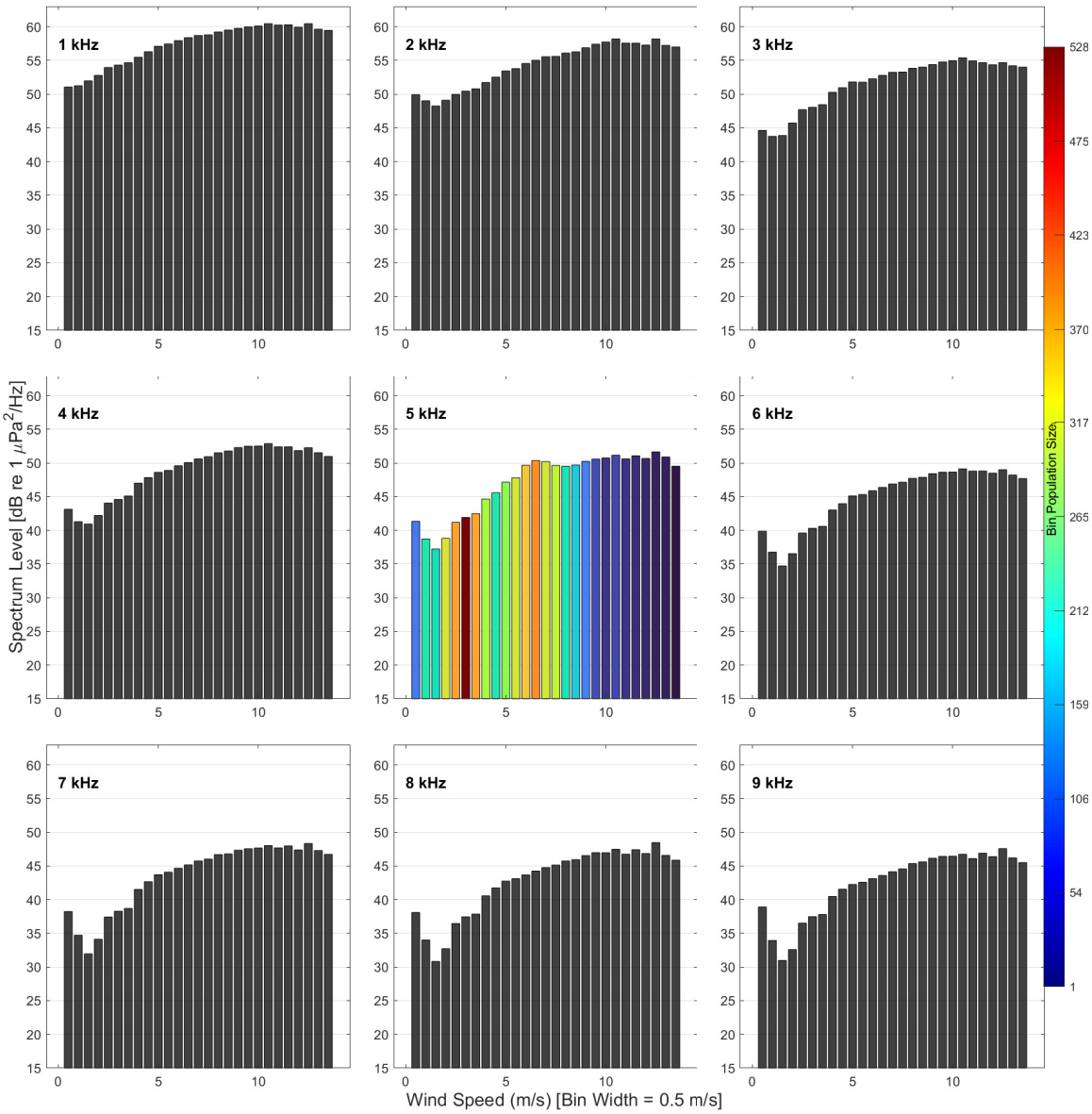

Figure 4.15. Histogram plot of spectrum level [dB re 1 μPa^2/Hz] compared to wind speed [m/s] for 1–9 kHz frequencies. A 1 minute sliding average is used with a bin width of 0.5 m/s. The color bar on the right side represents the bin population size (1 minute data points) and is shown in the subplot for 5 kHz since the population sizes are the same across all frequencies.

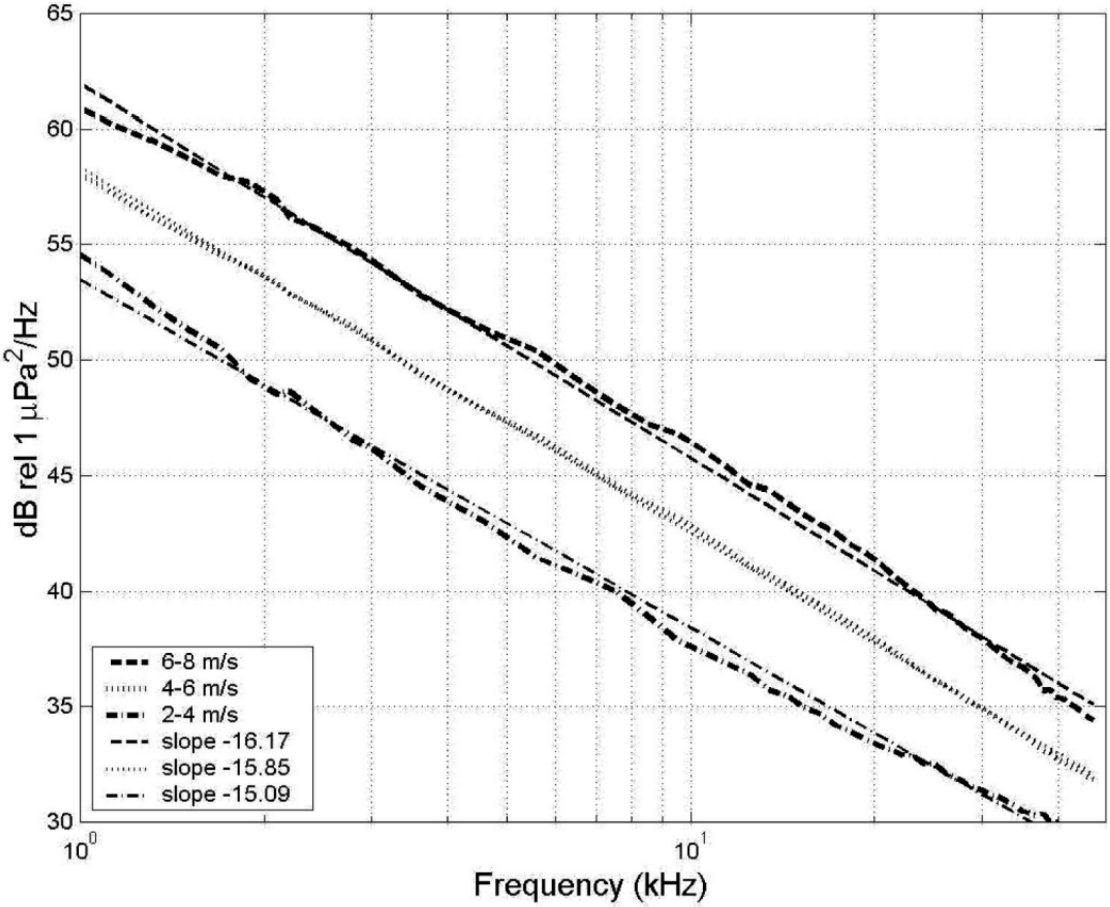

Figure 4.16. "The wind-only spectra and linear regressions for the wind speeds of 2–4, 4–6, and 6–8 m/s. This uniform slope –15.7 dB/decade is valid for the frequency band 1–50 kHz and wind speeds 2–14 m/s." Source: [29]

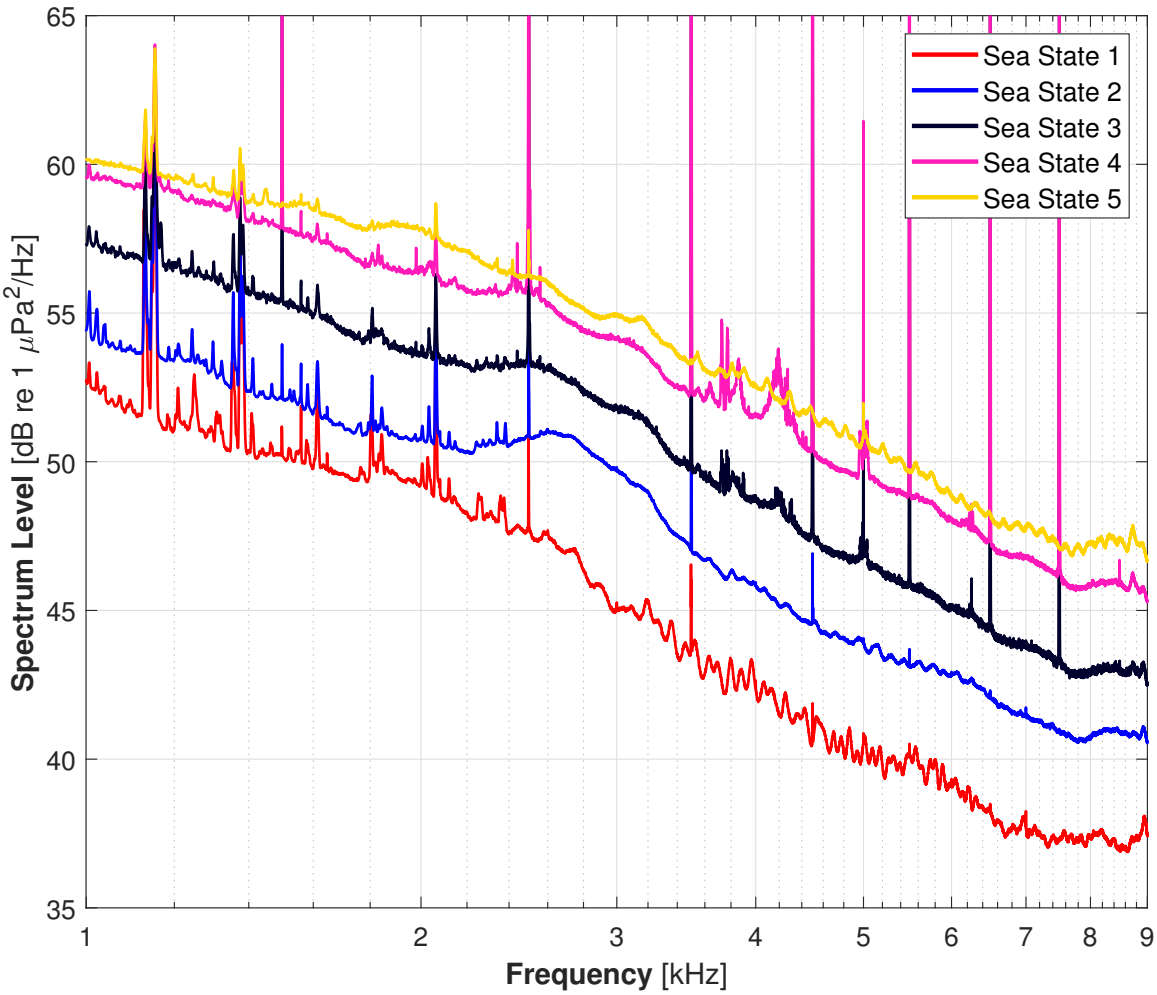

Figure 4.17. Spectrum level [dB re 1 μPa^2/Hz] versus frequency [kHz] for sea states 1–5. Sea states are derived from the wind speed using the Beaufort Scale (see Table 1.1). A one minute incoherent average of spectrum level is used. The distinct tonals in spectrum level are attributed to active source testing (see Table 4.1). These data came from deployment 1.

4.4 Data-Wind Model Comparison

The results in Sections 4.1, 4.2 and 4.3 are compared to an ambient noise model developed at the Applied Physics Lab at the University of Washington (APL-UW) [24]. The calculations and methodology for the model are detailed in Section 2.5.

Figures 4.18, 4.19 and 4.20 compare the model to the analyzed data for frequencies in the 1–9 kHz band. The result and figures for the second deployment (August 12-13) are located in Appendix A. A 10 minute sliding average is applied to both the acoustic and wind speed data. The wind based APL-UW model tracks predicted data spectrum levels reasonably well with a slight offset.

The only time period in which the model predicted spectrum level below recorded data spectrum value was around 0000Z on August 9th. The reason for this deviation is the dramatic drop in wind speed below 2 m/s (thus causing the model to drop predicted spectrum level significantly). This demonstrates model limitations because wind speed is only a proxy to ambient noise level. The cause for ambient noise levels due to wind is the energy imparted by the wind onto the waves causing breaking waves thus contributing to noise. When the wind slows down abruptly over a short time-span, the ambient noise level change will be delayed because the sea state is not affected instantaneously.

APL-UW recognized the model over/under predictions based on sea state [24]. For sea state 0, they found the model under predicted ambient noise compared to the Wenz curves based by about 5 dB. For sea states greater than 2, the model over predicts ambient noise PSD. Figure 4.22 from [24] shows the model prediction versus sea state. Figure 4.21 shows the misfit [dB] between the predicted model spectrum level and the recorded data spectrum level for 1–9 kHz as a function of sea state. The offset for the data in this thesis exhibits the same pattern in the findings made by [24] in Figure 4.22. Figure 4.21 is created using a 10 minute average on wind and acoustic data. The sea state bins are created based on the correlating wind speed on the Beaufort Scale in Table 1.1. PSD data is then sorted into each sea state bin based on the wind speed at the time. The numbers above the individual bars represent the population size (number of 10 minute bins) in each sea state. The populations of PSD data for the model prediction and the recorded data is then averaged. The misfit [dB] is the difference between the model and the data.

Figure 4.23 shows the misfit [dB] between the predicted model spectrum level and the data spectrum level at 4 kHz as a function of wind speed. Figure 4.23 is creating using the same technique described to create Figure 4.21. However, instead of sea state bins, a bin width of 0.1 m/s is used. Additionally, due to the higher number of bins, population size is instead denoted by a color bar at the top vice a number above the bar. Finally, a 1 minute sliding

average is used on the wind speed and the PSD data instead of a 10 minute average. Figures 4.21 and 4.23 show the same trends, yet Figure 4.23 offers more granularity. Due to the low population size, results at low and high wind speeds are not necessarily representative of the misfit. The best fit of the model to the data appears to be between sea states 1–2 and wind speeds between 1–3 m/s.

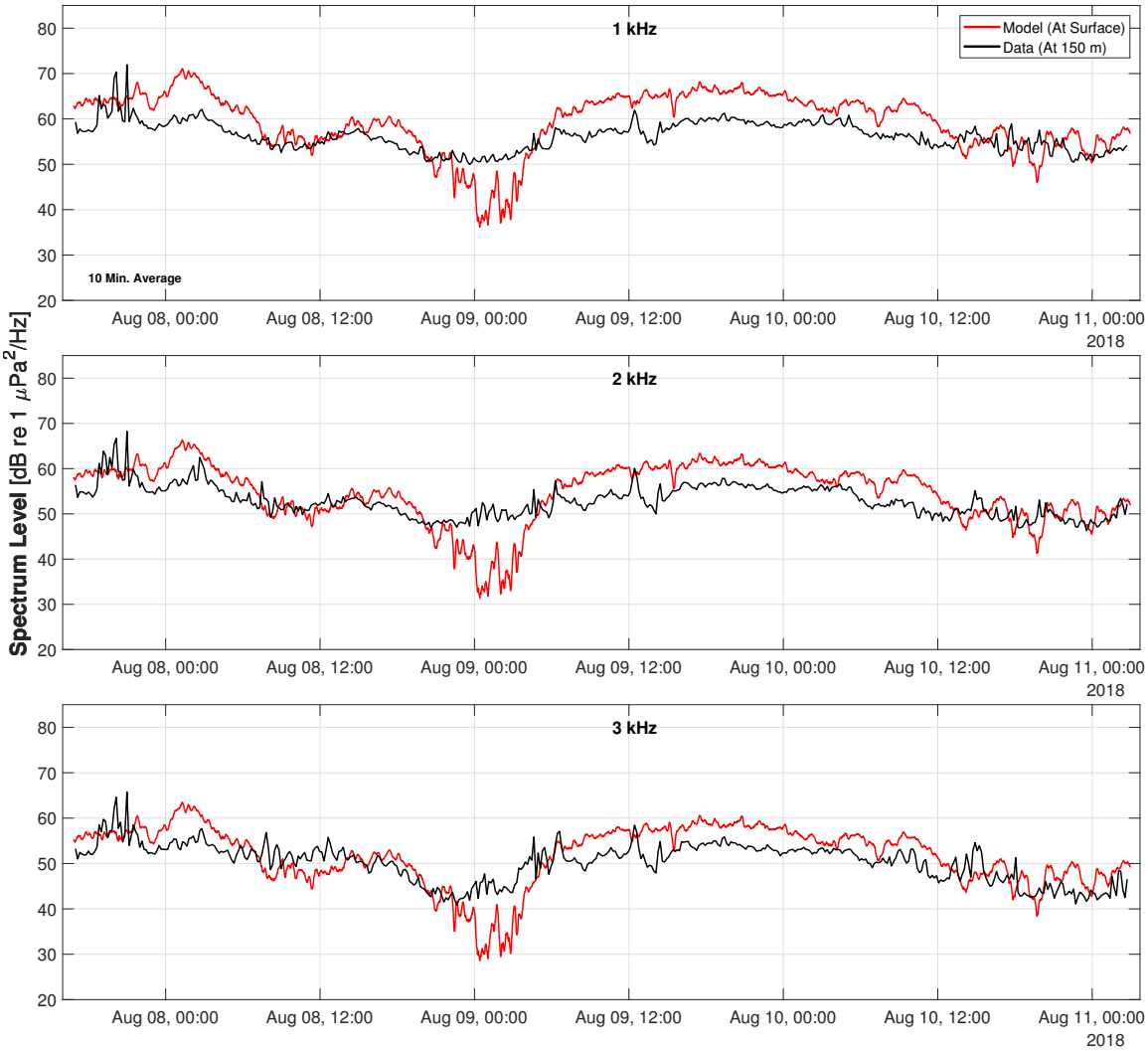

Figure 4.18. Spectrum Level [dB re 1 μPa^2/Hz] for both the APL-UW model and data for frequencies 1, 2 and 3 kHz. Both data were collected from 07AUG at 1650Z to 11AUG 0240Z using a 10 minute sliding average.

4.5 Conclusion

The objective of this thesis was to characterize mid-frequency ambient noise in the Norwegian Sea. The mid-frequency ambient noise in this important geographic region is highly wind dependent. Higher frequencies correlate with wind speed more than lower frequencies. The spectrum levels for the frequencies analyzed agree with prior results found elsewhere in the world and range from the high 50's dB re 1 μPa^2/Hz for 1 kHz down to the low 40's dB re 1 μPa^2/Hz for 9 kHz with a strong correlation to the prevailing wind speed. Figures 4.13 and Figures 4.14 show a time shift between the spectrum level and the wind speed. This is most likely due to the distance between the R/V Neil Armstrong (wind sensor) and the array. If one was shifted in time, the spectrum level and wind speed would most likely produce an even higher correlation. Spectrum levels for sea states 1–5 across 1–9 kHz are shown in Figure 4.17. The results show that ambient noise spectrum level can increase by as much as 12 dB re 1 μPa^2/Hz depending on sea state and frequency which is consistent with other studies. The APL-UW model tracks relatively well with the data presented with a slight offset. Based on historic model performance, the offset gives insight into the prevailing sea state. Future research is needed to characterize the directionality of ambient noise in this region as well as further exploring individual noise sources beyond wind, such as biologic sources.

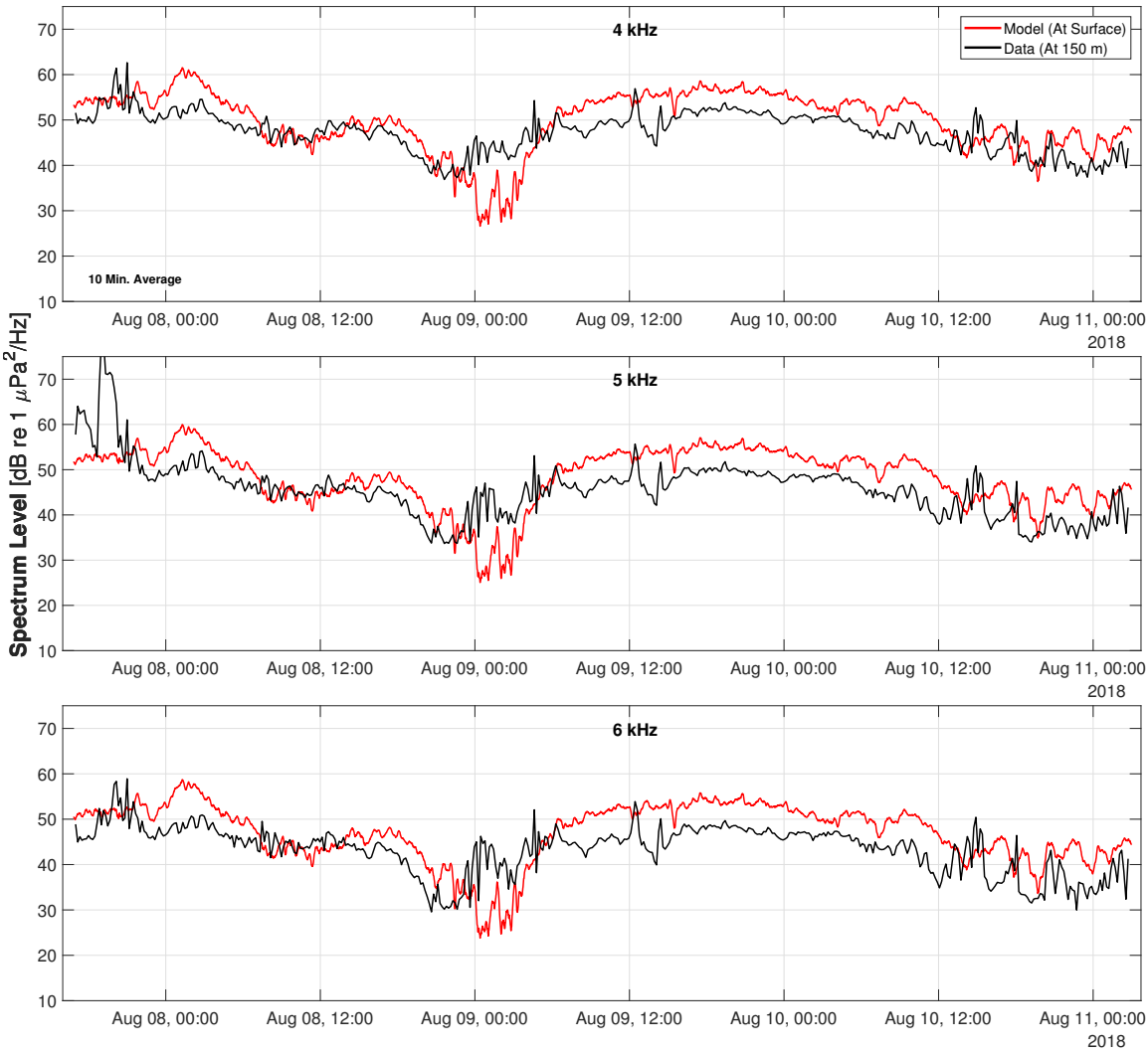

Figure 4.19. Spectrum Level [dB re 1 μPa^2/Hz] for both the APL-UW model and data for frequencies 4, 5 and 6 kHz. Both data were collected from 07AUG at 1650Z to 11AUG 0240Z using a 10 minute sliding average.

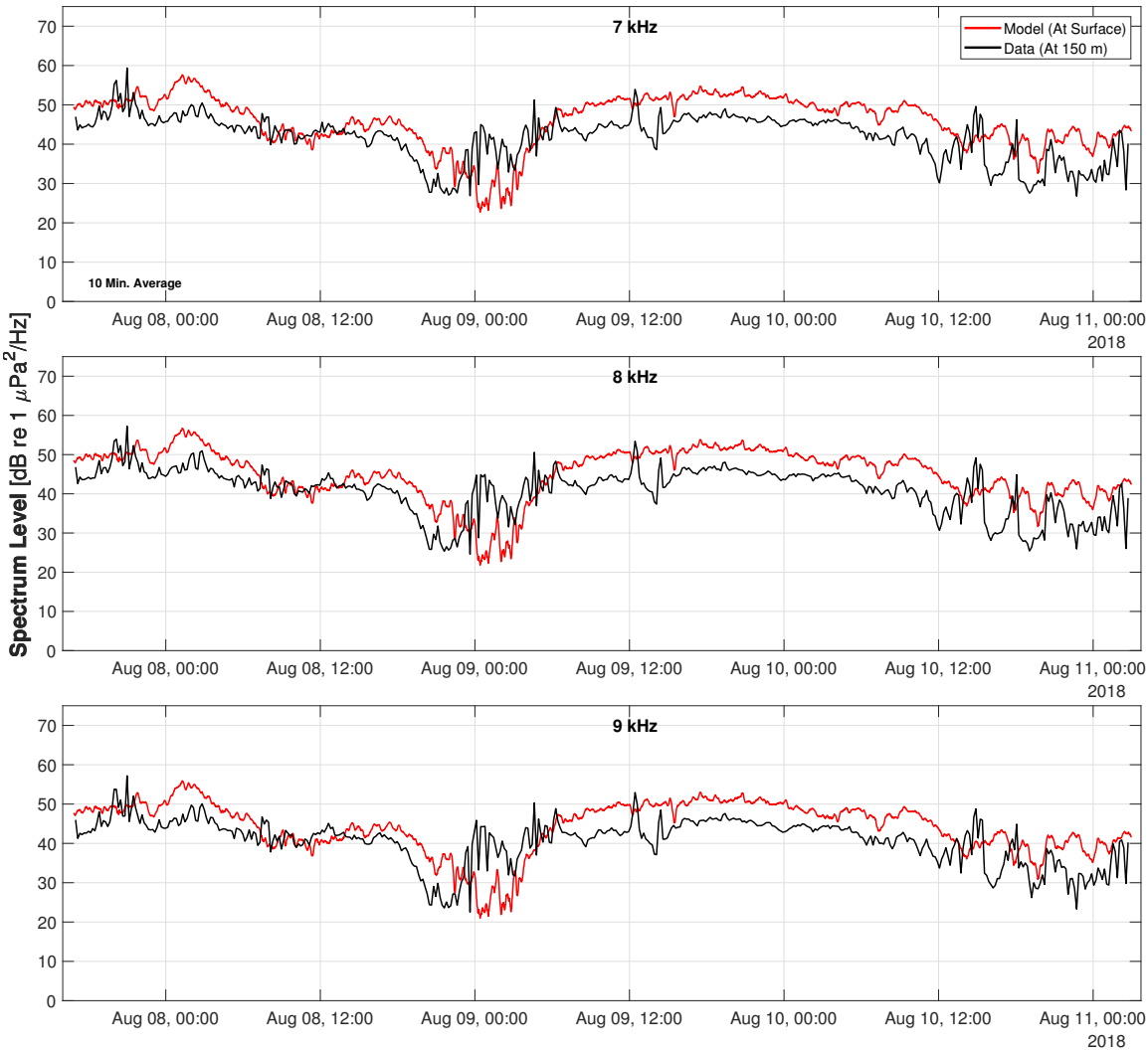

Figure 4.20. Spectrum Level [dB re 1 μPa^2/Hz] for both the APL-UW model and data for frequencies 7, 8 and 9 kHz. Both data were collected from 07AUG at 1650Z to 11AUG 0240Z using a 10 minute sliding average.

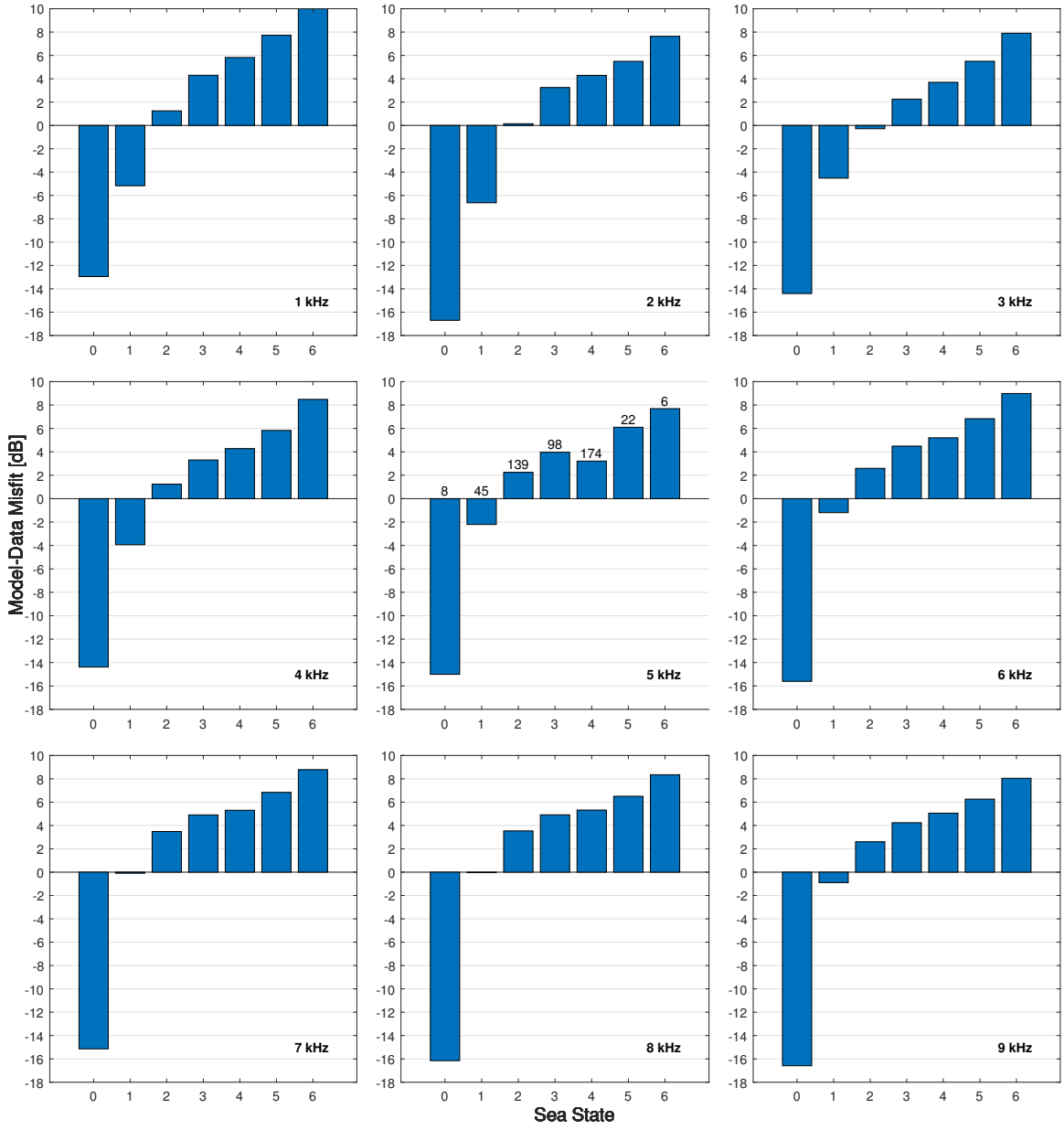

Figure 4.21. Misfit between the APL-UW model and recorded data [dB] for 1–9 kHz based on the sea state. The numbers above each sea state on the 5 kHz subplot indicate the population size (i.e. 10 minute bins) contributing to the average. Sea state is based on the Beaufort scale chosen from the corresponding wind speed Table 1.1. 10 minute average is used on the wind speed and the PSD data.

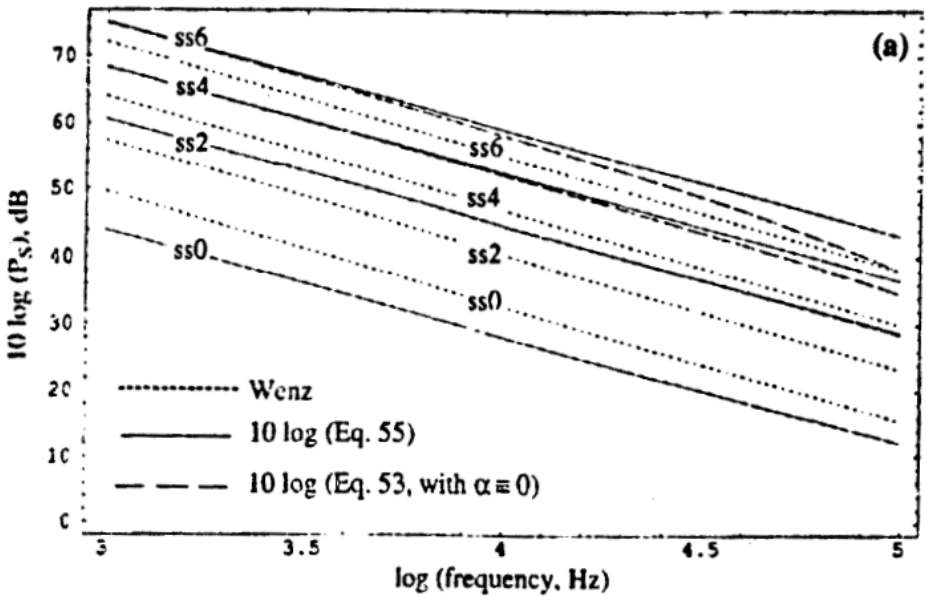

Figure 4.22. APL-UW model (Labeled as Eq. 55 solid line) PSD and Wenz curves compared against frequency. Source: [24].

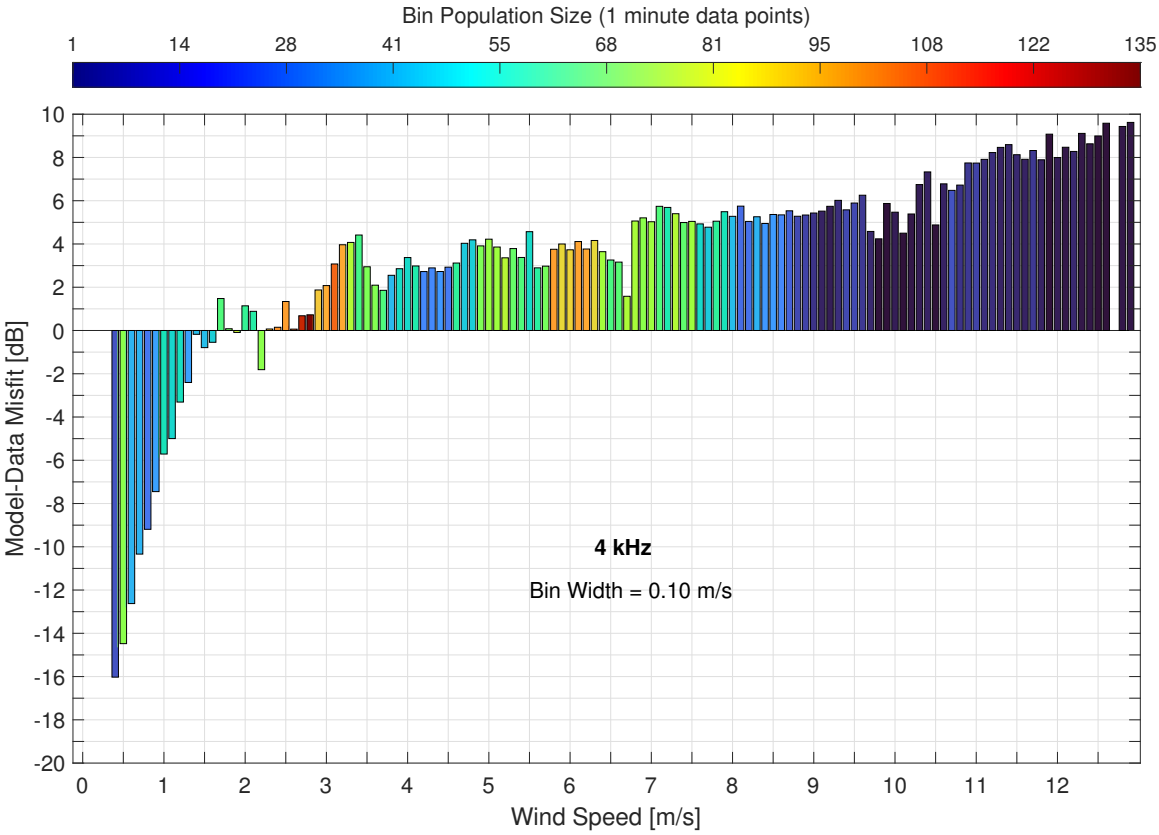

Figure 4.23. As Figure 4.21 but with 1 minute sliding average and bin width of 0.1 m/s wind speed.

APPENDIX A:
Supplemental Figures

This appendix contains supplemental figures not contained in the body. Section A.1 and Section A.2 contains figures with additional sliding time averages of 1, 2, 5, 15, 30 and 60 minutes. The figures are separated by frequency and time (first or second deployment). 10 minute sliding time average results are in Chapter 4. Section A.3 contains additional model-data comparisons for the second deployment. Additionally, Section A.3 contains additional frequencies for Figure 4.23.

A.1 Supplemental Narrowband Figures

A.1.1 Additional time averages for frequencies 1, 2, and 3 kHz for the first deployment.

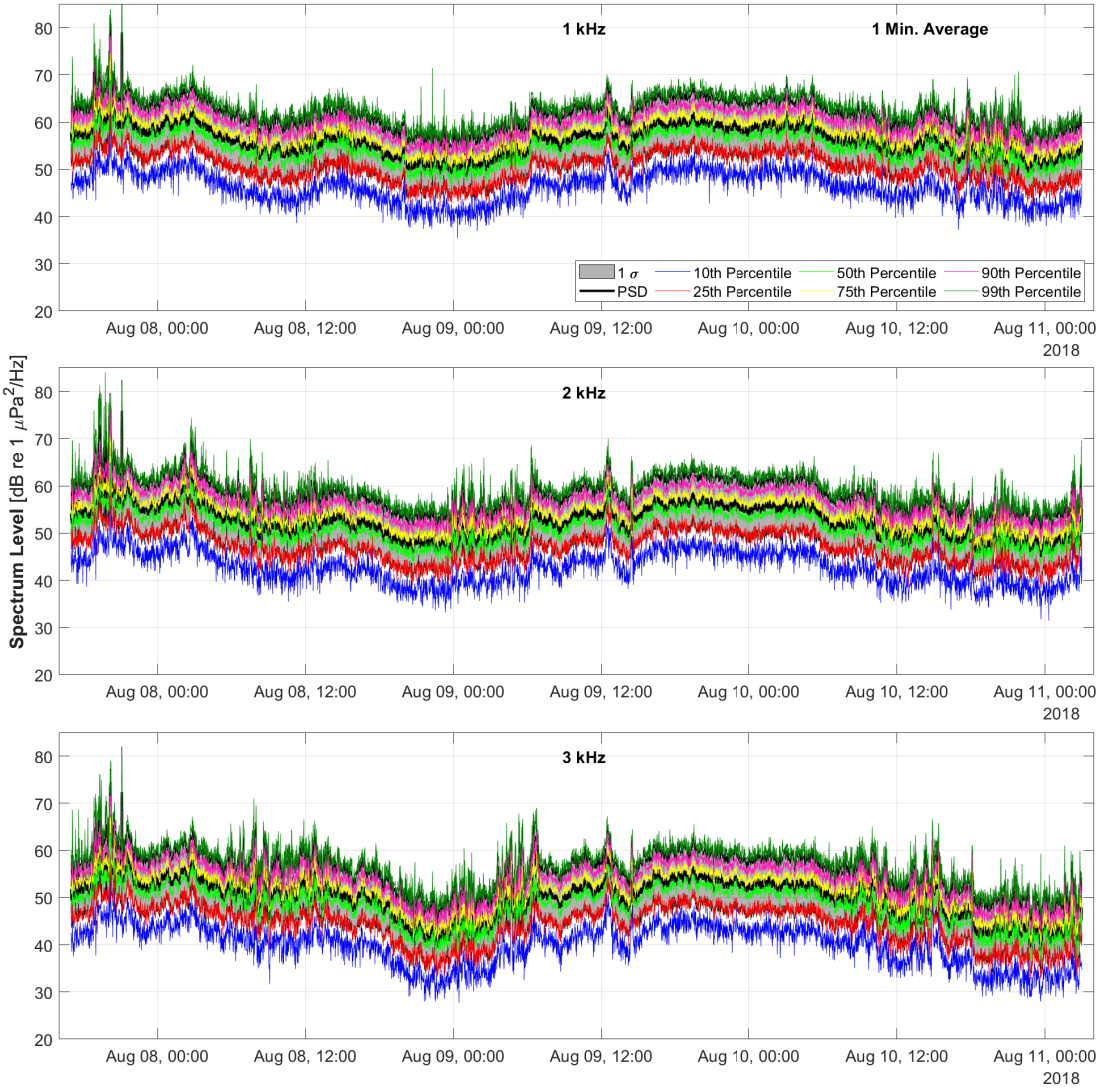

Figure A.1. Spectrum Level [dB re 1 μPa^2/Hz] of frequencies 1, 2, and 3 kHz from 8AUG18 to 11AUG18 using a 1 minute sliding average. The statistics are described in Section 2.4.

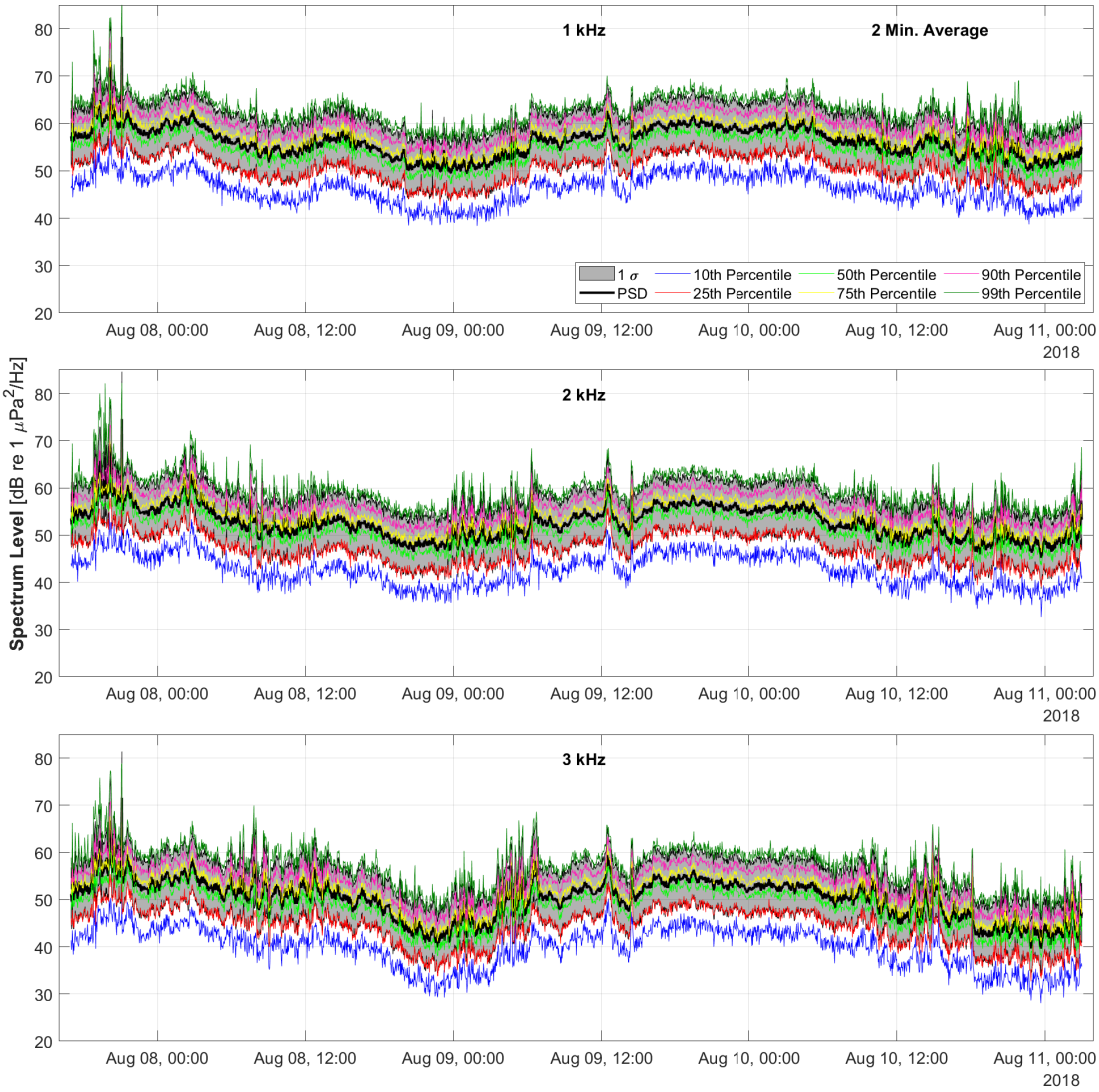

Figure A.2. Spectrum Level [dB re 1 μPa^2/Hz] of frequencies 1, 2, and 3 kHz from 8AUG18 to 11AUG18 using a 2 minute sliding average. The statistics are described in Section 2.4.

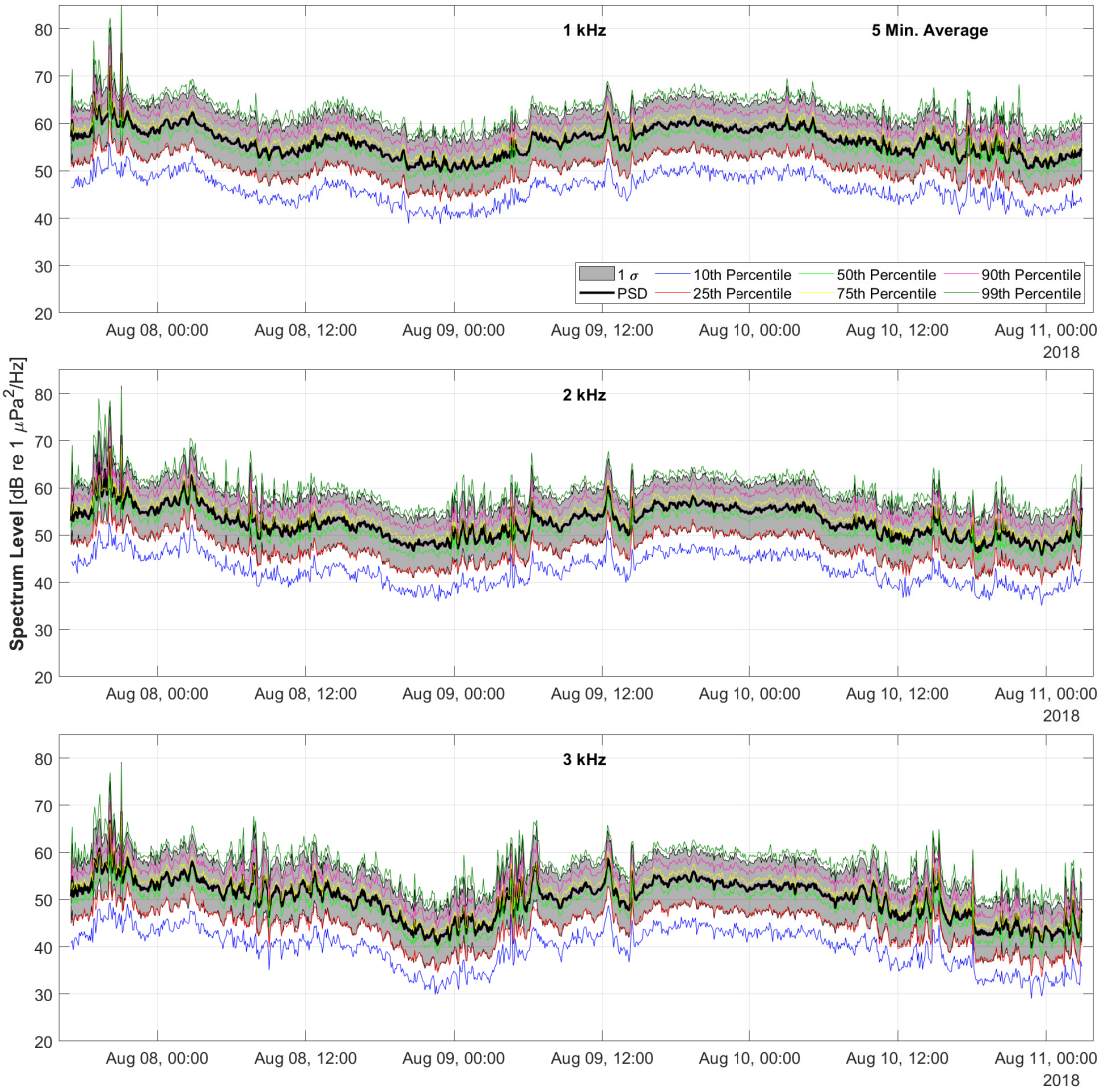

Figure A.3. Spectrum Level [dB re 1 μPa^2/Hz] of frequencies 1, 2, and 3 kHz from 8AUG18 to 11AUG18 using a 5 minute sliding average. The statistics are described in Section 2.4.

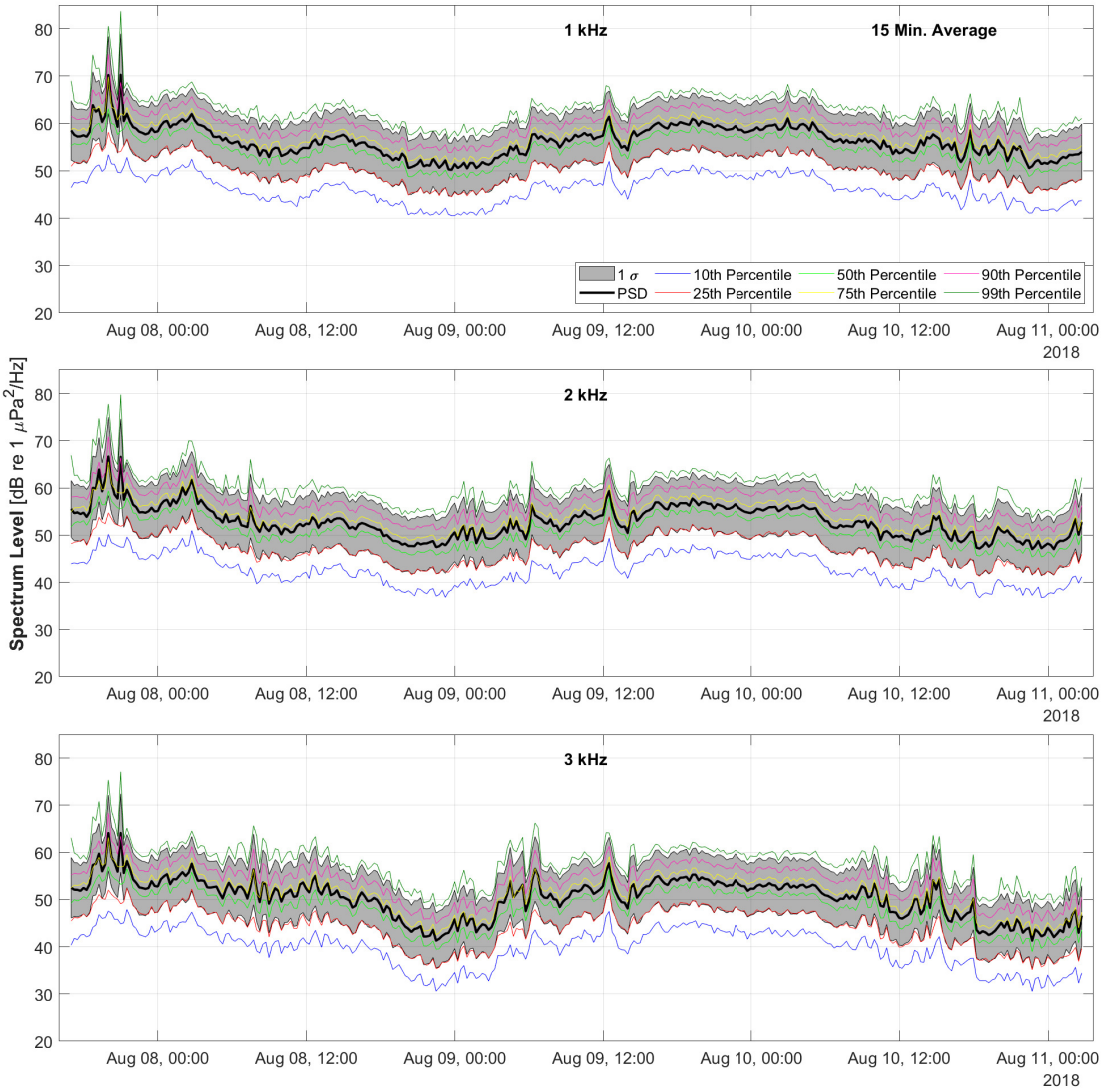

Figure A.4. Spectrum Level [dB re 1 μPa^2/Hz] of frequencies 1, 2, and 3 kHz from 8AUG18 to 11AUG18 using a 15 minute sliding average. The statistics are described in Section 2.4.

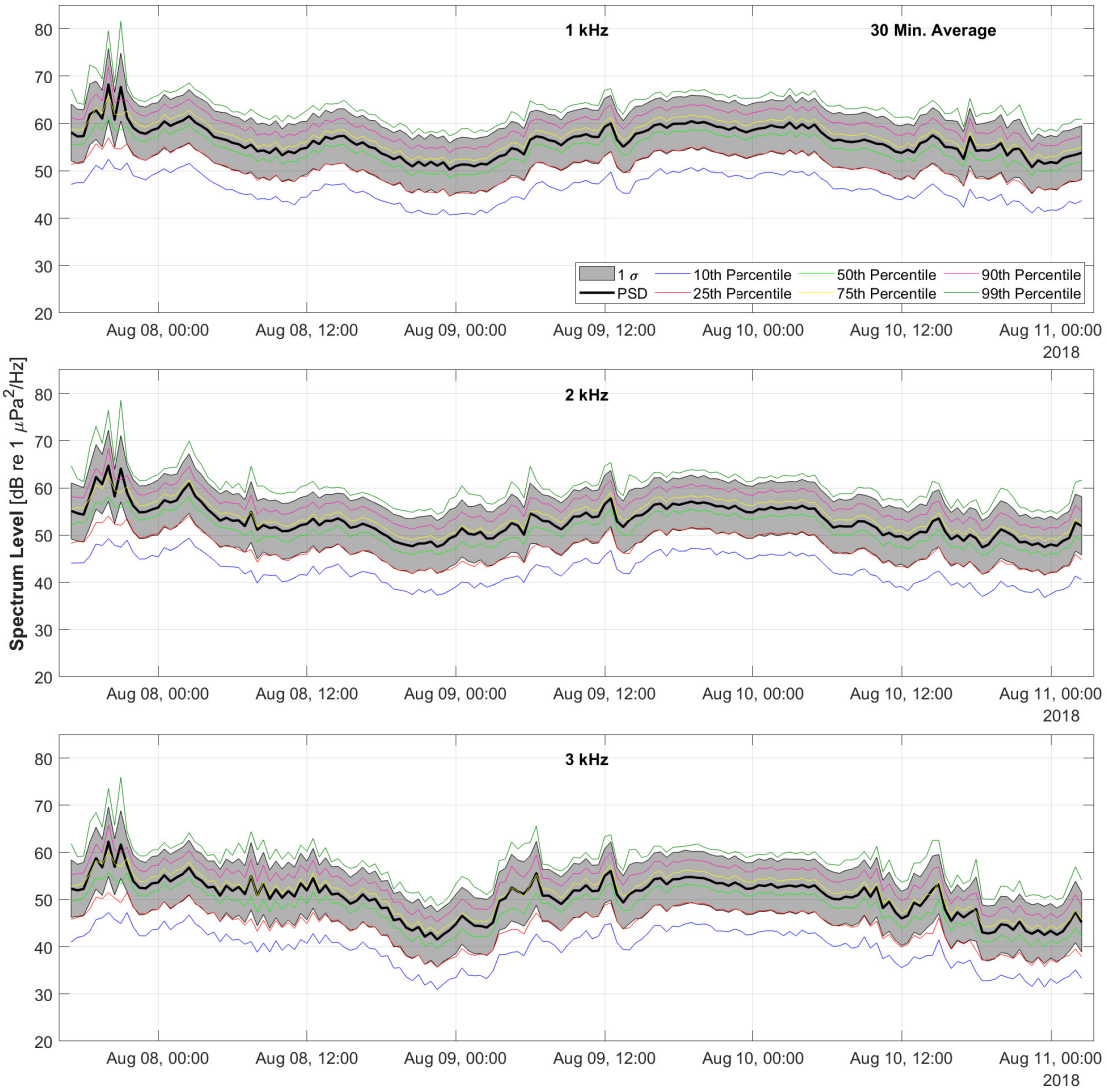

Figure A.5. Spectrum Level [dB re 1 μPa^2/Hz] of frequencies 1, 2, and 3 kHz from 8AUG18 to 11AUG18 using a 30 minute sliding average. The statistics are described in Section 2.4.

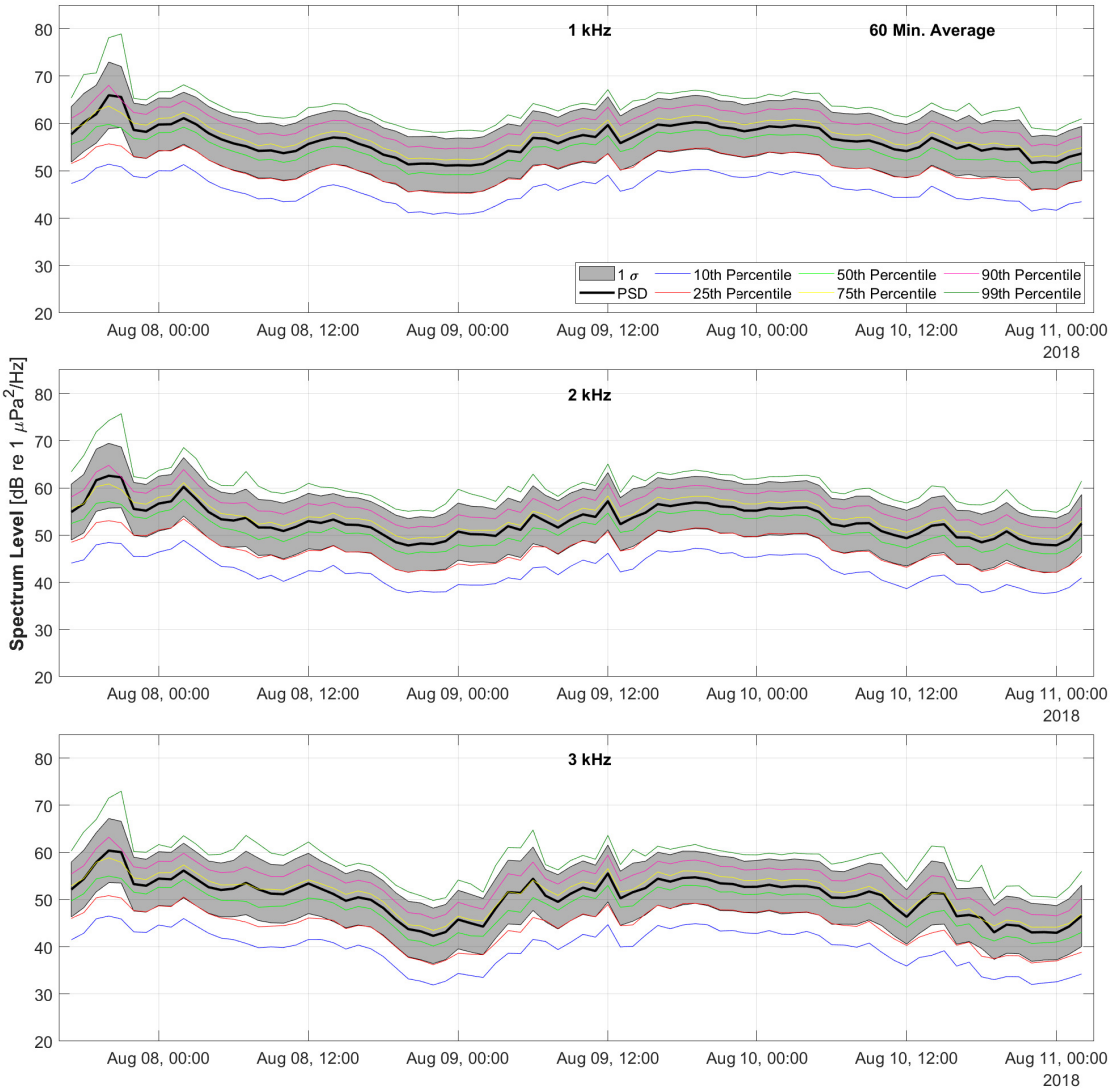

Figure A.6. Spectrum Level [dB re 1 μPa^2/Hz] of frequencies 1, 2, and 3 kHz from 8AUG18 to 11AUG18 using a 60 minute sliding average. The statistics are described in Section 2.4.

A.1.2 Additional time averages for frequencies 1, 2, and 3 kHz for the second deployment.

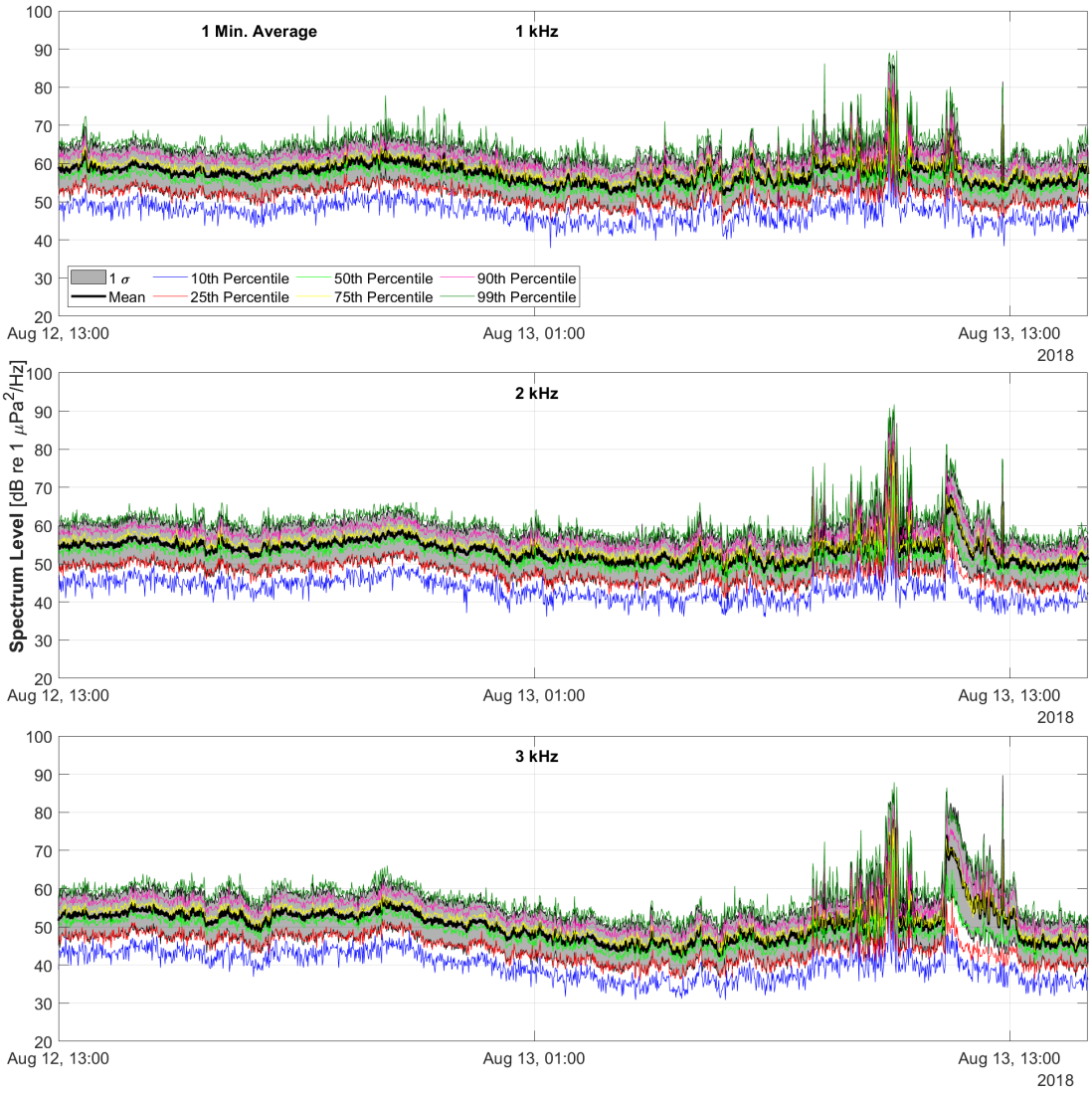

Figure A.7. Spectrum Level [dB re 1 µPa^2/Hz] of frequencies 1, 2, and 3 kHz for the second deployment using a 1 minute sliding average. The statistics are described in Section 2.4. Of note, the spike and rapidly changing PSD around 1000 on 13 AUG is due to various noise testing. See Table 4.1.

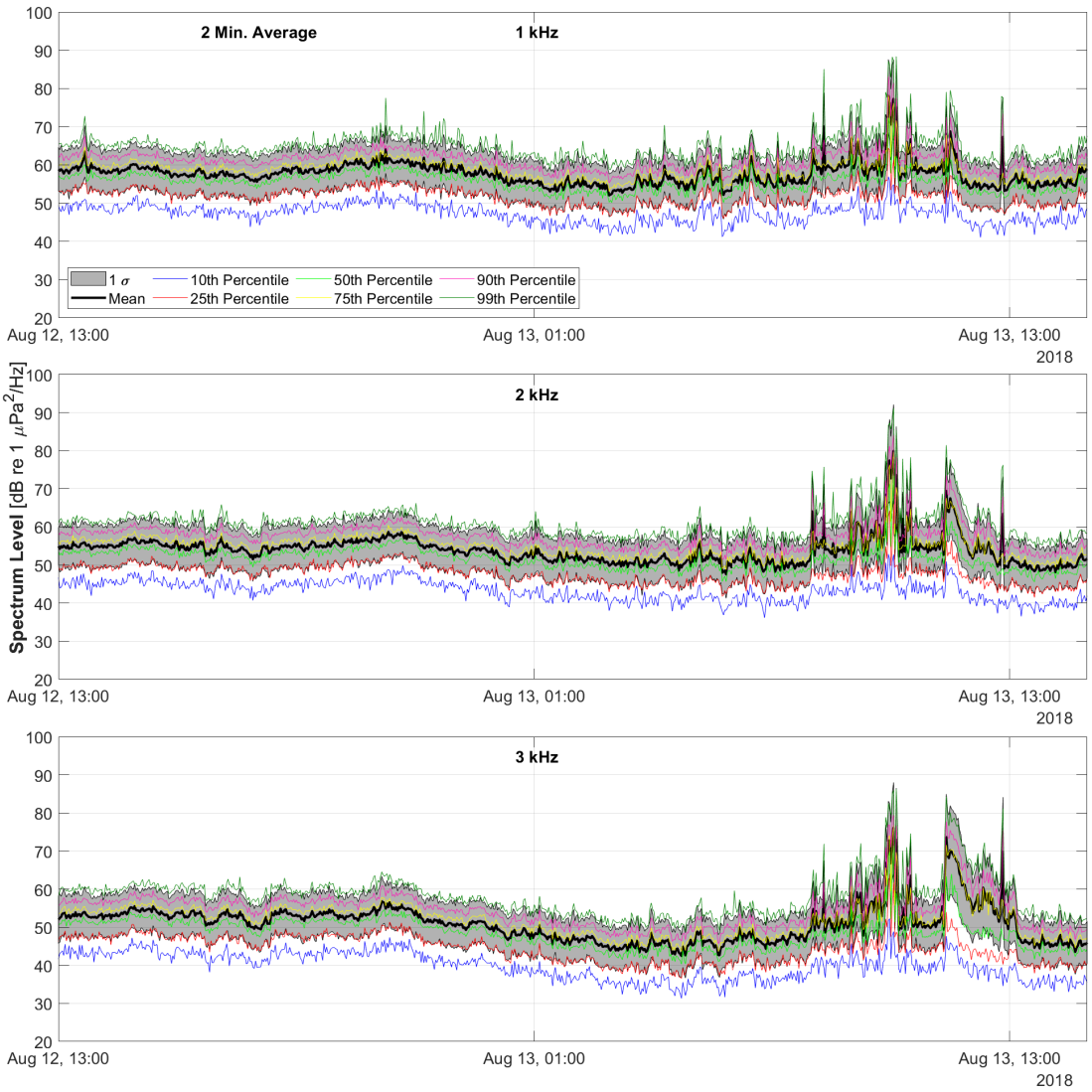

Figure A.8. Spectrum Level [dB re 1 μPa^2/Hz] of frequencies 1, 2, and 3 kHz for the second deployment using a 2 minute sliding average. The statistics are described in Section 2.4. Of note, the spike and rapidly changing PSD around 1000 on 13 AUG is due to various noise testing. See Table 4.1.

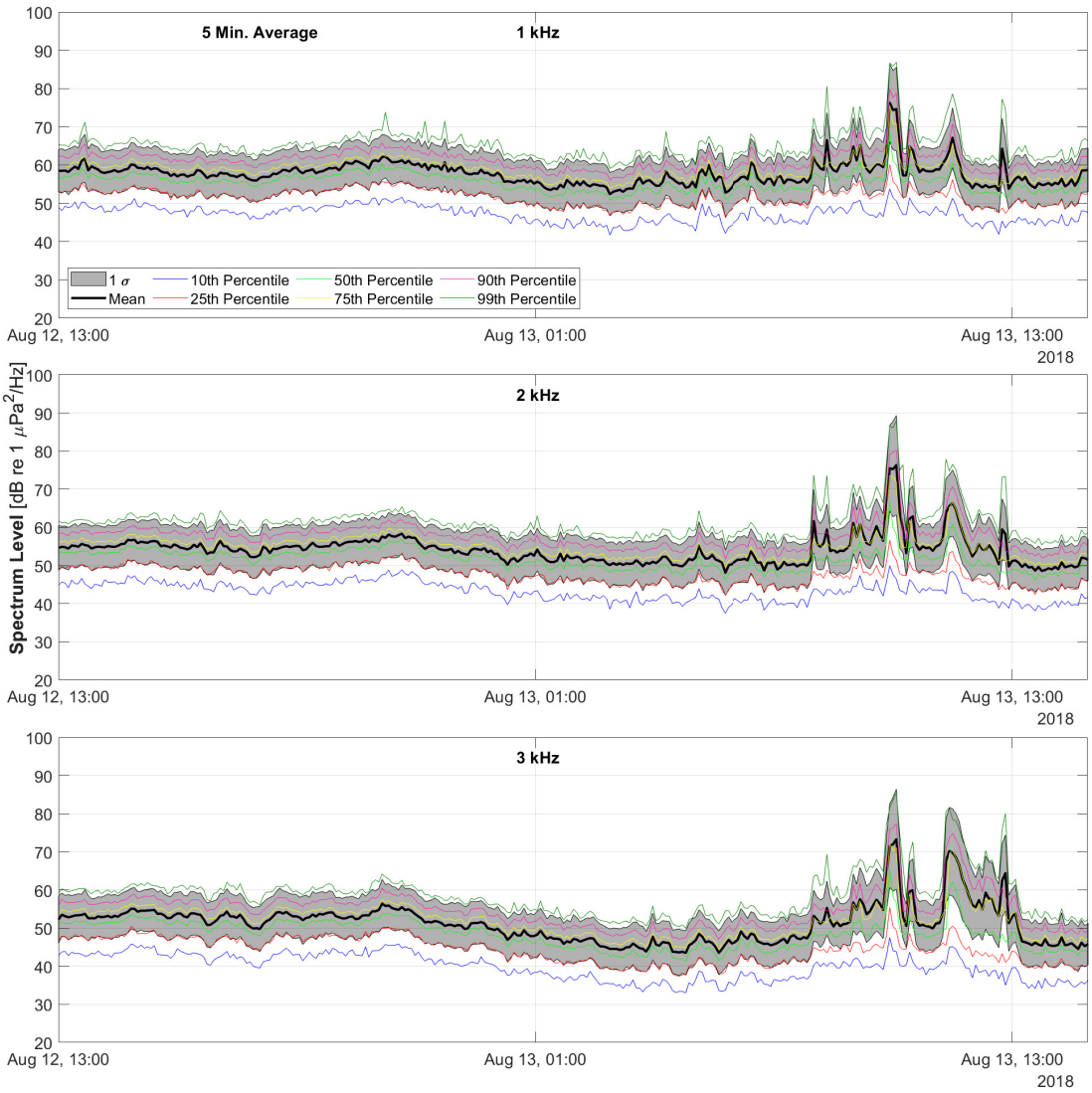

Figure A.9. Spectrum Level [dB re 1 μPa^2/Hz] of frequencies 1, 2, and 3 kHz for the second deployment using a 5 minute sliding average. The statistics are described in Section 2.4. Of note, the spike and rapidly changing PSD around 1000 on 13 AUG is due to various noise testing. See Table 4.1.

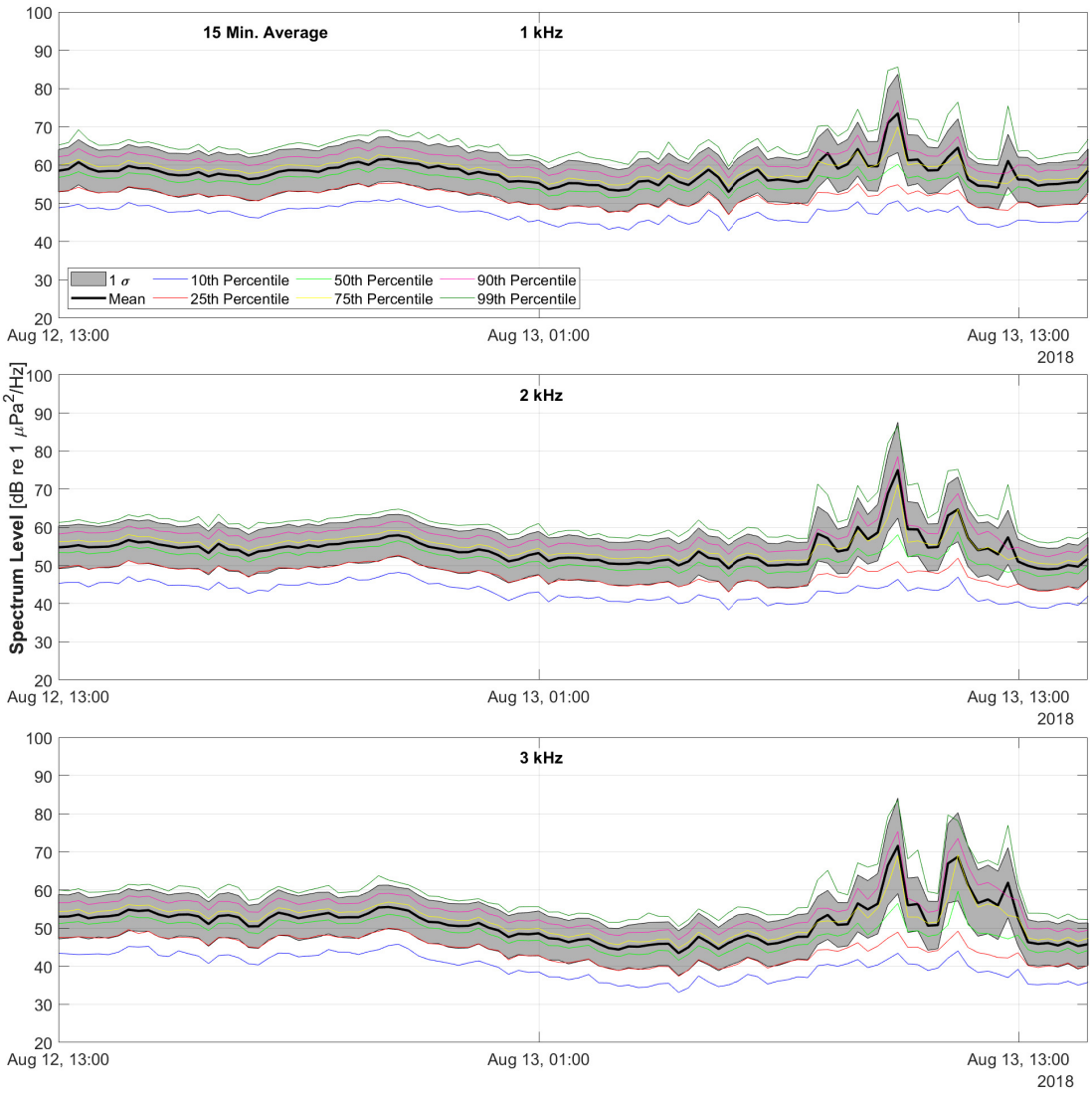

Figure A.10. Spectrum Level [dB re 1 μPa^2/Hz] of frequencies 1, 2, and 3 kHz for the second deployment using a 15 minute sliding average. The statistics are described in Section 2.4. Of note, the spike and rapidly changing PSD around 1000 on 13 AUG is due to various noise testing. See Table 4.1.

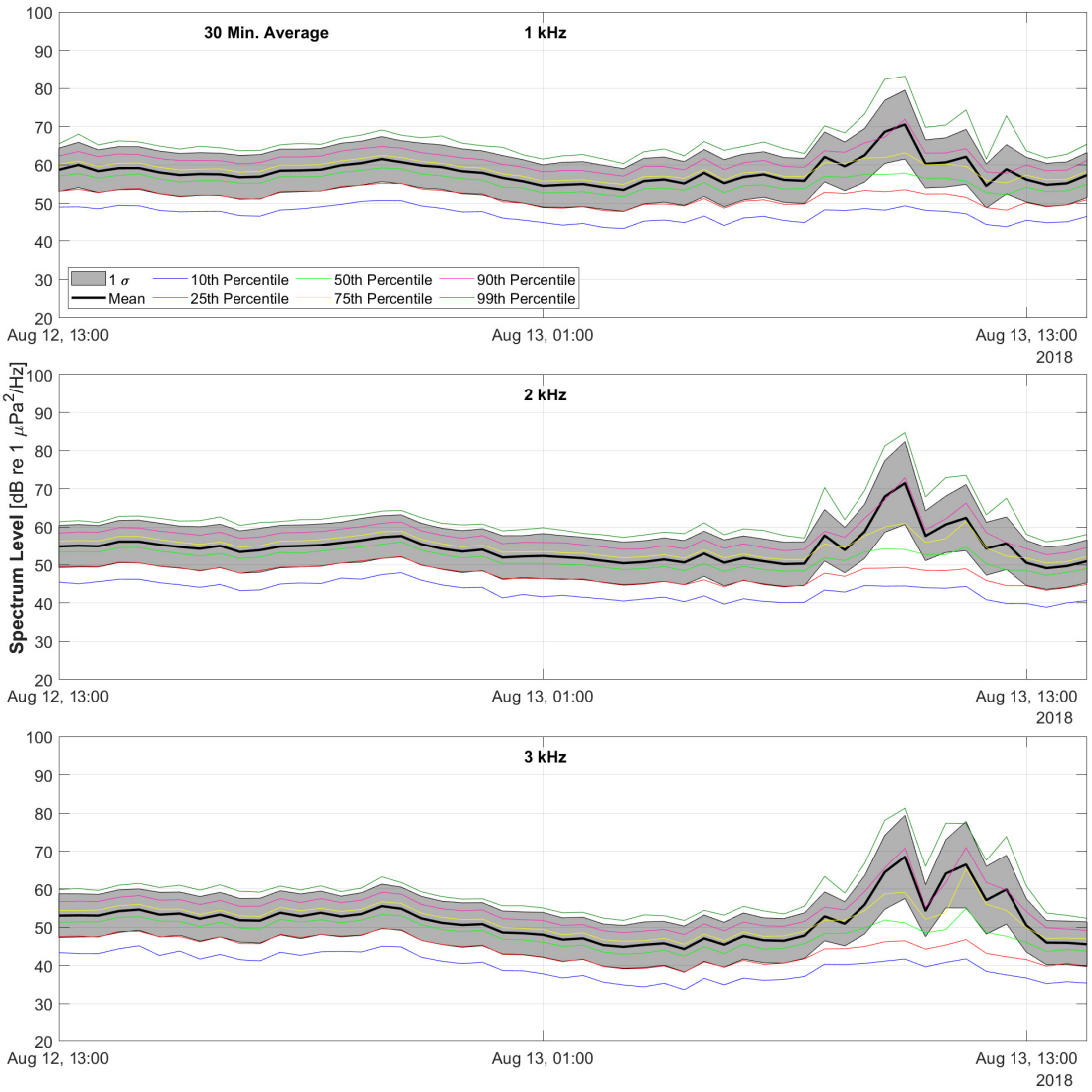

Figure A.11. Spectrum Level [dB re 1 μPa^2/Hz] of frequencies 1, 2, and 3 kHz for the second deployment using a 30 minute sliding average. The statistics are described in Section 2.4. Of note, the spike and rapidly changing PSD around 1000 on 13 AUG is due to various noise testing. See Table 4.1.

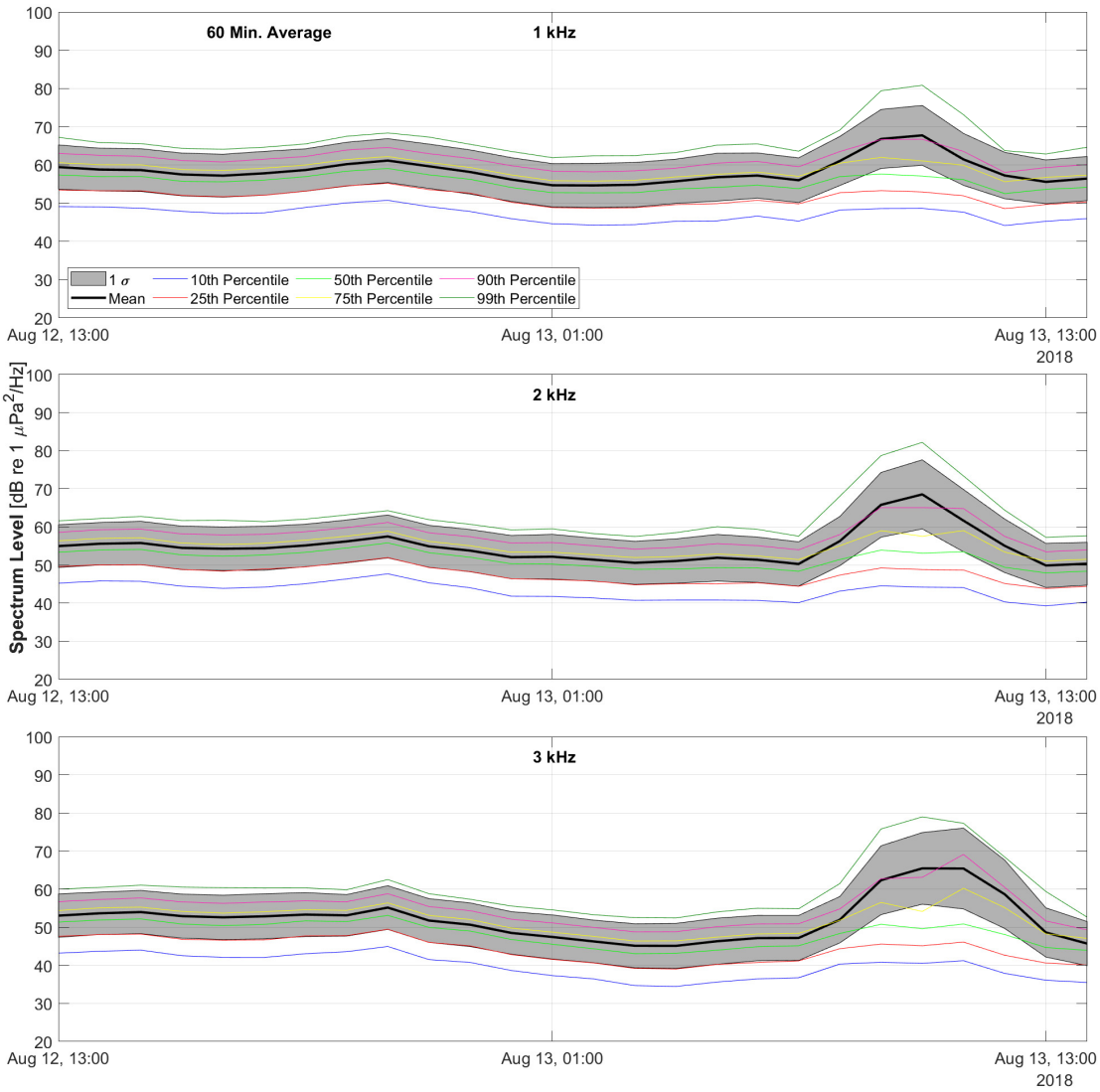

Figure A.12. Spectrum Level [dB re 1 μPa^2/Hz] of frequencies 1, 2, and 3 kHz for the second deployment using a 60 minute sliding average. The statistics are described in Section 2.4. Of note, the spike and rapidly changing PSD around 1000 on 13 AUG is due to various noise testing. See Table 4.1.

A.1.3 Additional time averages for frequencies 4, 5, and 6 kHz for the first deployment.

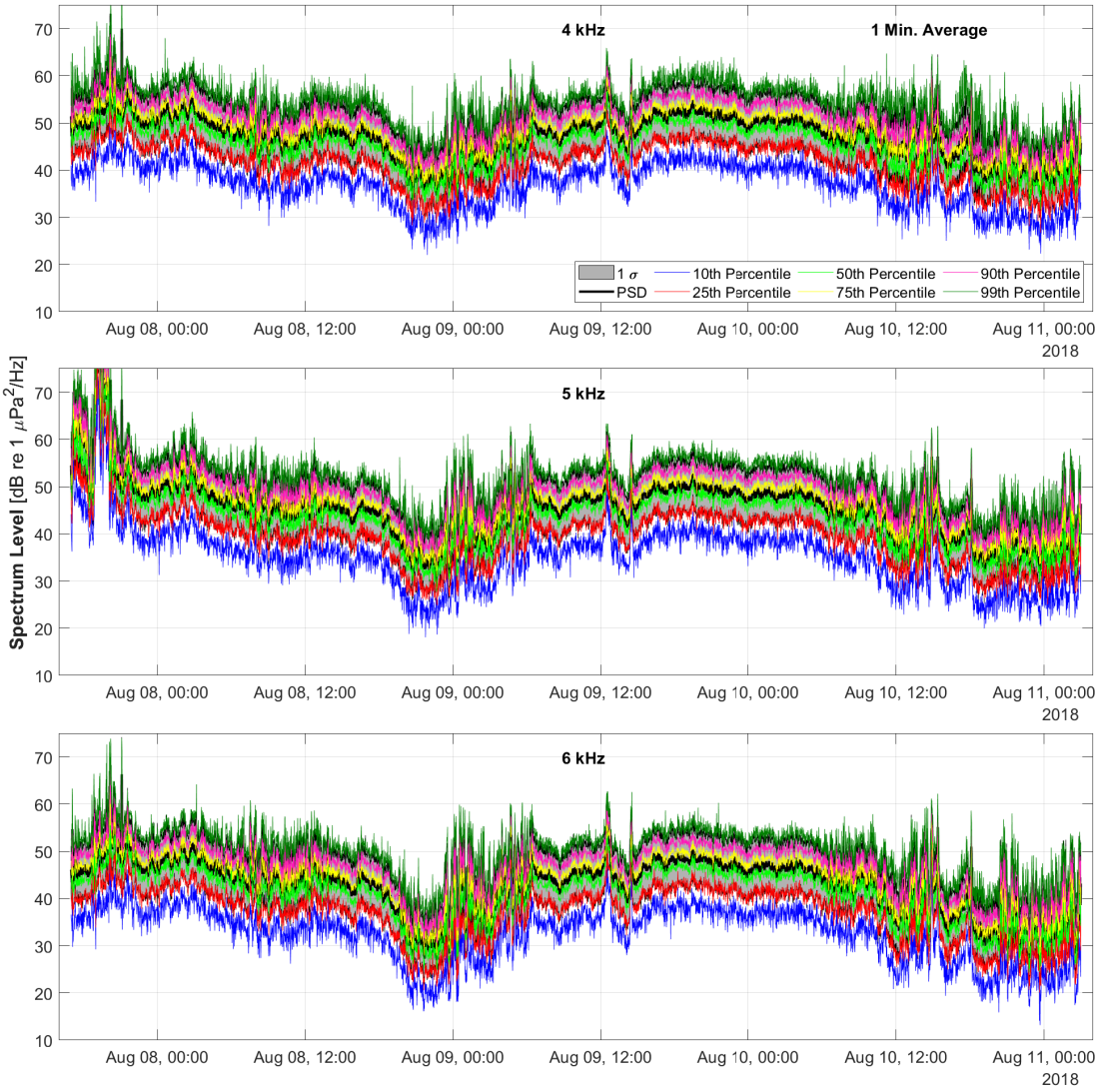

Figure A.13. Spectrum Level [dB re 1 μPa^2/Hz] of frequencies 4, 5, and 6 kHz from 8AUG18 to 11AUG18 using a 1 minute sliding average. The statistics are described in Section 2.4.

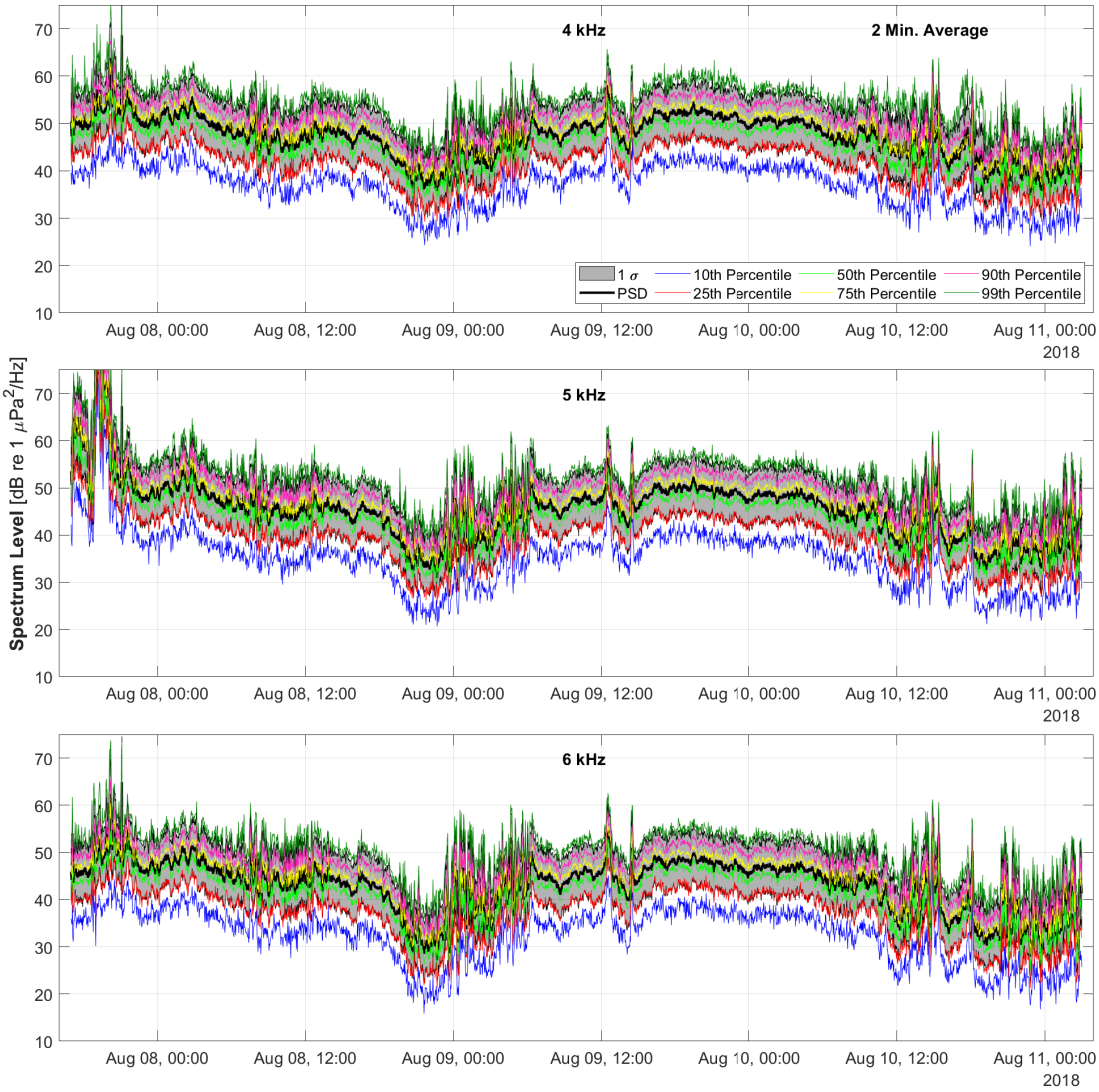

Figure A.14. Spectrum Level [dB re 1 μPa^2/Hz] of frequencies 4, 5, and 6 kHz from 8AUG18 to 11AUG18 using a 2 minute sliding average. The statistics are described in Section 2.4.

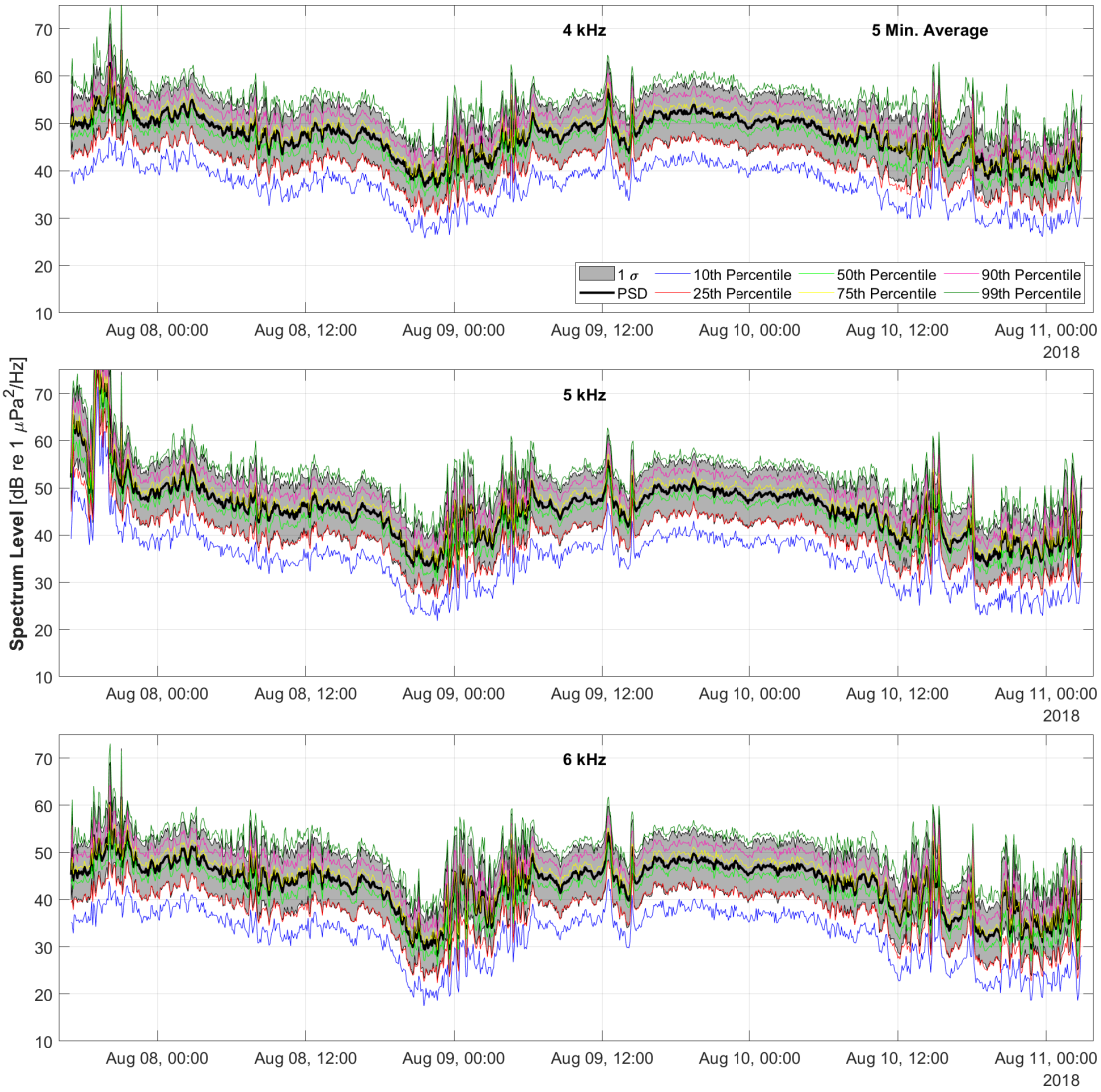

Figure A.15. Spectrum Level [dB re 1 μPa^2/Hz] of frequencies 4, 5, and 6 kHz from 8AUG18 to 11AUG18 using a 5 minute sliding average. The statistics are described in Section 2.4.

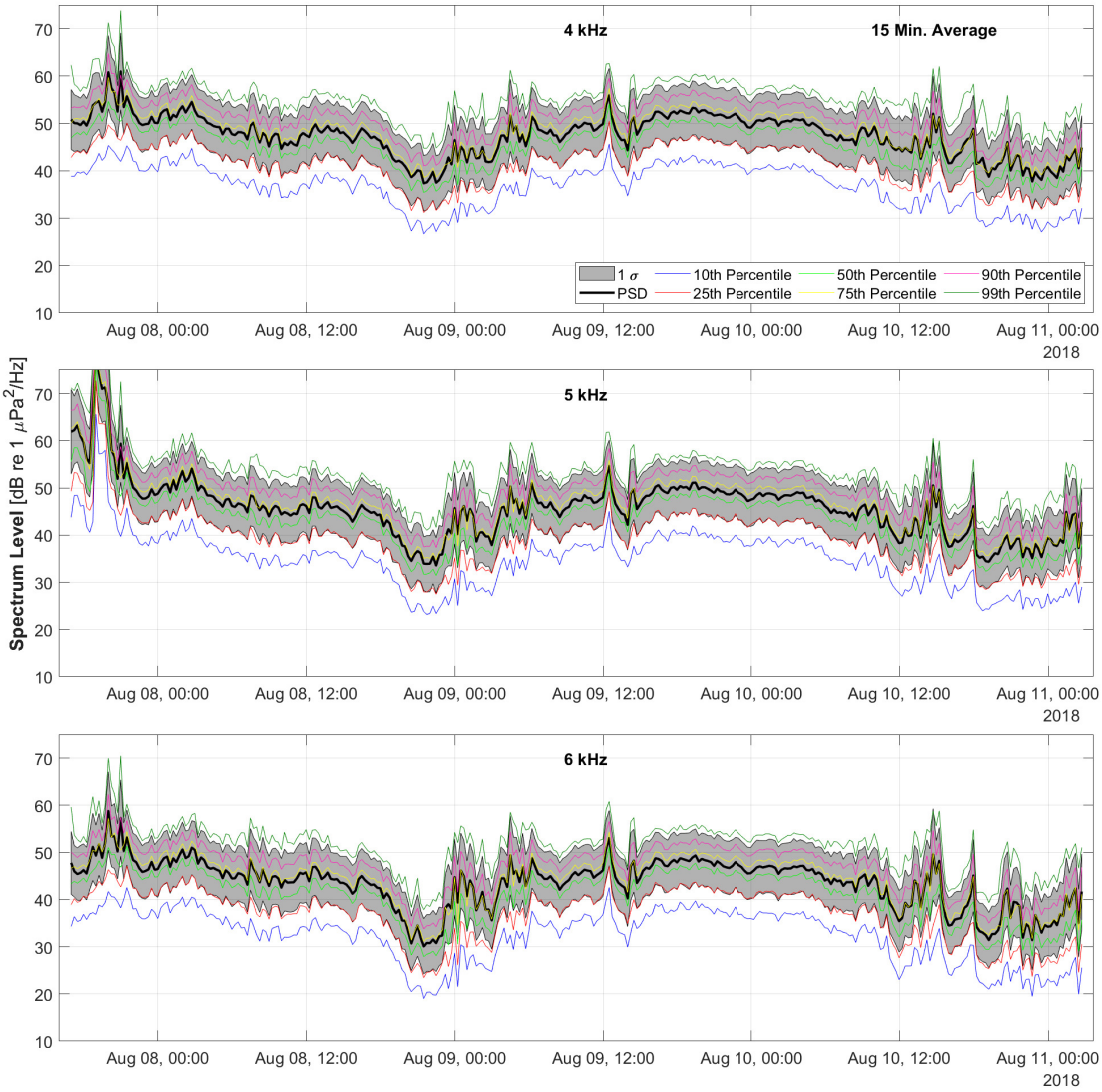

Figure A.16. Spectrum Level [dB re 1 μPa^2/Hz] of frequencies 4, 5, and 6 kHz from 8AUG18 to 11AUG18 using a 15 minute sliding average. The statistics are described in Section 2.4.

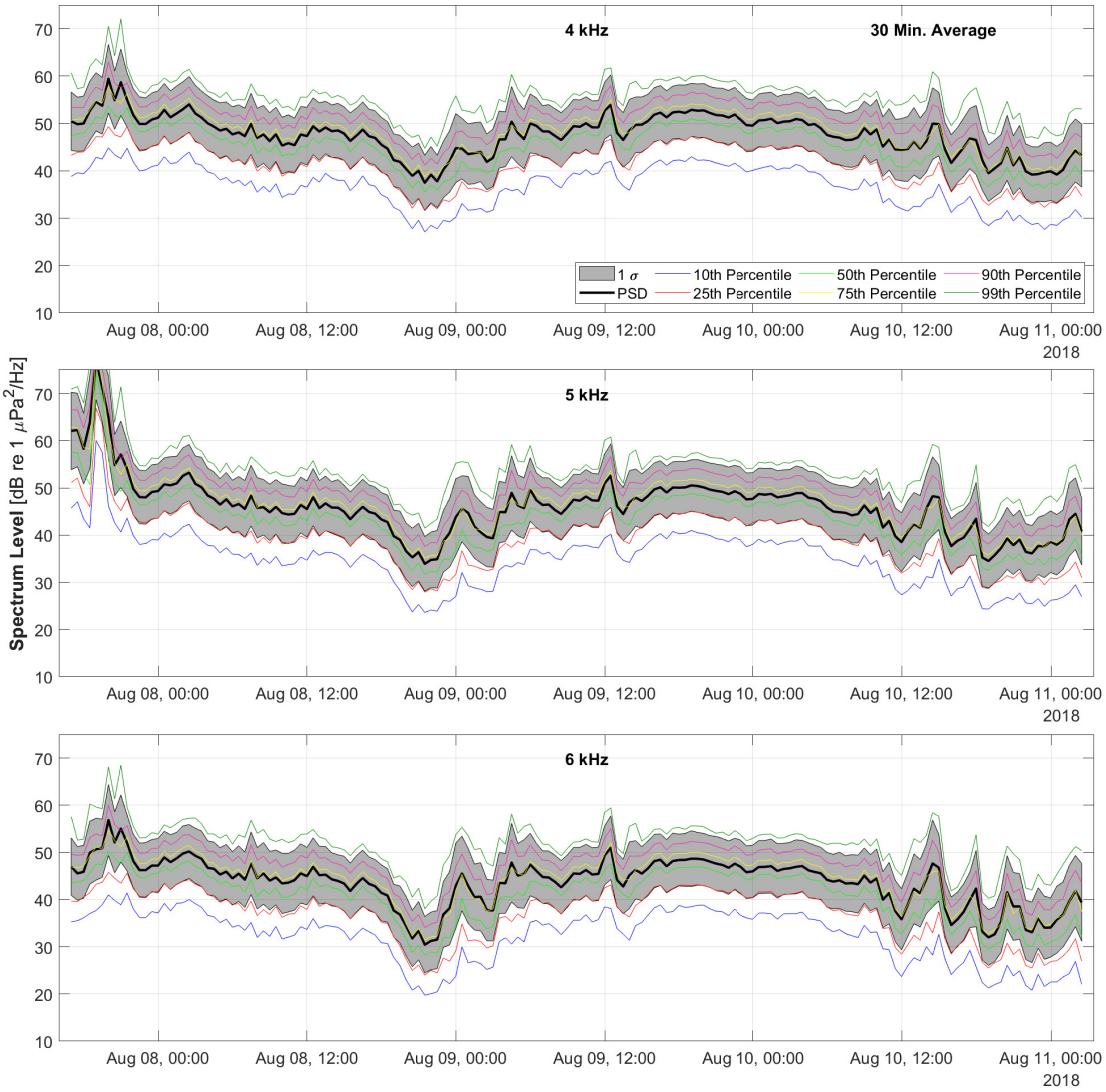

Figure A.17. Spectrum Level [dB re 1 μPa^2/Hz] of frequencies 4, 5, and 6 kHz from 8AUG18 to 11AUG18 using a 30 minute sliding average. The statistics are described in Section 2.4.

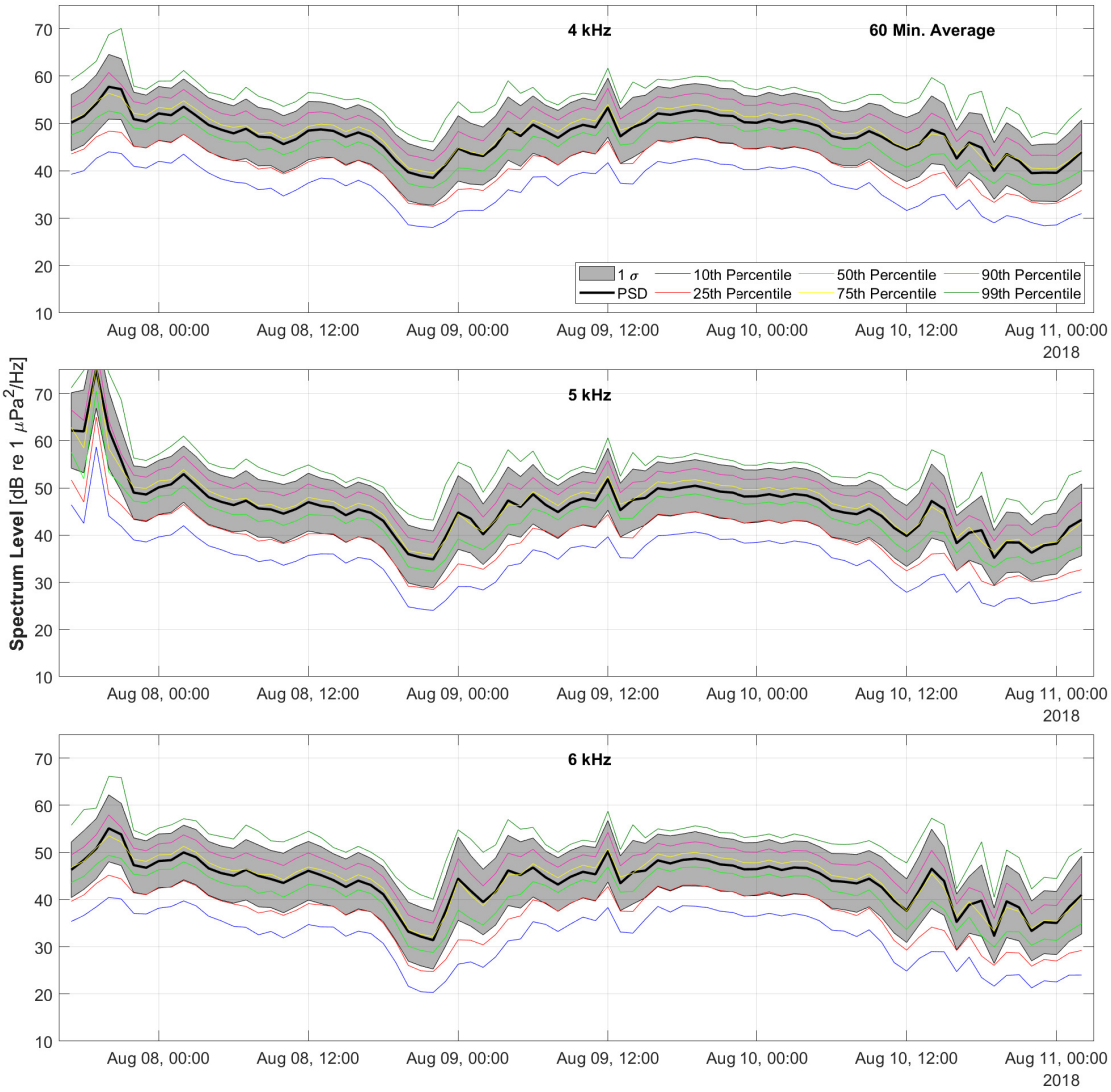

Figure A.18. Spectrum Level [dB re 1 μPa^2/Hz] of frequencies 4, 5, and 6 kHz from 8AUG18 to 11AUG18 using a 60 minute sliding average. The statistics are described in Section 2.4.

A.1.4 Additional time averages for frequencies 4, 5, and 6 kHz for the second deployment.

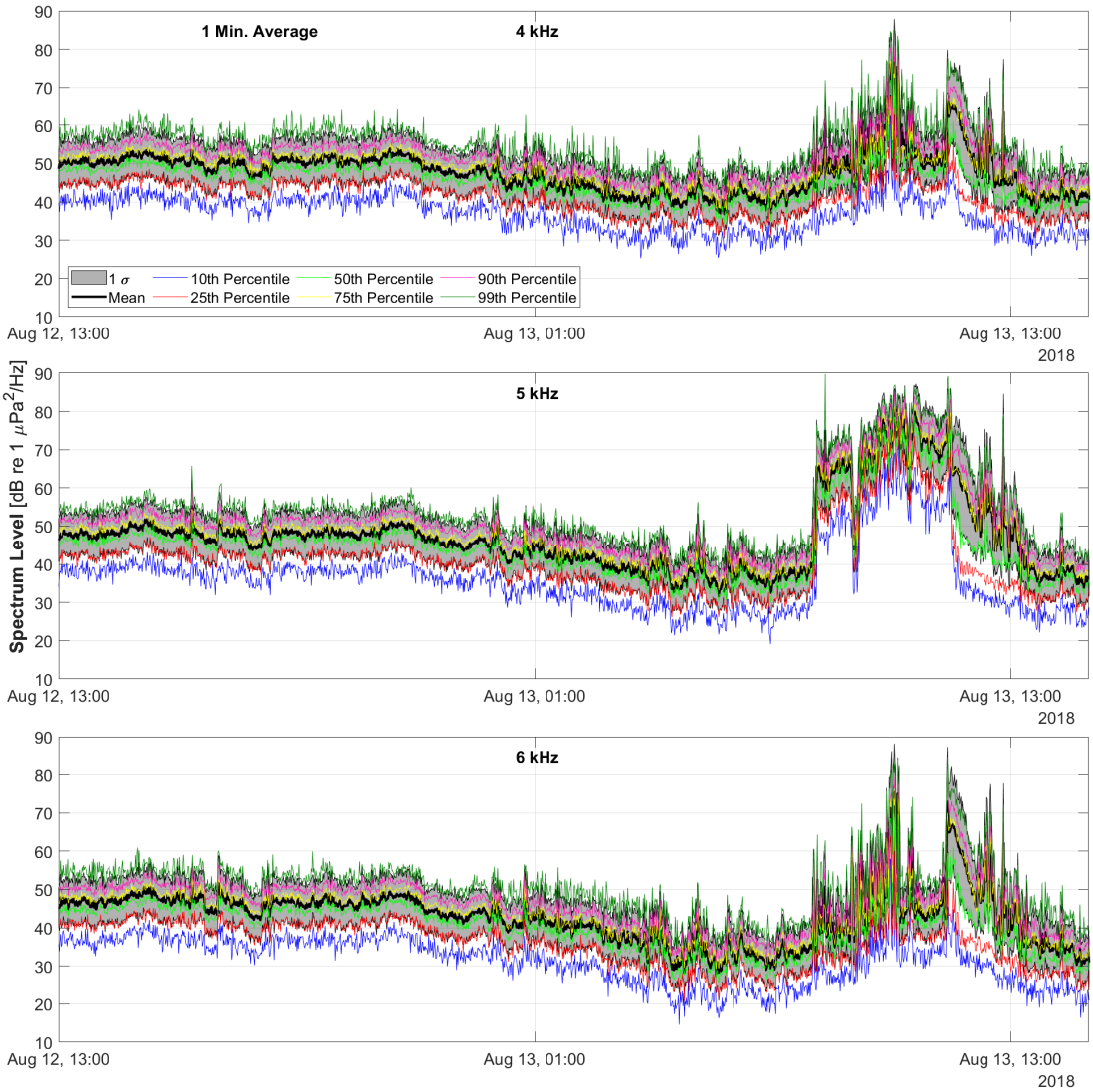

Figure A.19. Spectrum Level [dB re 1 μPa^2/Hz] of frequencies 4, 5, and 6 kHz for the second deployment using a 1 minute sliding average. The statistics are described in Section 2.4. Of note, the spike and rapidly changing PSD around 1000 on 13 AUG is due to various noise testing. See Table 4.1.

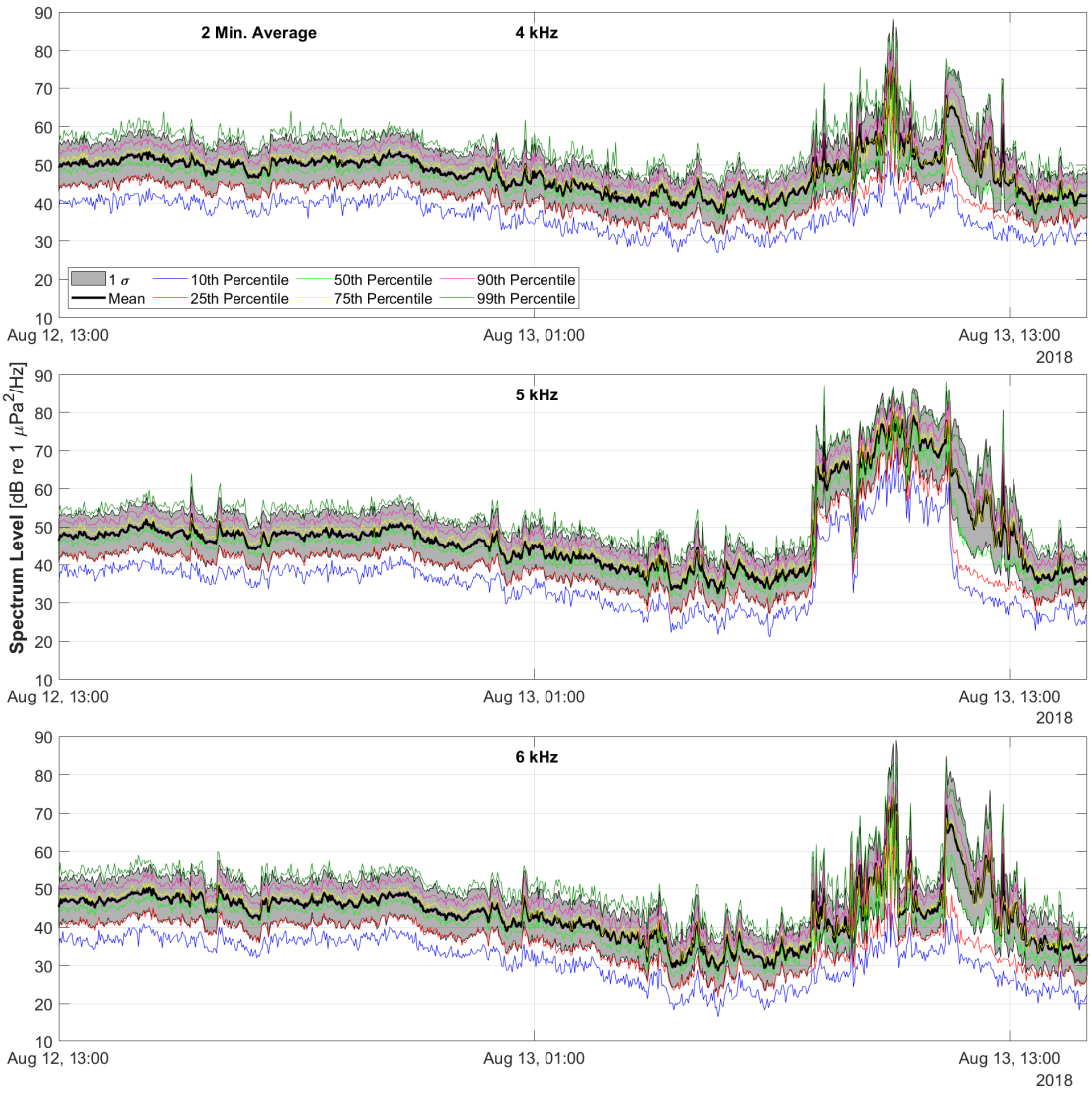

Figure A.20. Spectrum Level [dB re 1 μPa^2/Hz] of frequencies 4, 5, and 6 kHz for the second deployment using a 2 minute sliding average. The statistics are described in Section 2.4. Of note, the spike and rapidly changing PSD around 1000 on 13 AUG is due to various noise testing. See Table 4.1.

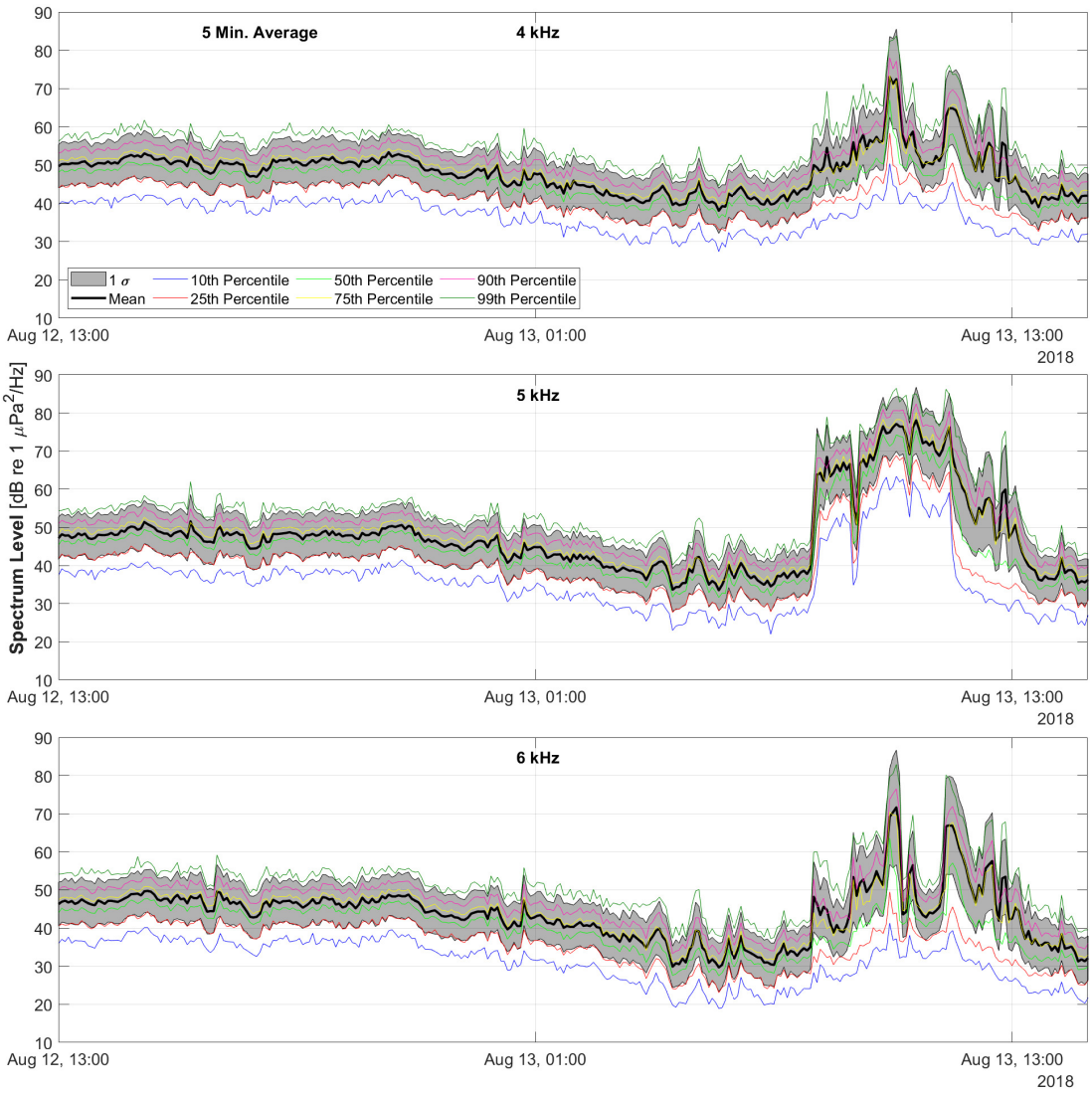

Figure A.21. Spectrum Level [dB re 1 μPa^2/Hz] of frequencies 4, 5, and 6 kHz for the second deployment using a 5 minute sliding average. The statistics are described in Section 2.4. Of note, the spike and rapidly changing PSD around 1000 on 13 AUG is due to various noise testing. See Table 4.1.

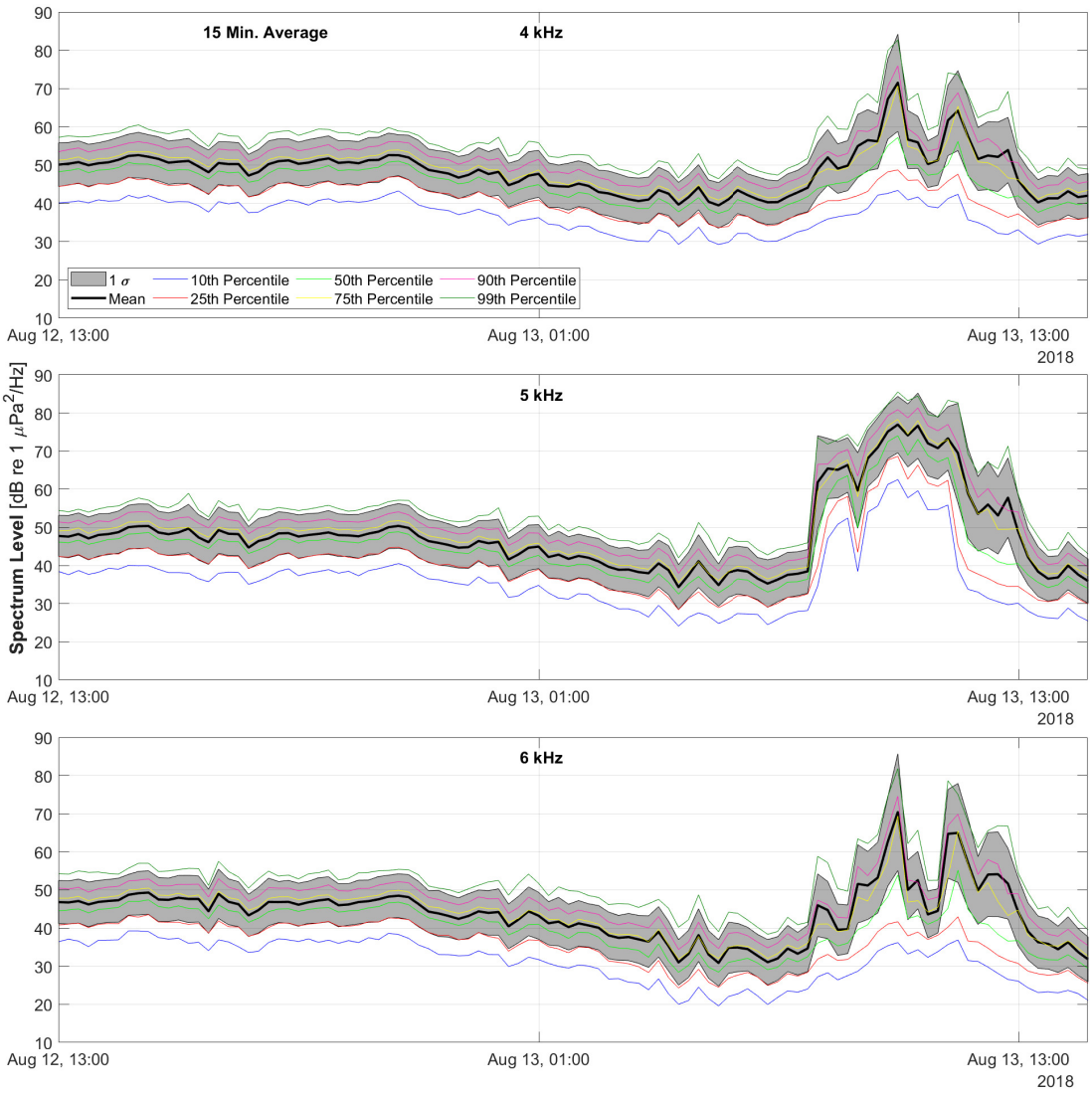

Figure A.22. Spectrum Level [dB re 1 μPa^2/Hz] of frequencies 4, 5, and 6 kHz for the second deployment using a 15 minute sliding average. The statistics are described in Section 2.4. Of note, the spike and rapidly changing PSD around 1000 on 13 AUG is due to various noise testing. See Table 4.1.

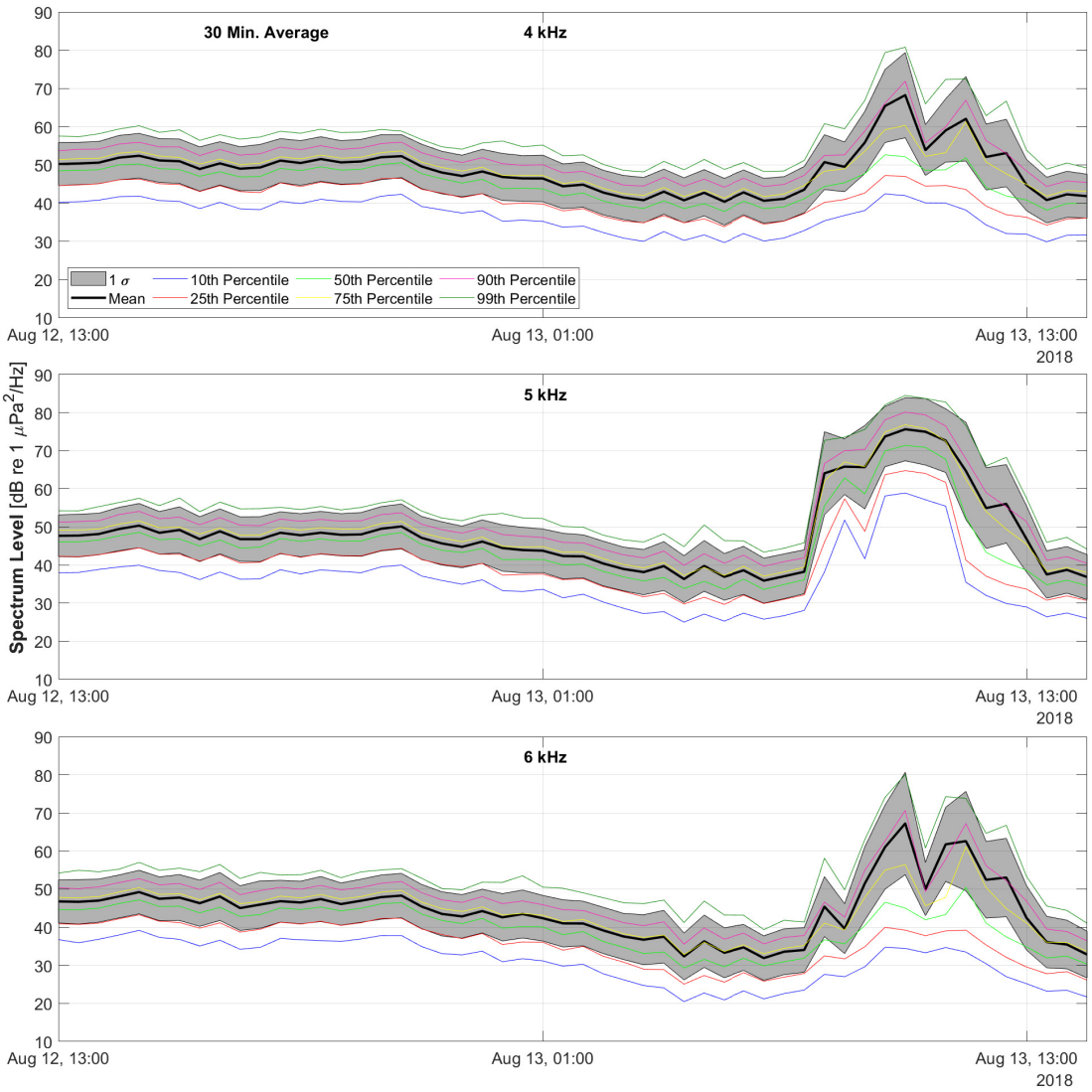

Figure A.23. Spectrum Level [dB re 1 μPa^2/Hz] of frequencies 4, 5, and 6 kHz for the second deployment using a 30 minute sliding average. The statistics are described in Section 2.4. Of note, the spike and rapidly changing PSD around 1000 on 13 AUG is due to various noise testing. See Table 4.1.

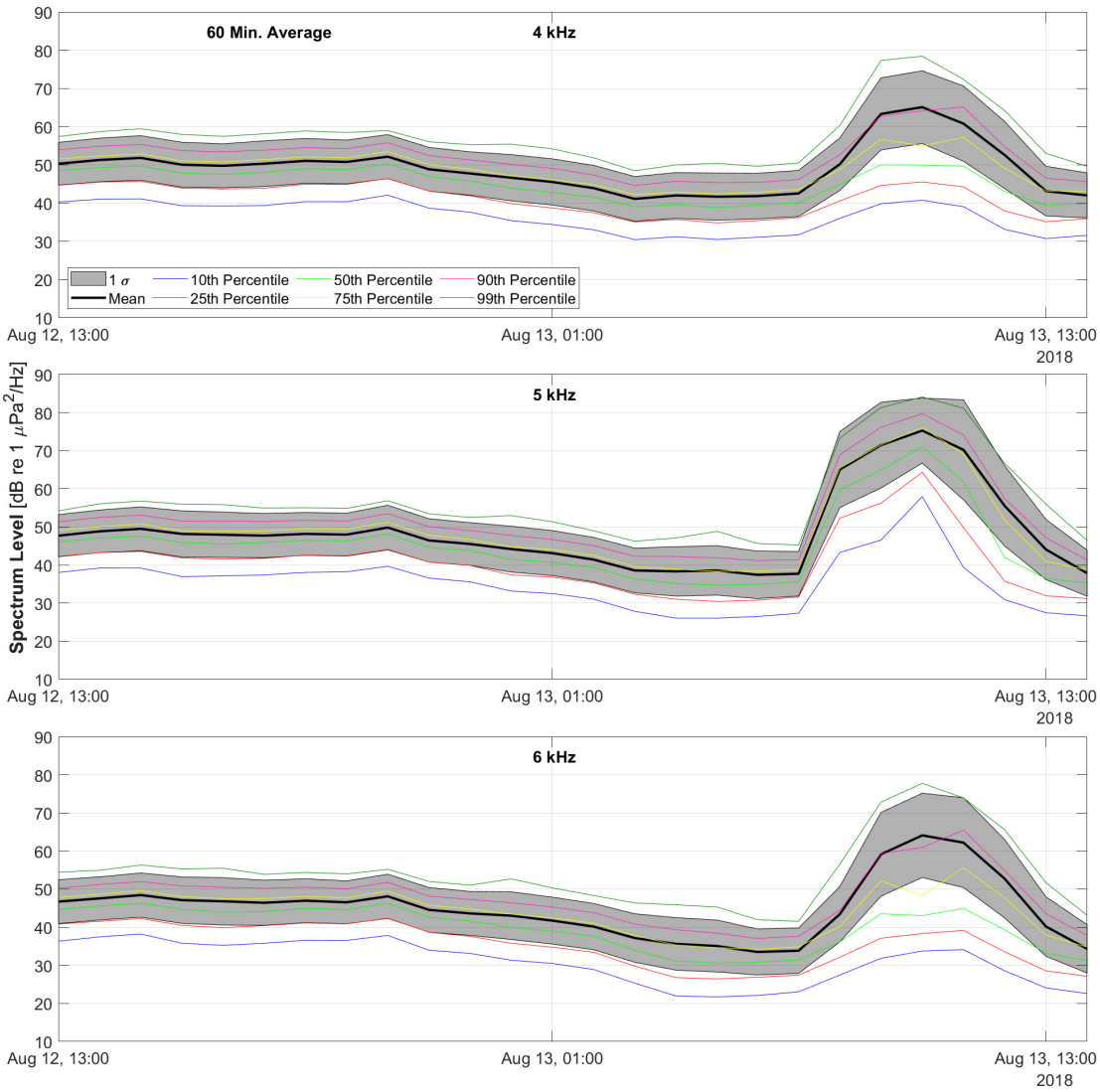

Figure A.24. Spectrum Level [dB re 1 μPa^2/Hz] of frequencies 4, 5, and 6 kHz for the second deployment using a 60 minute sliding average. The statistics are described in Section 2.4. Of note, the spike and rapidly changing PSD around 1000 on 13 AUG is due to various noise testing. See Table 4.1.

A.1.5 Additional time averages for frequencies 7, 8, and 9 kHz for the first deployment.

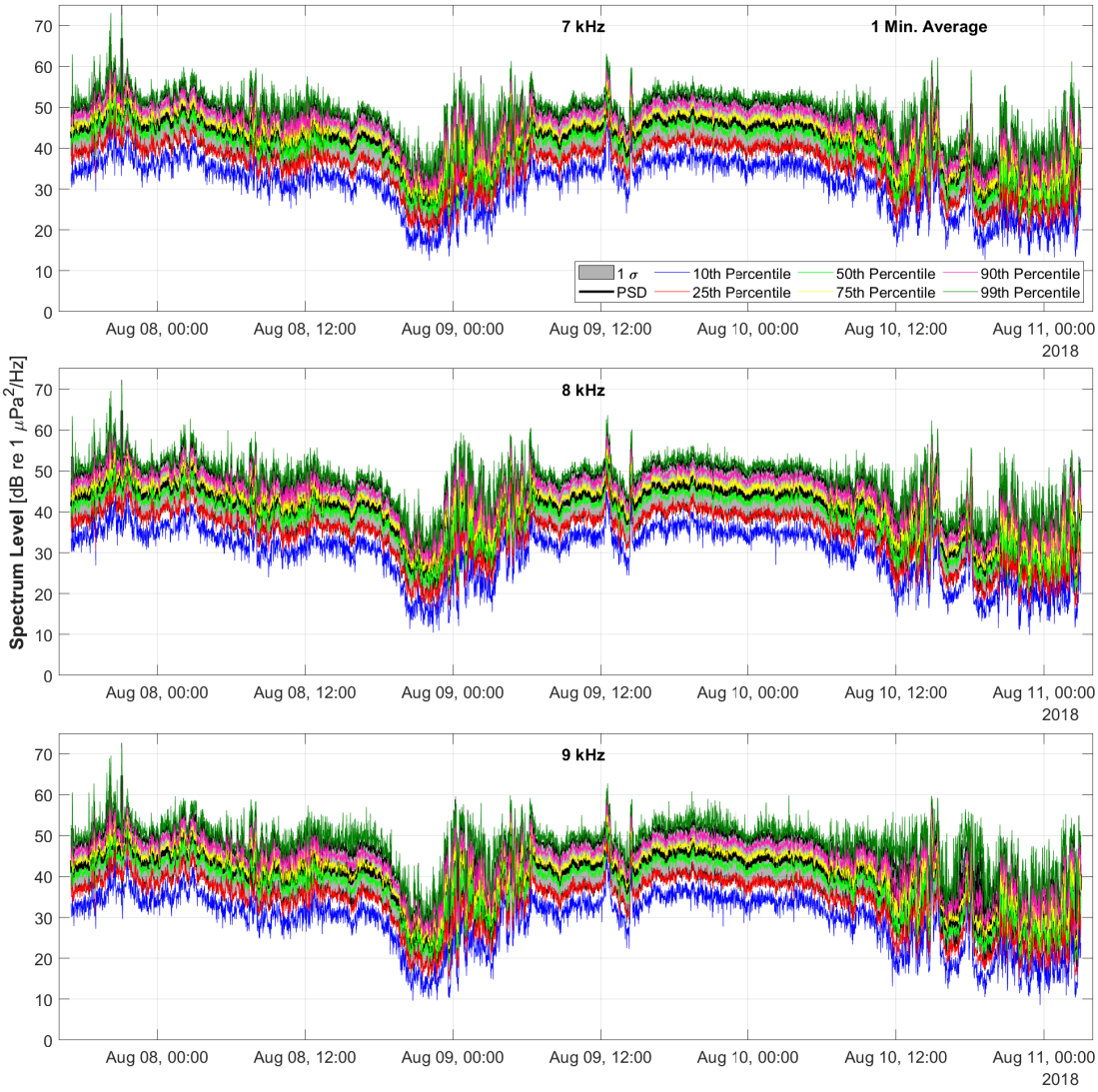

Figure A.25. Spectrum Level [dB re 1 μPa^2/Hz] of frequencies 7, 8, and 9 kHz from 8AUG18 to 11AUG18 using a 1 minute sliding average. The statistics are described in Section 2.4.

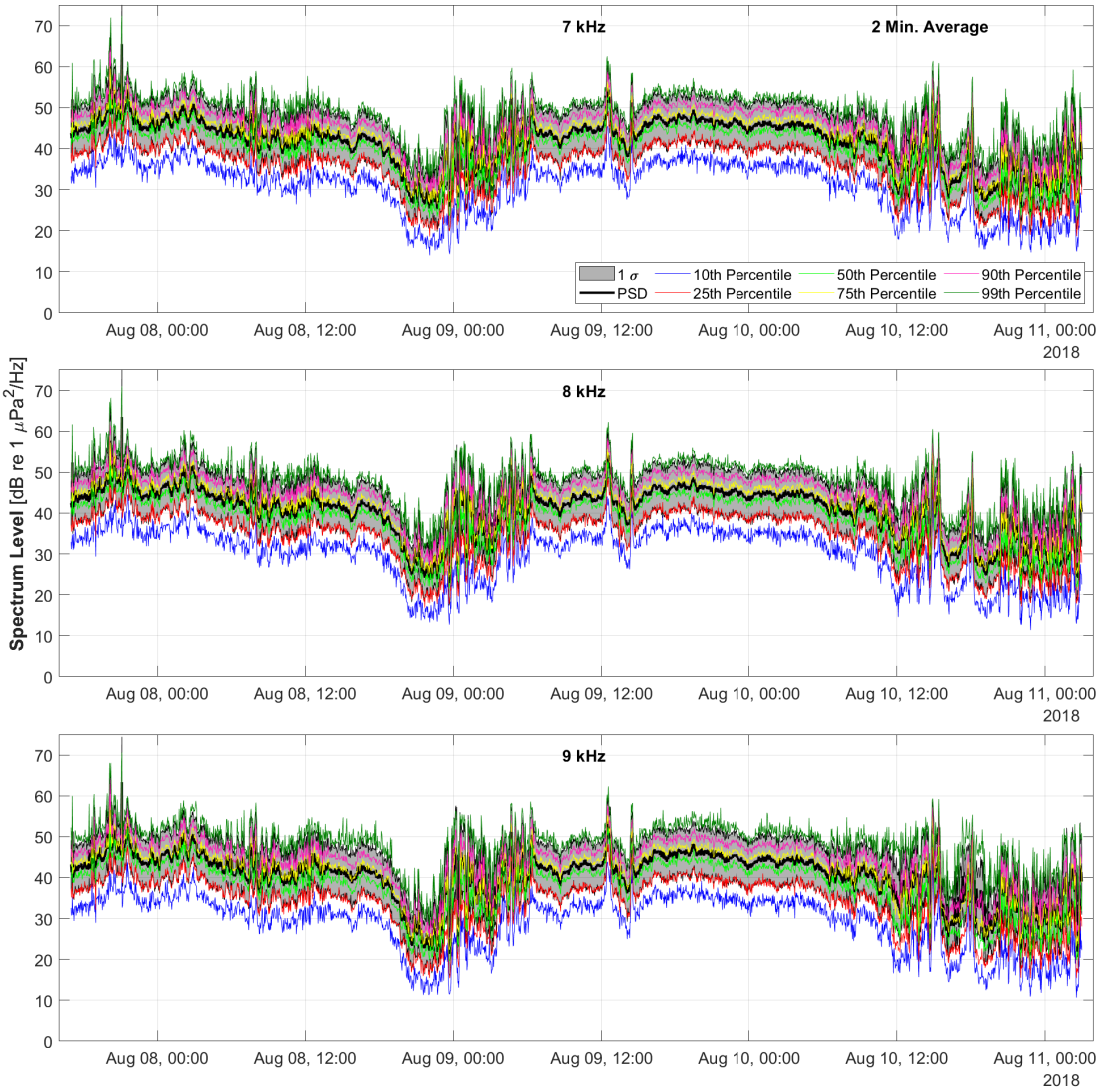

Figure A.26. Spectrum Level [dB re 1 μPa^2/Hz] of frequencies 7, 8, and 9 kHz from 8AUG18 to 11AUG18 using a 2 minute sliding average. The statistics are described in Section 2.4.

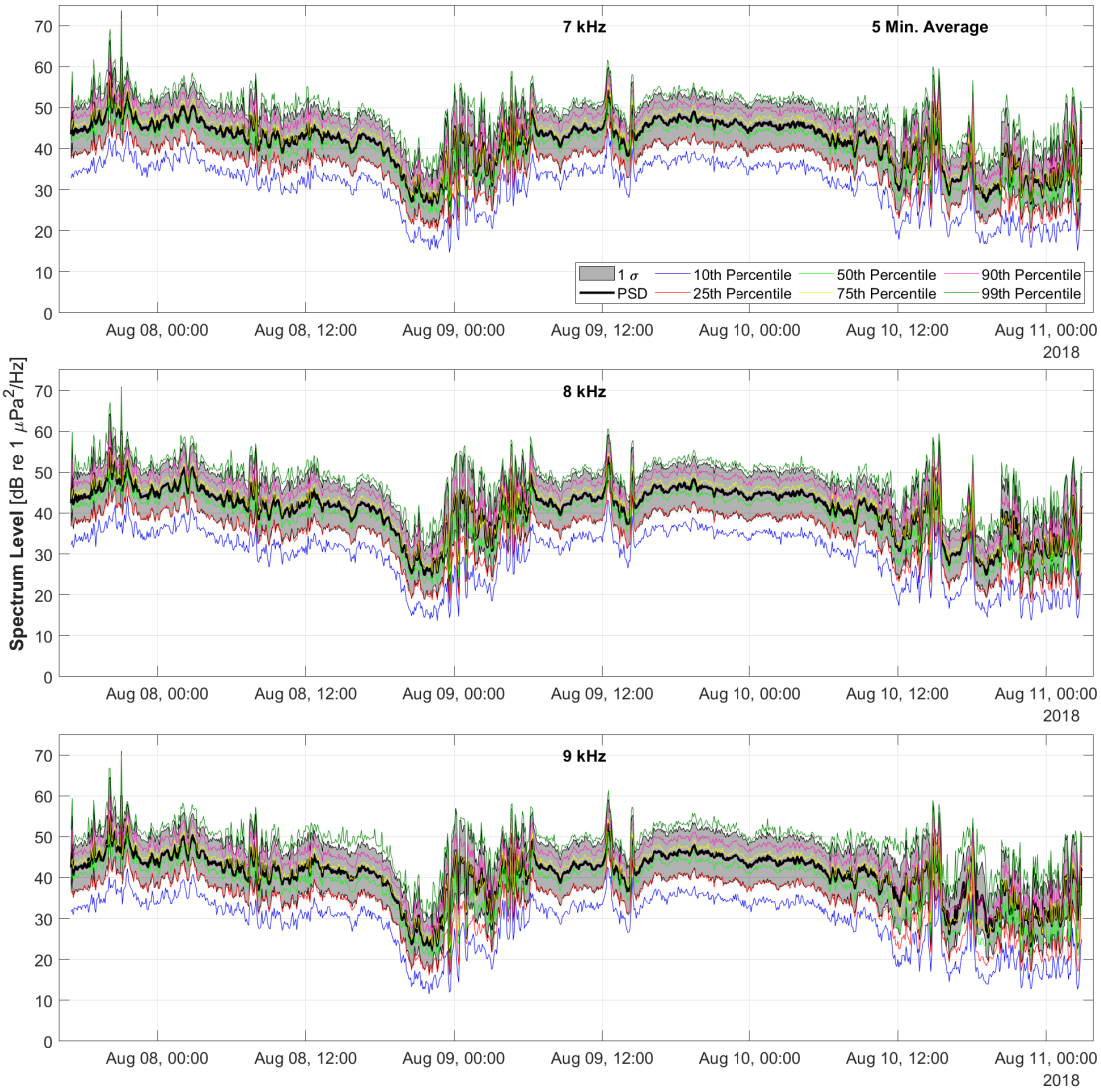

Figure A.27. Spectrum Level [dB re 1 μPa^2/Hz] of frequencies 7, 8, and 9 kHz from 8AUG18 to 11AUG18 using a 5 minute sliding average. The statistics are described in Section 2.4.

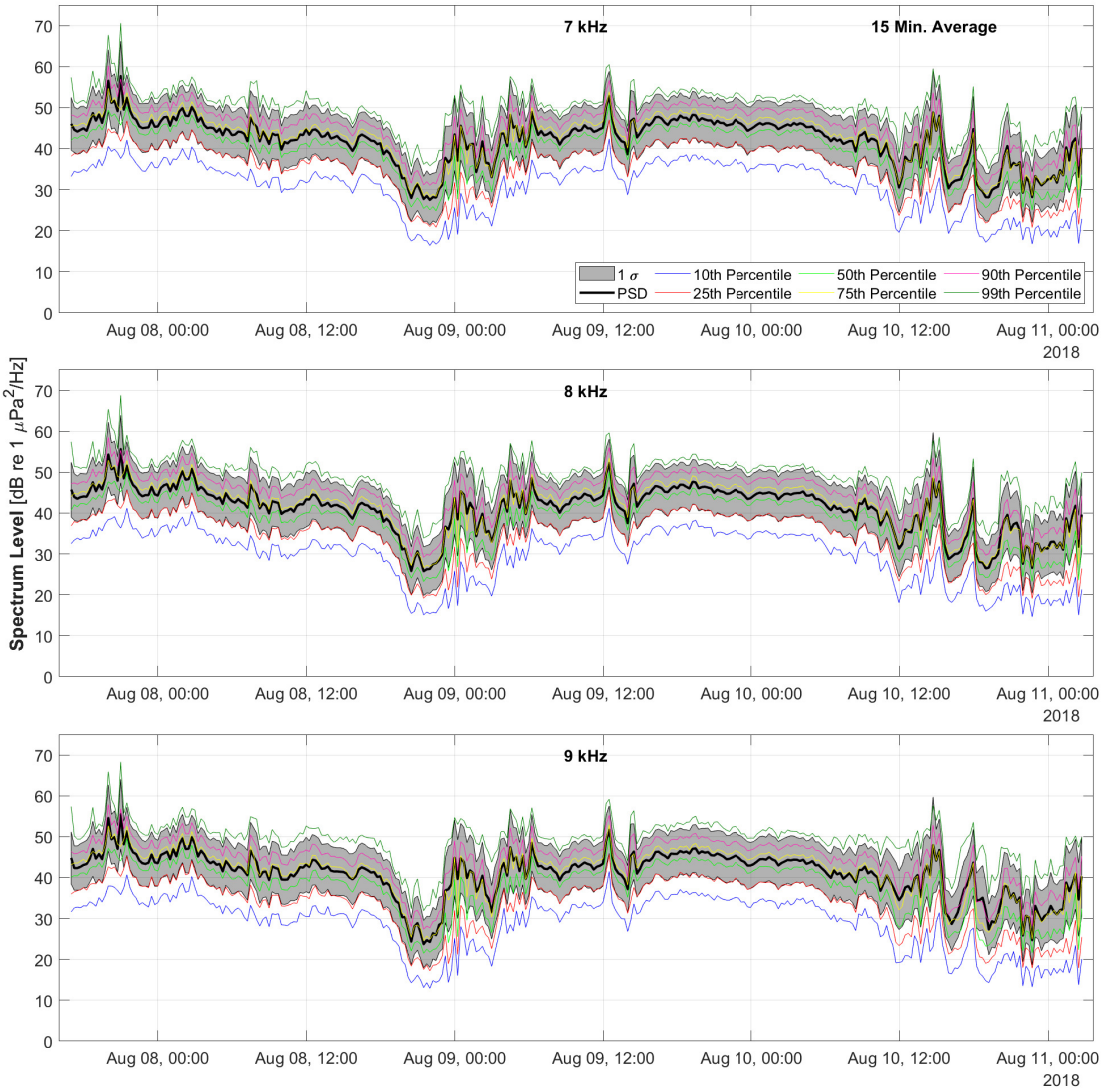

Figure A.28. Spectrum Level [dB re 1 μPa^2/Hz] of frequencies 7, 8, and 9 kHz from 8AUG18 to 11AUG18 using a 15 minute sliding average. The statistics are described in Section 2.4.

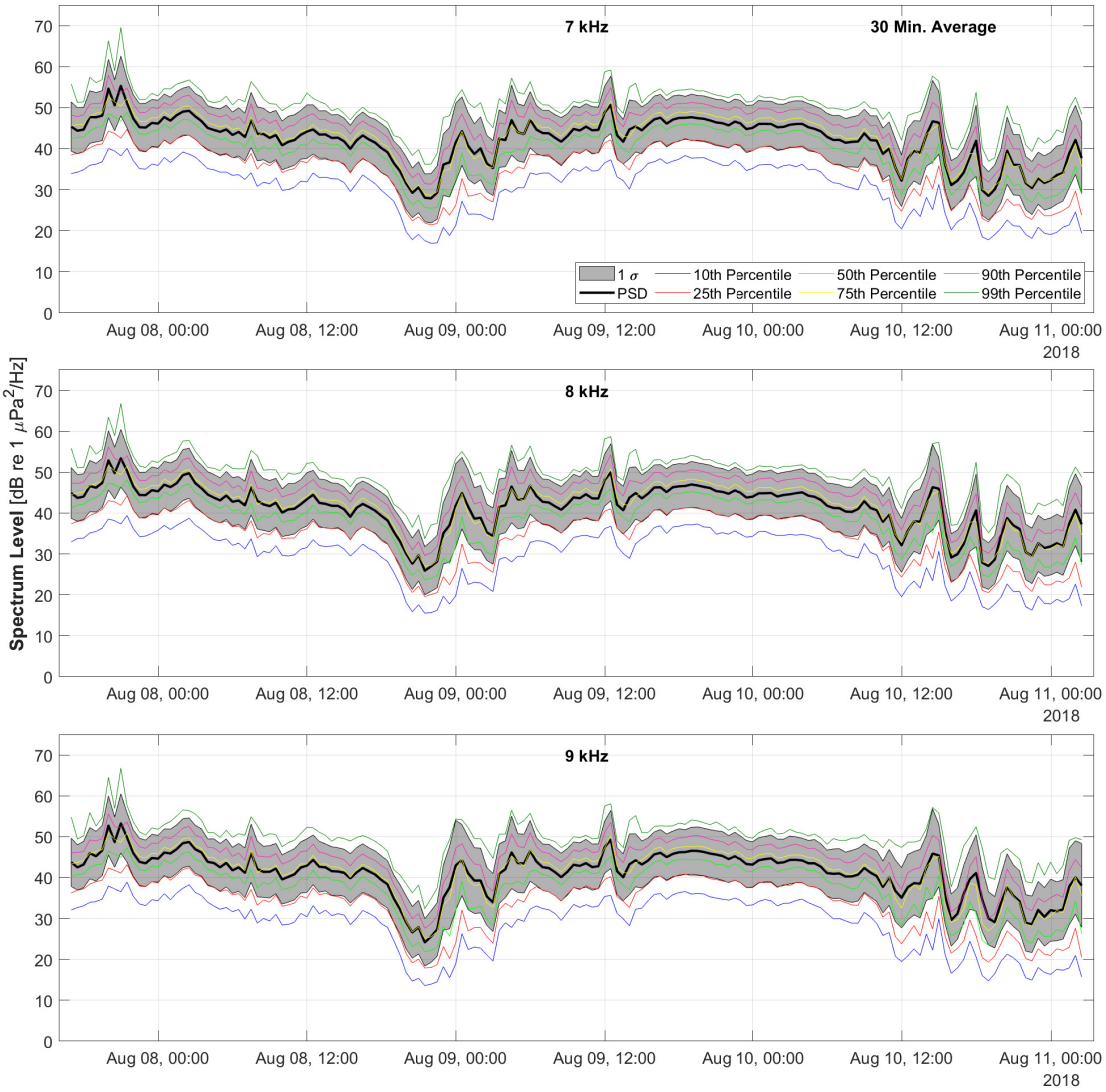

Figure A.29. Spectrum Level [dB re 1 μPa^2/Hz] of frequencies 7, 8, and 9 kHz from 8AUG18 to 11AUG18 using a 30 minute sliding average. The statistics are described in Section 2.4.

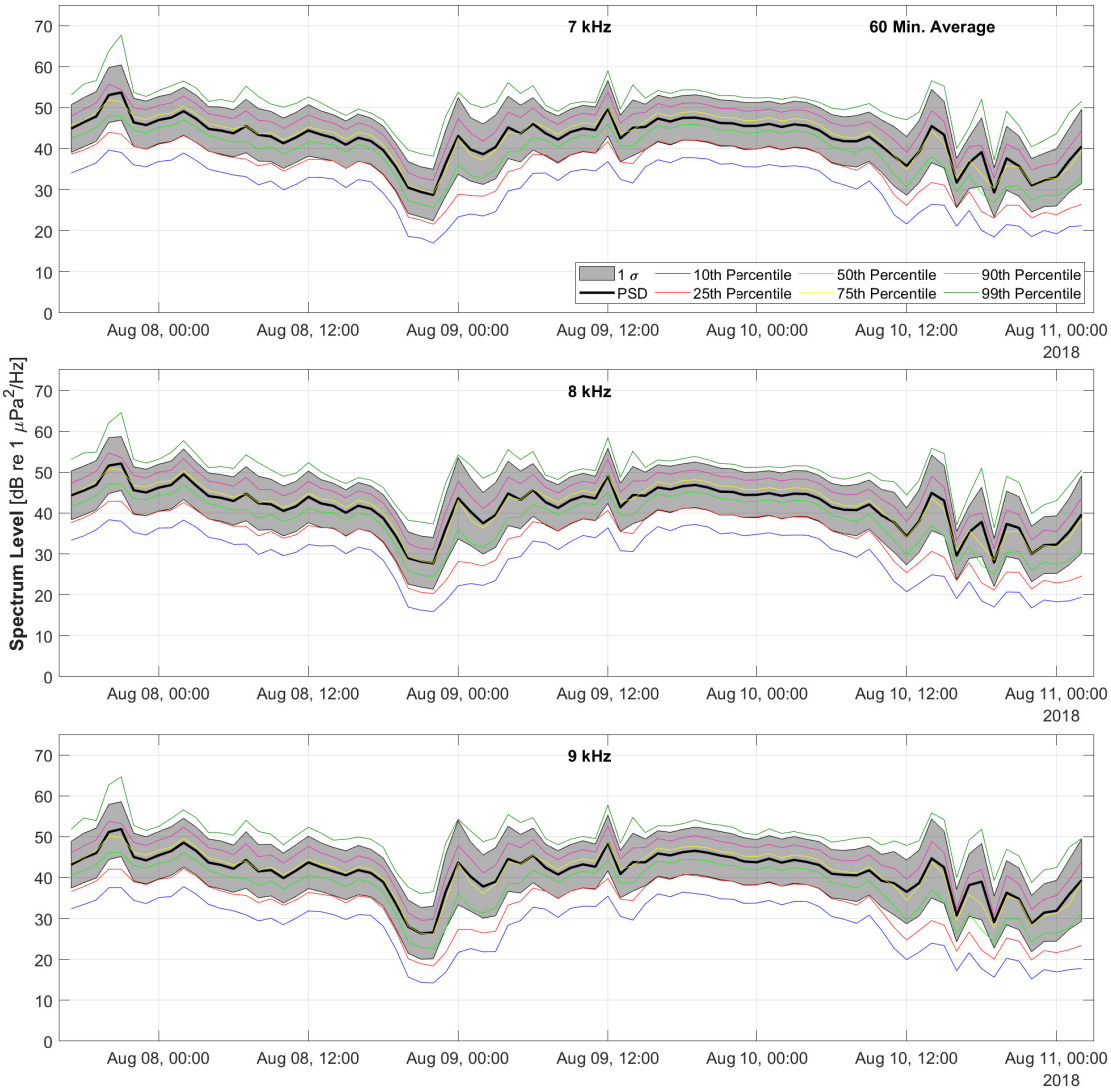

Figure A.30. Spectrum Level [dB re 1 μPa^2/Hz] of frequencies 7, 8, and 9 kHz from 8AUG18 to 11AUG18 using a 60 minute sliding average. The statistics are described in Section 2.4.

A.1.6 Additional time averages for frequencies 7, 8, and 9 kHz for the second deployment.

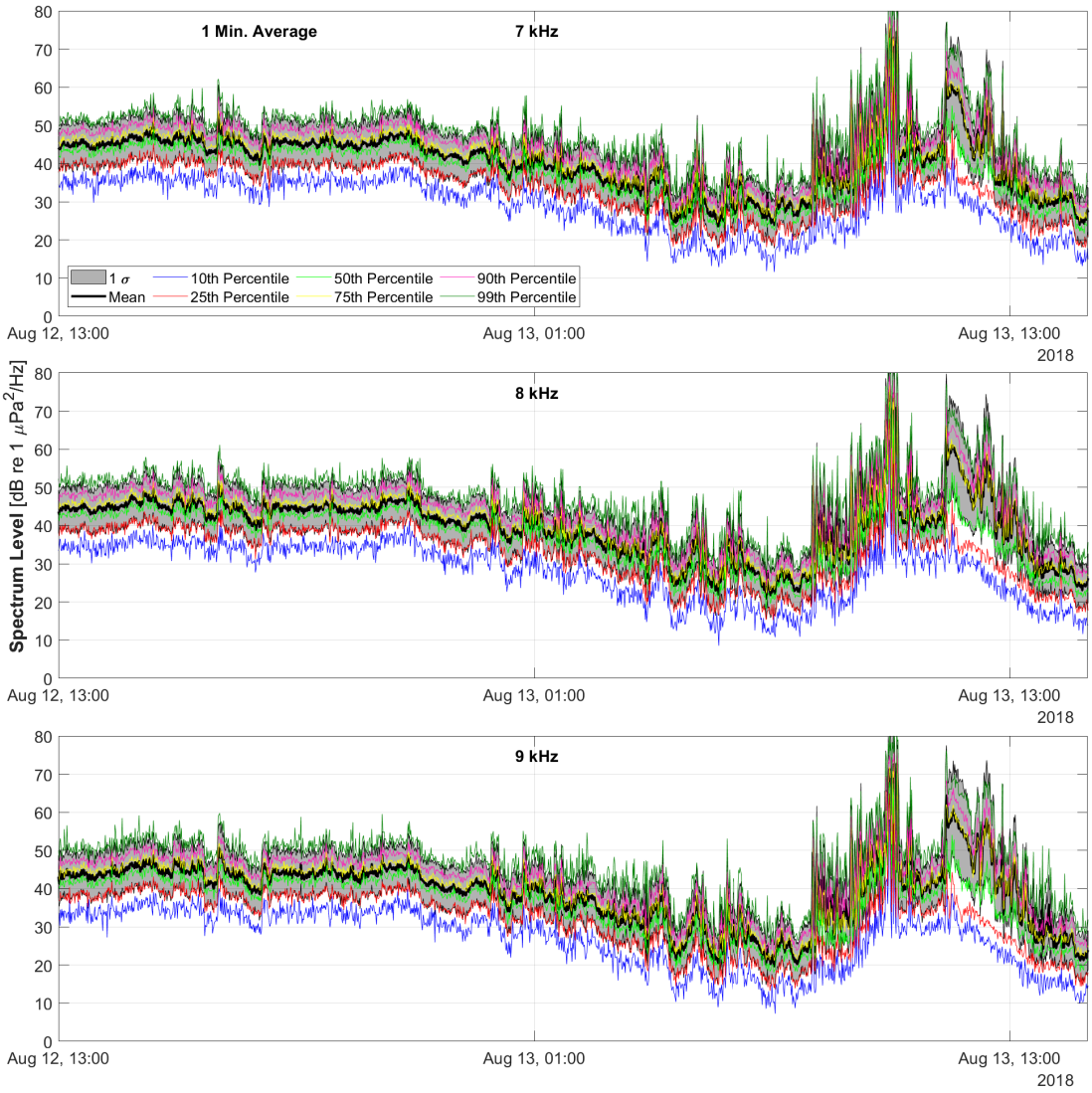

Figure A.31. Spectrum Level [dB re 1 μPa^2/Hz] of frequencies 7, 8, and 9 kHz for the second deployment using a 1 minute sliding average. The statistics are described in Section 2.4. Of note, the spike and rapidly changing PSD around 1000 on 13 AUG is due to various noise testing. See Table 4.1.

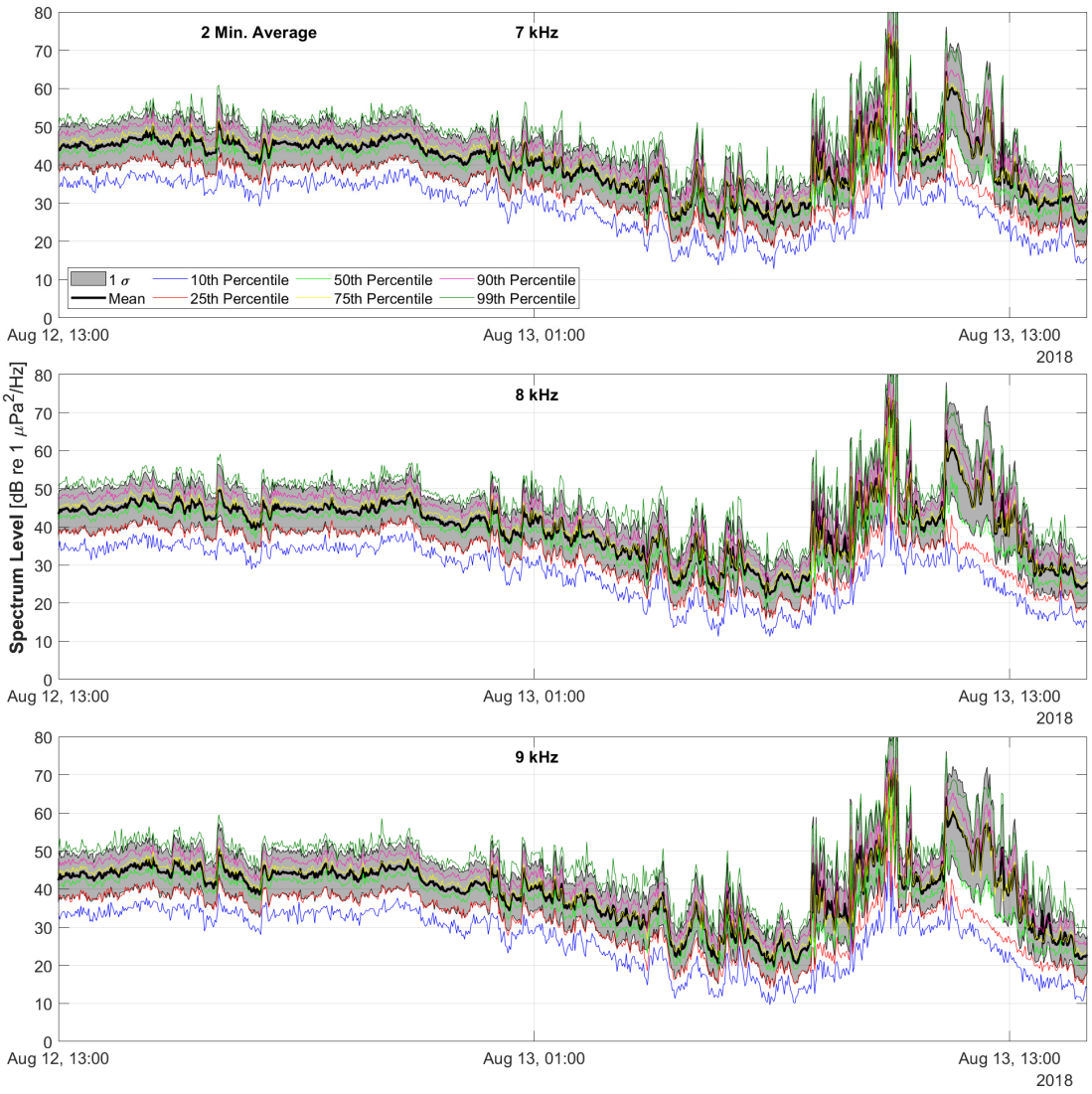

Figure A.32. Spectrum Level [dB re 1 μPa^2/Hz] of frequencies 7, 8, and 9 kHz for the second deployment using a 2 minute sliding average. The statistics are described in Section 2.4. Of note, the spike and rapidly changing PSD around 1000 on 13 AUG is due to various noise testing. See Table 4.1.

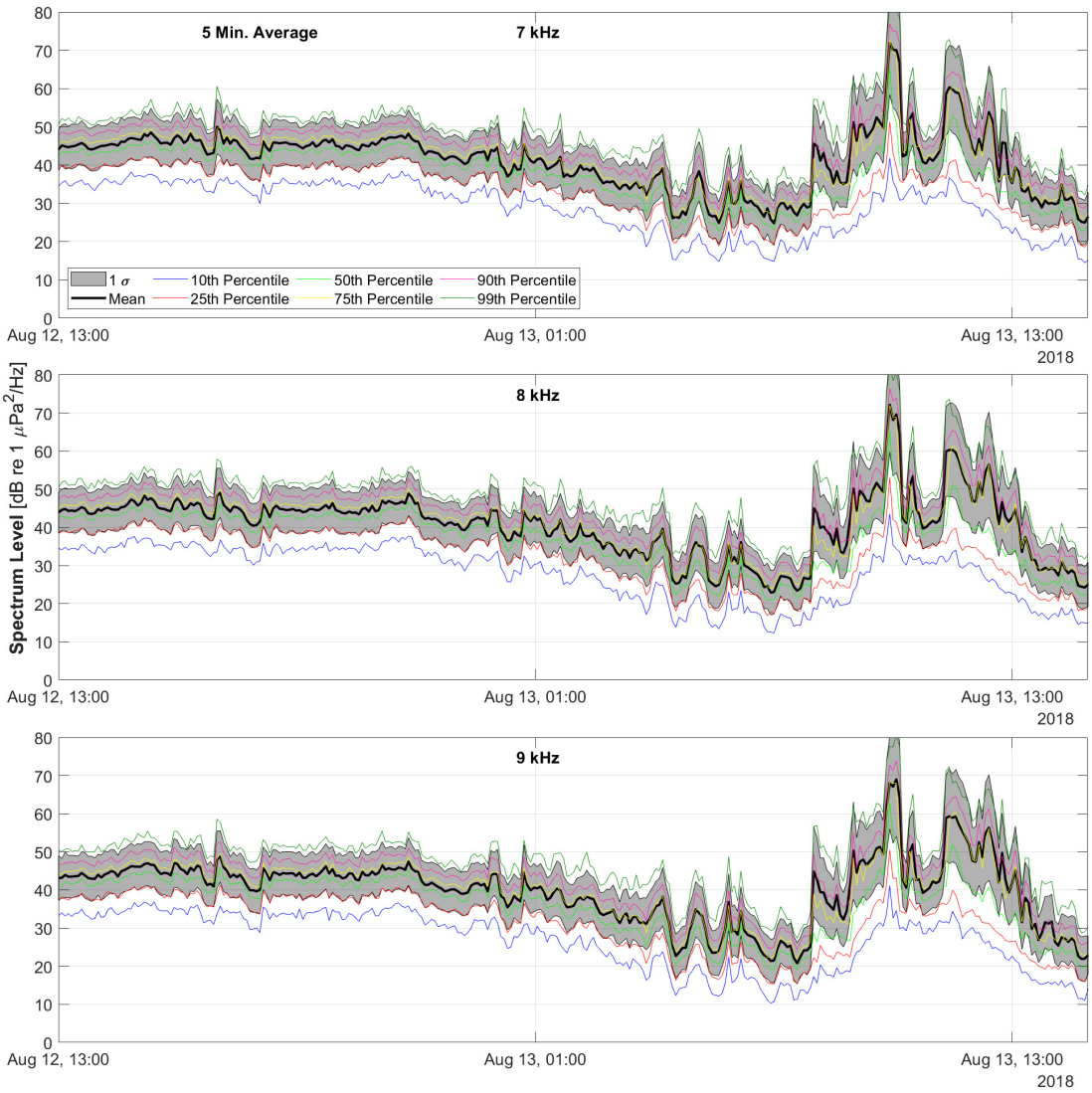

Figure A.33. Spectrum Level [dB re 1 μPa^2/Hz] of frequencies 7, 8, and 9 kHz for the second deployment using a 5 minute sliding average. The statistics are described in Section 2.4. Of note, the spike and rapidly changing PSD around 1000 on 13 AUG is due to various noise testing. See Table 4.1.

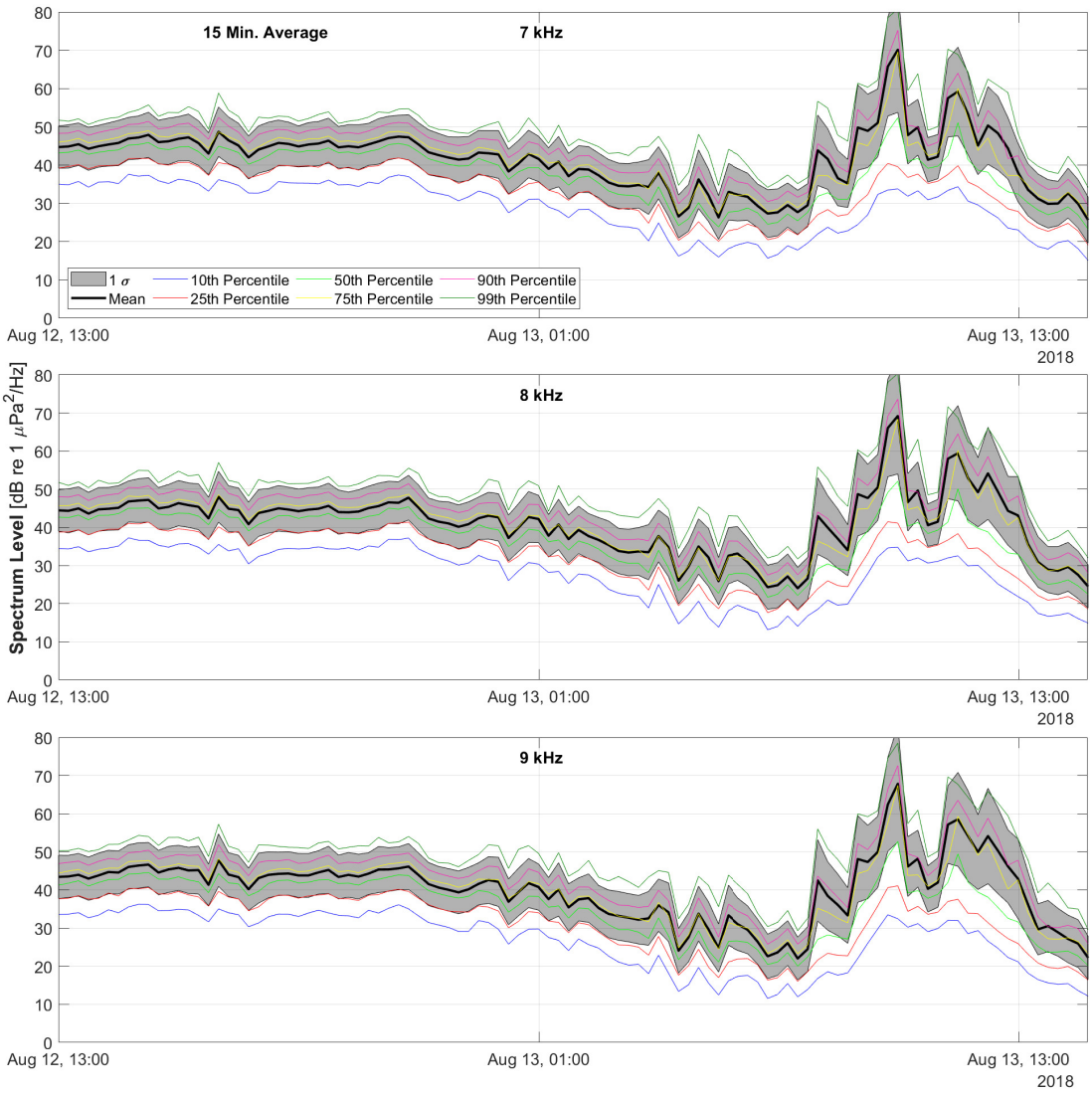

Figure A.34. Spectrum Level [dB re 1 μPa^2/Hz] of frequencies 7, 8, and 9 kHz for the second deployment using a 15 minute sliding average. The statistics are described in Section 2.4. Of note, the spike and rapidly changing PSD around 1000 on 13 AUG is due to various noise testing. See Table 4.1.

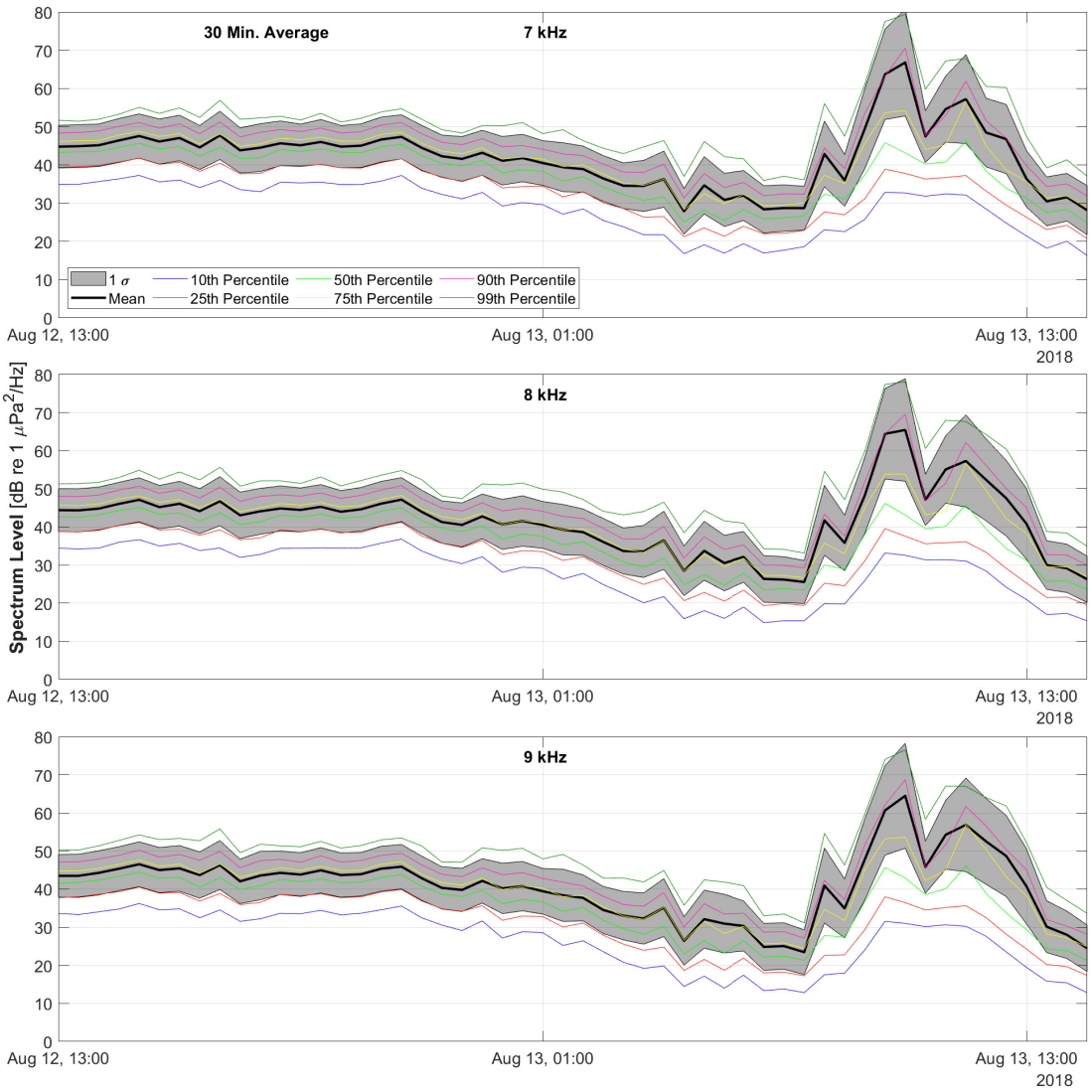

Figure A.35. Spectrum Level [dB re 1 μPa^2/Hz] of frequencies 7, 8, and 9 kHz for the second deployment using a 30 minute sliding average. The statistics are described in Section 2.4. Of note, the spike and rapidly changing PSD around 1000 on 13 AUG is due to various noise testing. See Table 4.1.

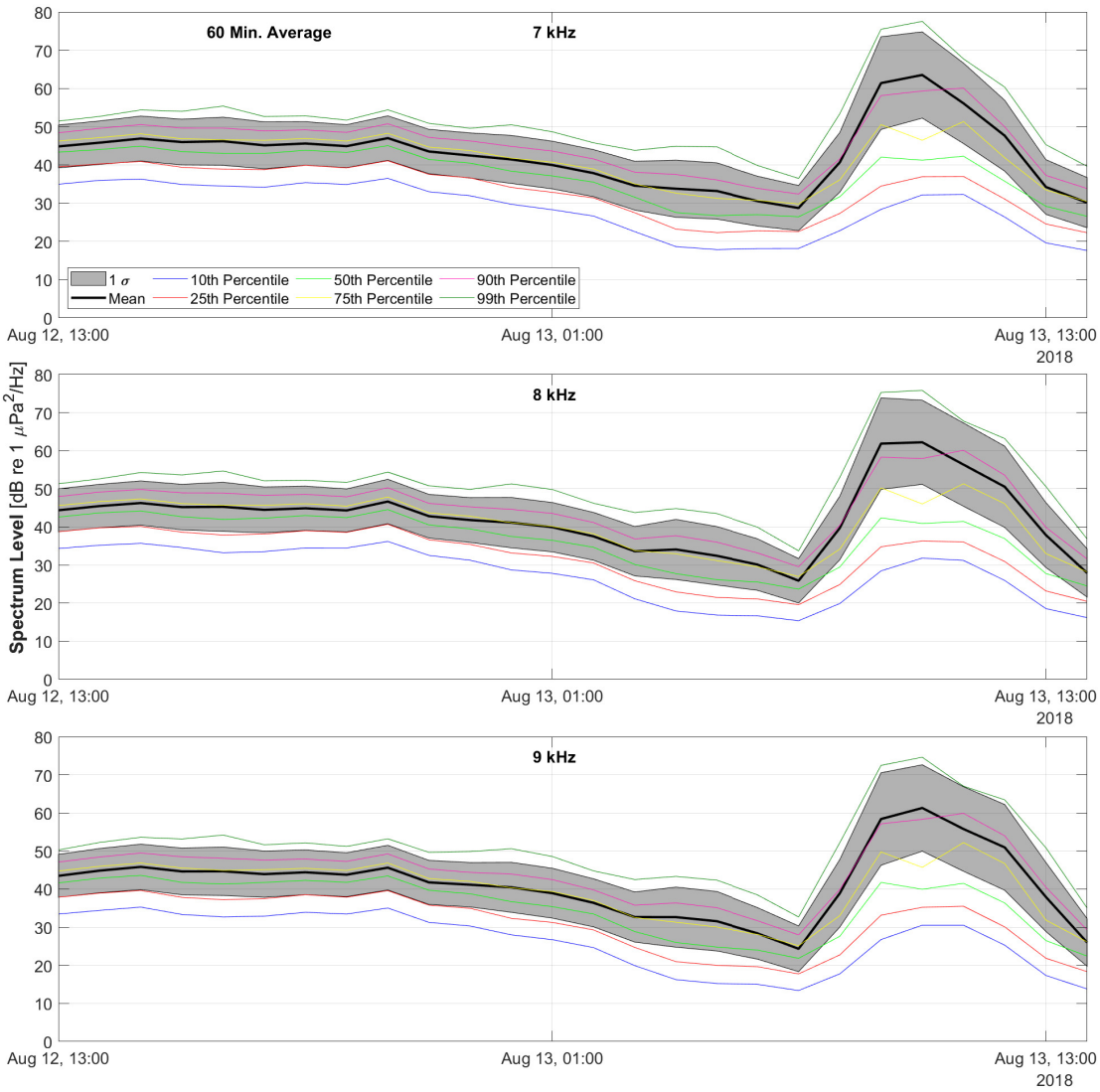

Figure A.36. Spectrum Level [dB re 1 μPa^2/Hz] of frequencies 7, 8, and 9 kHz for the second deployment using a 60 minute sliding average. The statistics are described in Section 2.4. Of note, the spike and rapidly changing PSD around 1000 on 13 AUG is due to various noise testing. See Table 4.1.

A.2 Supplemental Broadband Figures

A.2.1 Additional time averages for Figure 4.1

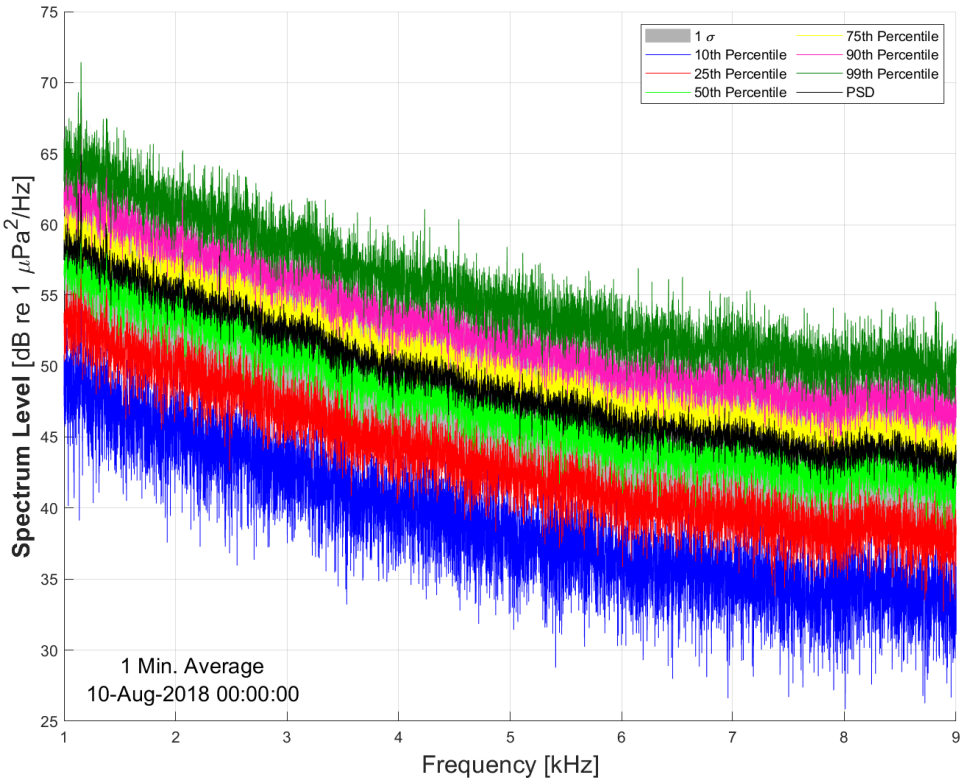

Figure A.37. Spectrum Level [dB re 1 μPa^2/Hz] versus frequency [kHz] using a 1 minute average. This data is taken from midnight on 10AUG2018. The statistics are described in Section 2.4.

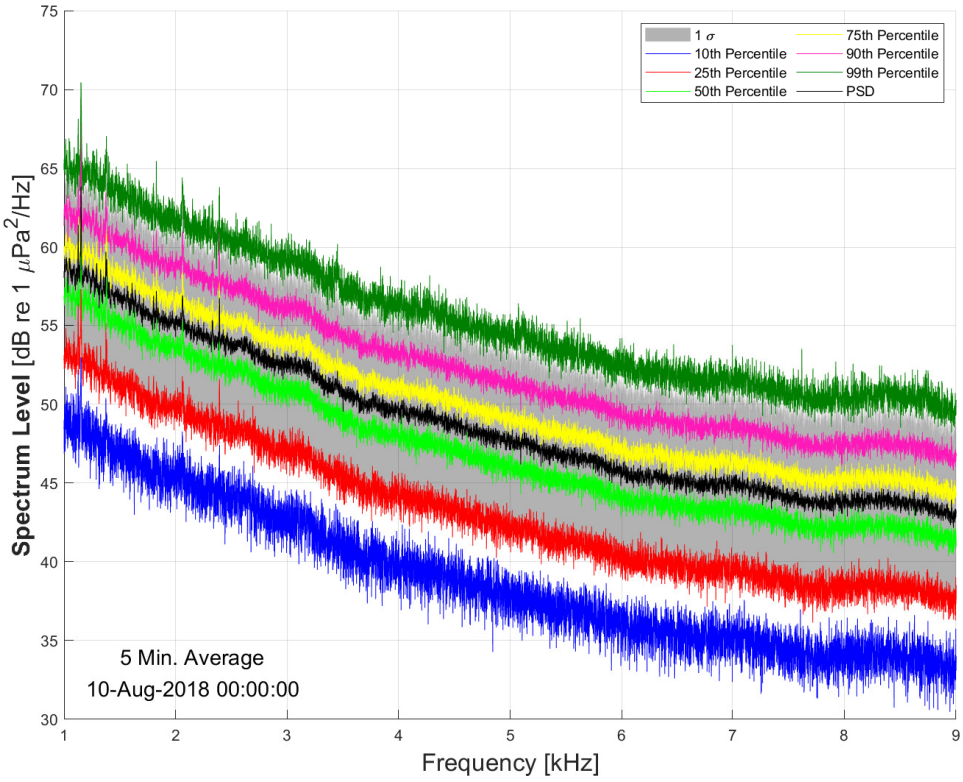

Figure A.38. Spectrum Level [dB re 1 μPa^2/Hz] versus frequency [kHz] using a 10 minute average. This data is taken from midnight on 10AUG2018. The statistics are described in Section 2.4.

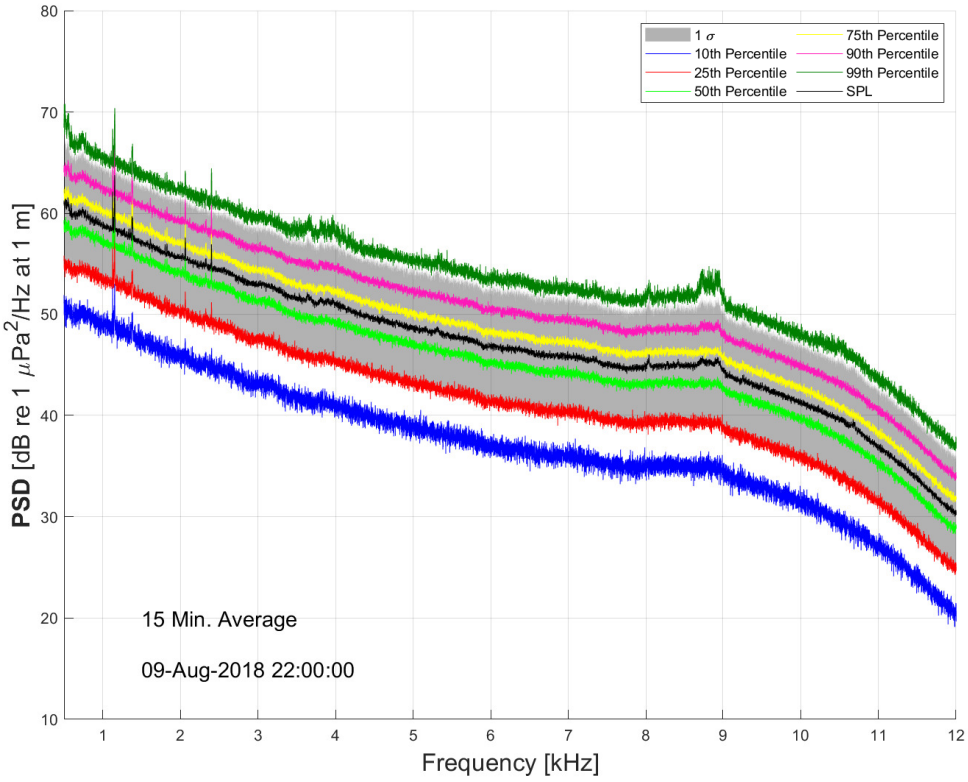

Figure A.39. Spectrum Level [dB re 1 μPa^2/Hz] versus frequency [kHz] using a 15 minute average. This data is taken from midnight on 10AUG2018. The statistics are described in Section 2.4.

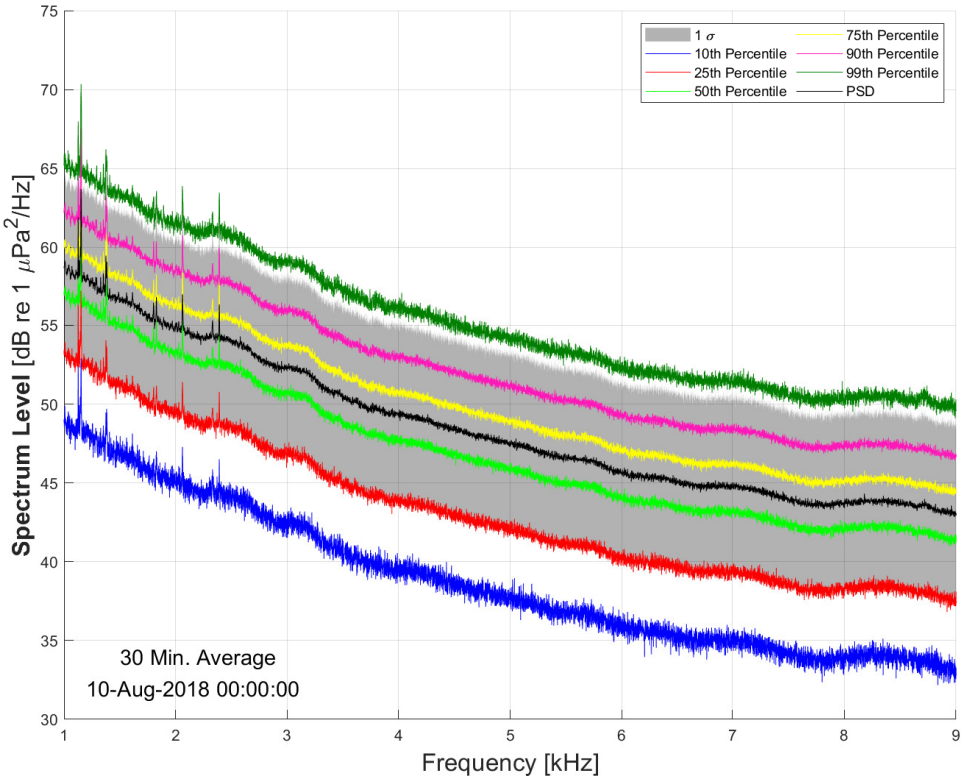

Figure A.40. Spectrum Level [dB re 1 μPa^2/Hz] versus frequency [kHz] using a 30 minute average. This data is taken from midnight on 10AUG2018. The statistics are described in Section 2.4.

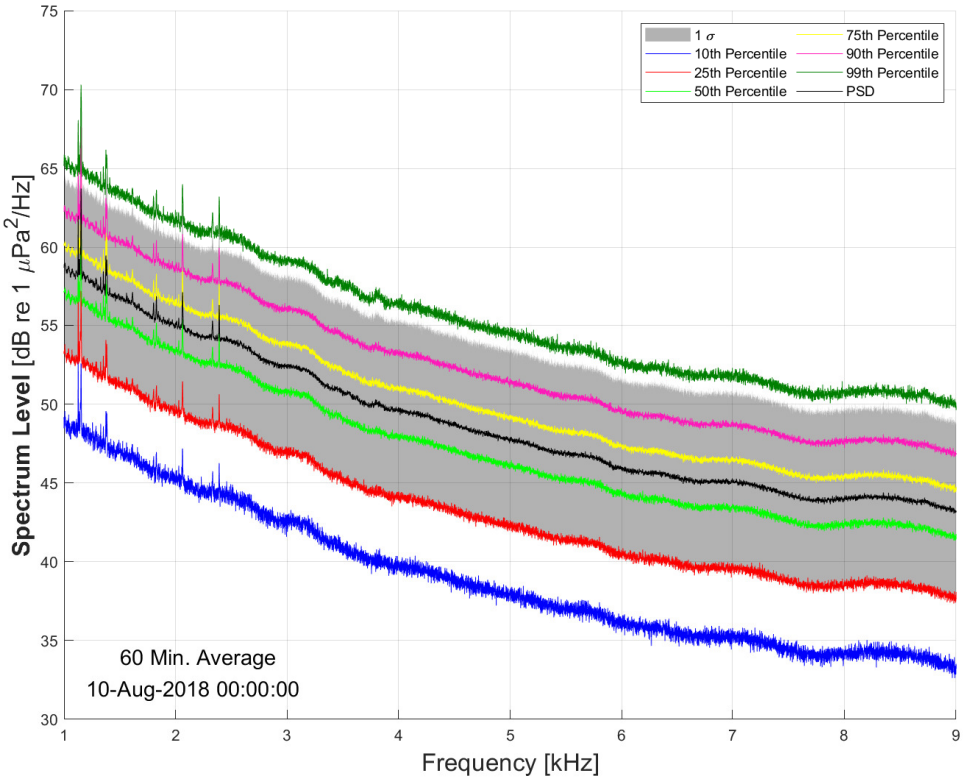

Figure A.41. Spectrum Level [dB re 1 μPa^2/Hz] versus frequency [kHz] using a 60 minute sliding average. This data is taken from midnight on 10AUG2018. The statistics are described in Section 2.4.

A.2.2 Additional time averages for Figure 4.2

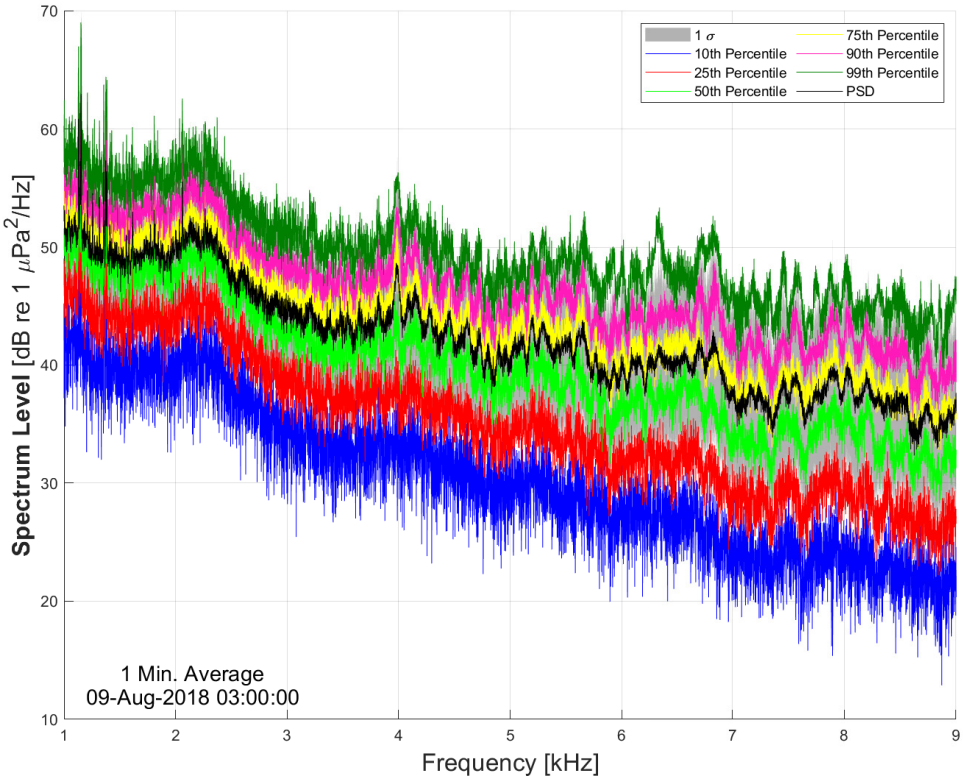

Figure A.42. Spectrum Level [dB re 1 μPa^2/Hz] versus frequency [kHz] using a 1 minute average. This data is taken from 0300Z on 09AUG2018. The statistics are described in Section 2.4.

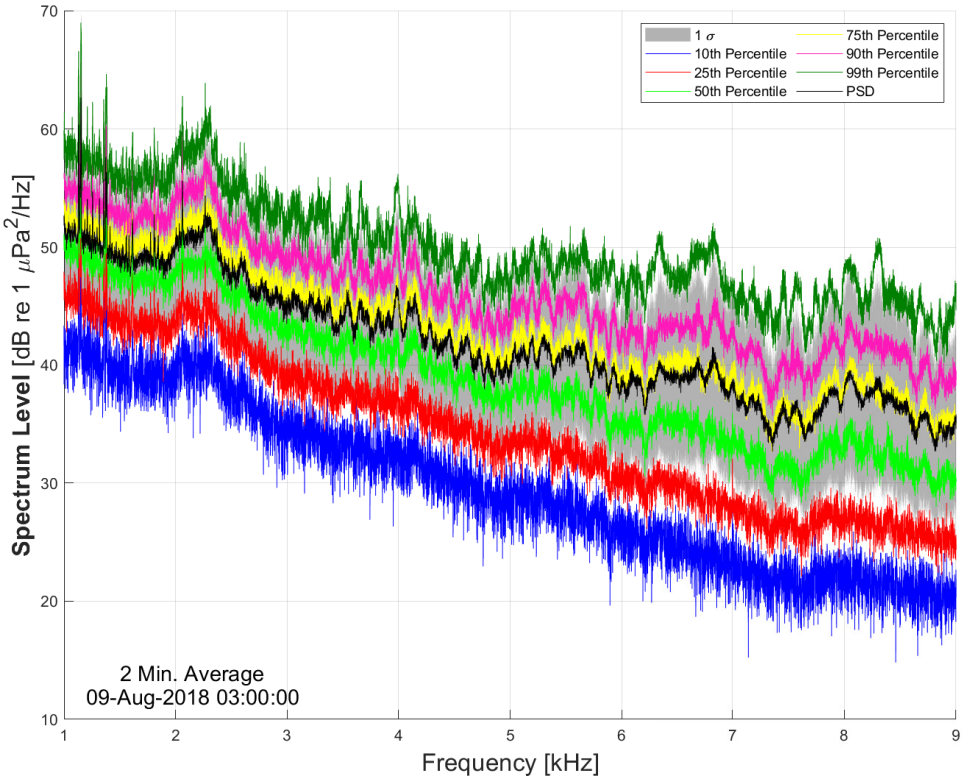

Figure A.43. Spectrum Level [dB re 1 μPa^2/Hz] versus frequency [kHz] using a 2 minute average. This data is taken from 0300Z on 09AUG2018. The statistics are described in Section 2.4.

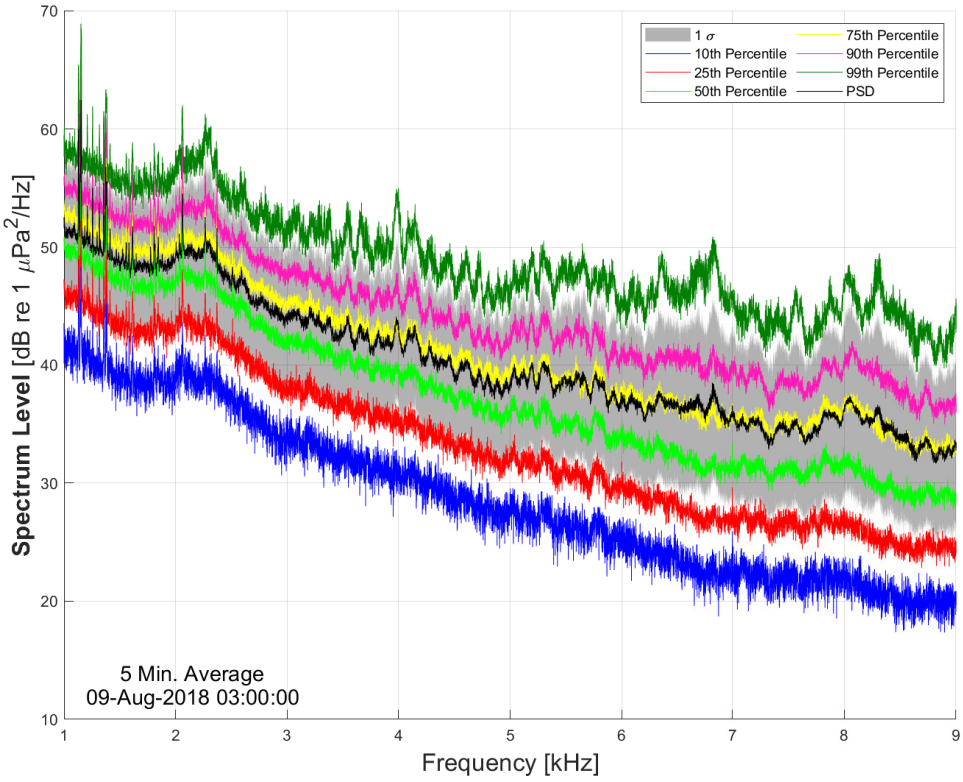

Figure A.44. Spectrum Level [dB re 1 μPa^2/Hz] versus frequency [kHz] using a 5 minute average. This data is taken from 0300Z on 09AUG2018. The statistics are described in Section 2.4.

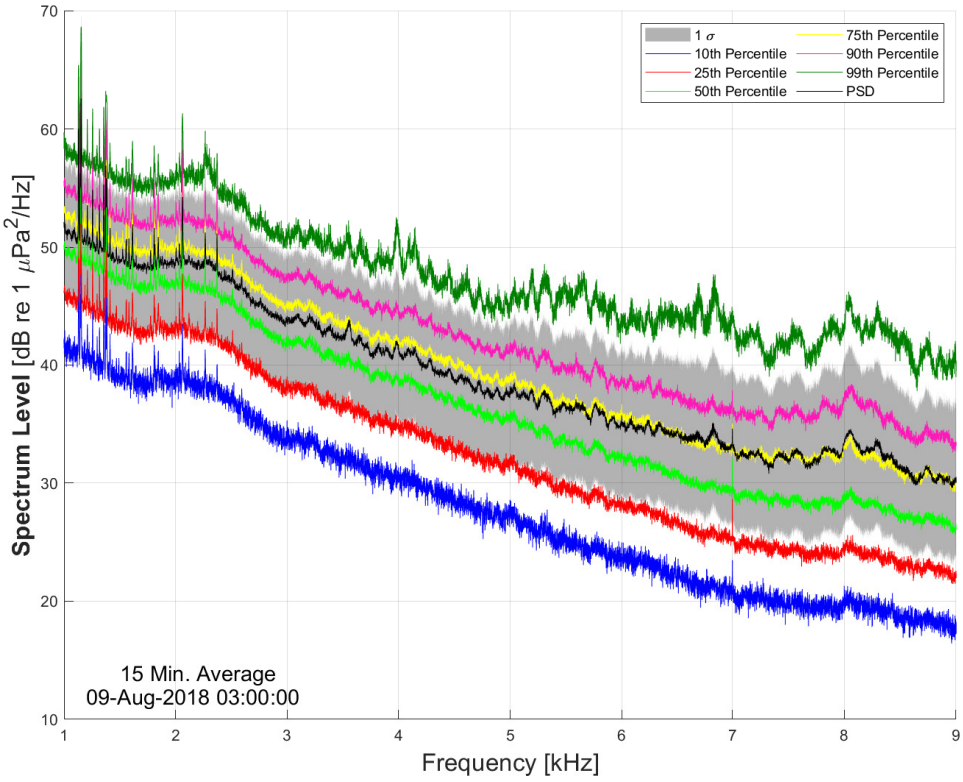

Figure A.45. Spectrum Level [dB re 1 μPa^2/Hz] versus frequency [kHz] using a 15 minute average. This data is taken from 0300Z on 09AUG2018. The statistics are described in Section 2.4.

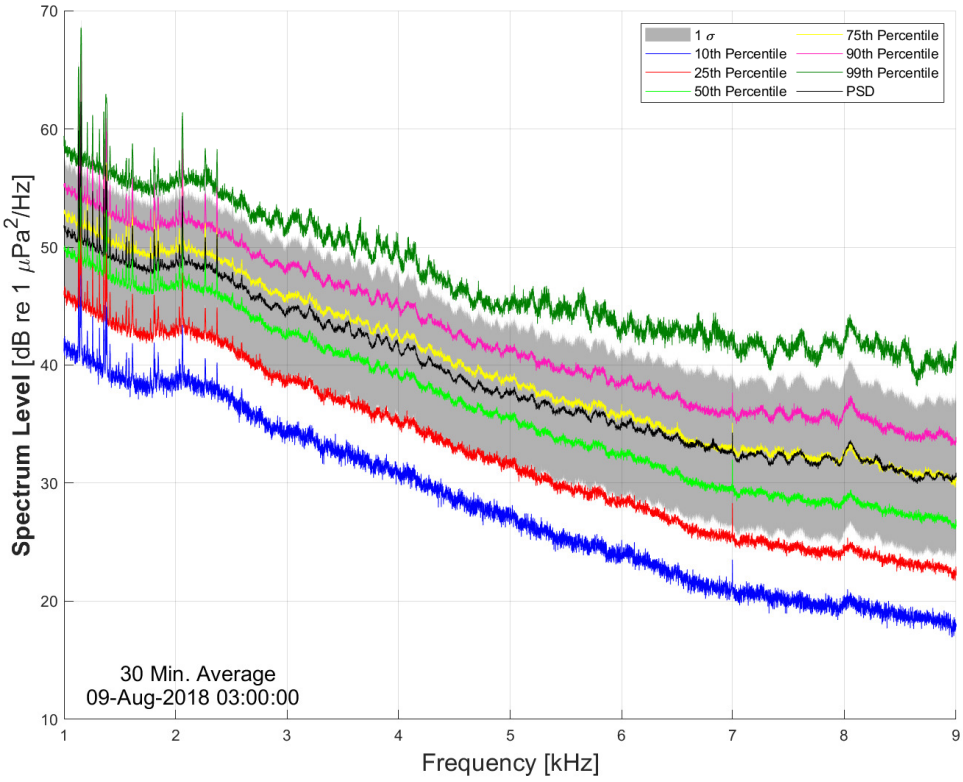

Figure A.46. Spectrum Level [dB re 1 μPa^2/Hz] versus frequency [kHz] using a 30 minute average. This data is taken from 0300Z on 09AUG2018. The statistics are described in Section 2.4.

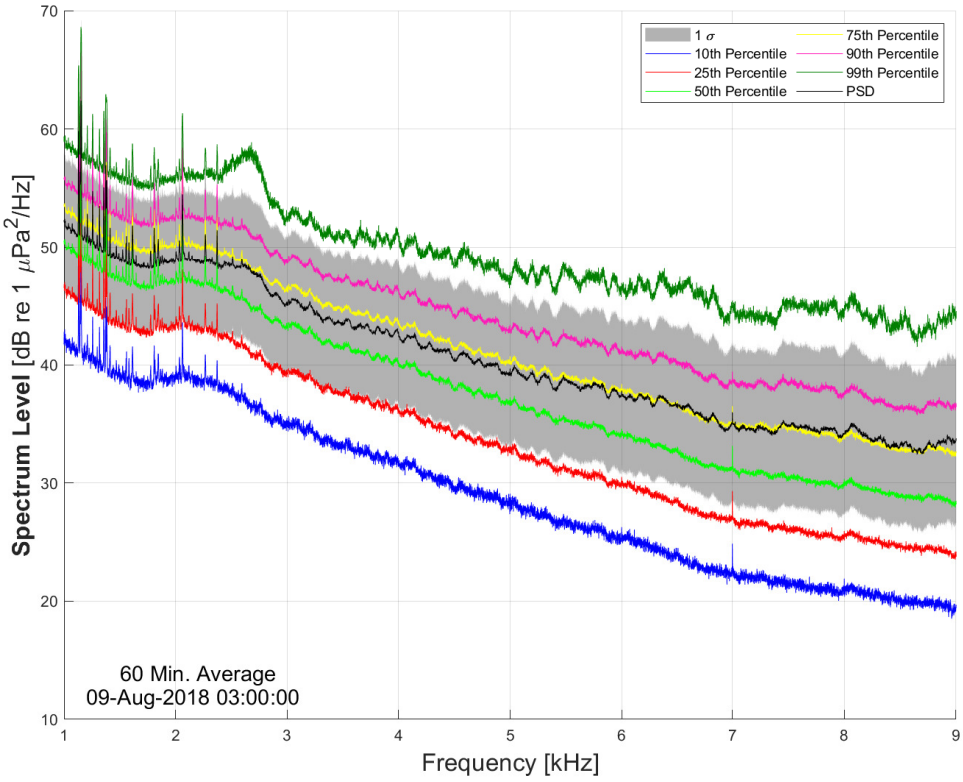

Figure A.47. Spectrum Level [dB re 1 μPa^2/Hz] versus frequency [kHz] using a 60 minute average. This data is taken from 0300Z on 09AUG2018. The statistics are described in Section 2.4.

A.2.3 Additional time averages for Figure 4.3

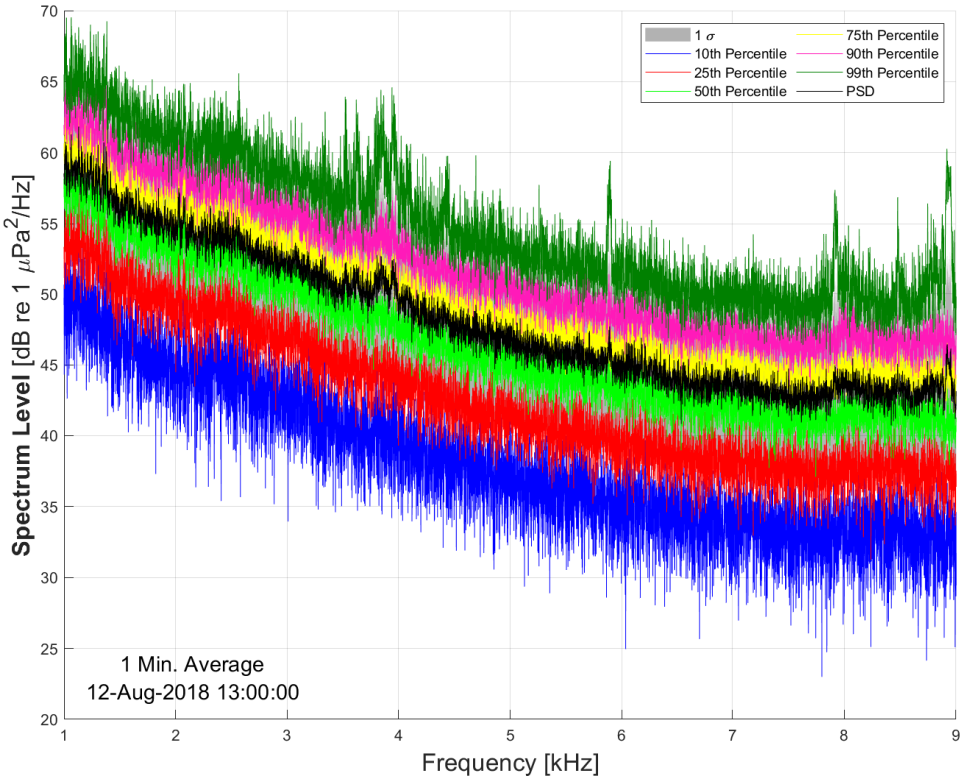

Figure A.48. Spectrum Level [dB re 1 μPa^2/Hz] versus frequency [kHz] using a 1 minute average. This data is taken from 1300Z on 12AUG2018. The statistics are described in Section 2.4.

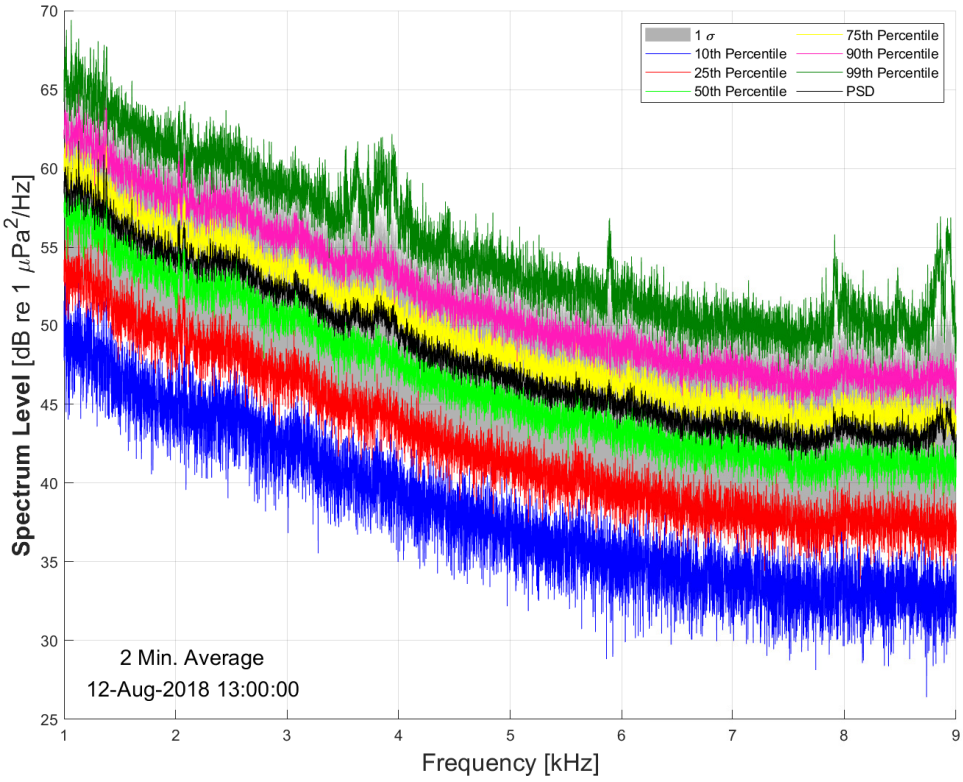

Figure A.49. Spectrum Level [dB re 1 μPa^2/Hz] versus frequency [kHz] using a 2 minute average. This data is taken from 1300Z on 12AUG2018. The statistics are described in Section 2.4.

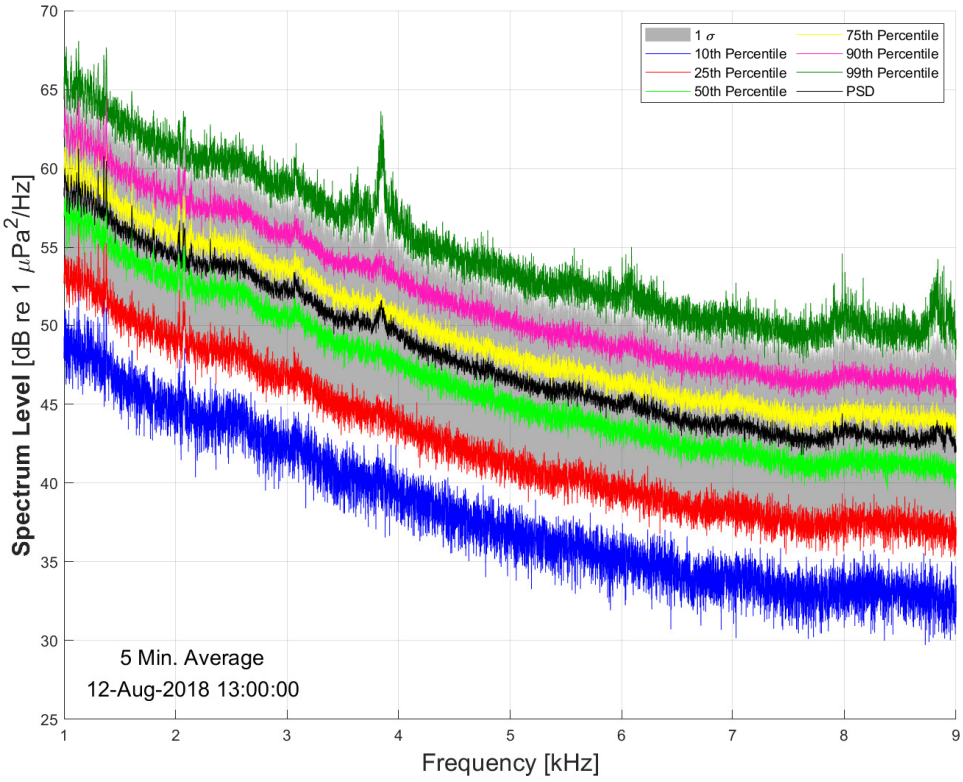

Figure A.50. Spectrum Level [dB re 1 μPa^2/Hz] versus frequency [kHz] using a 5 minute average. This data is taken from 1300Z on 12AUG2018. The statistics are described in Section 2.4.

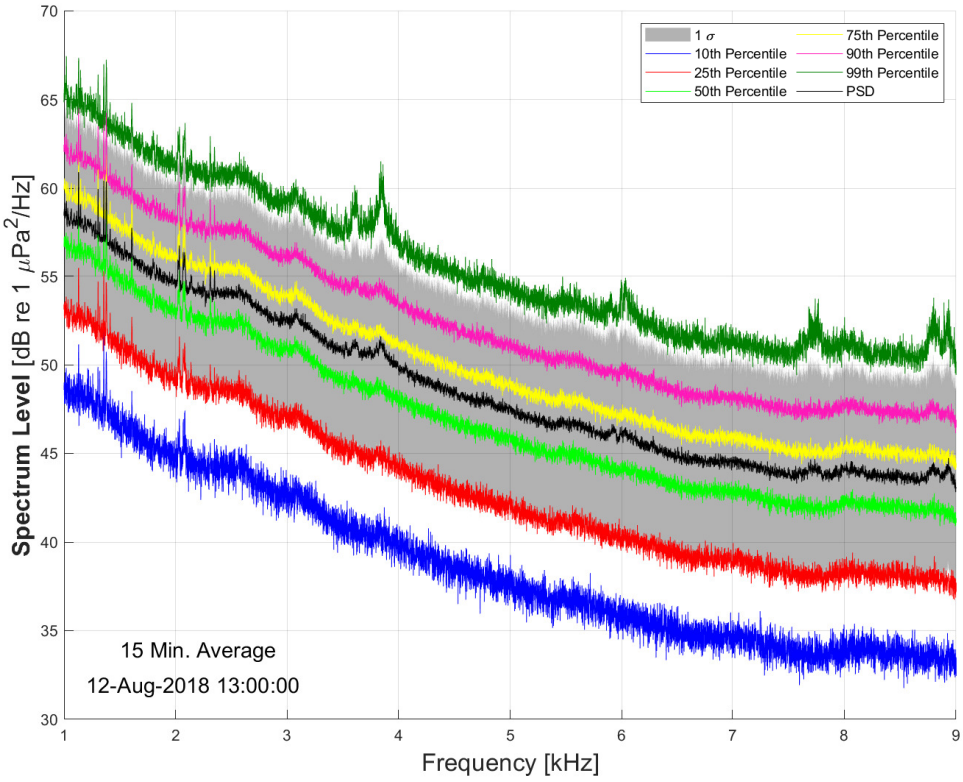

Figure A.51. Spectrum Level [dB re 1 μPa^2/Hz] versus frequency [kHz] using a 15 minute average. This data is taken from 1300Z on 12AUG2018. The statistics are described in Section 2.4.

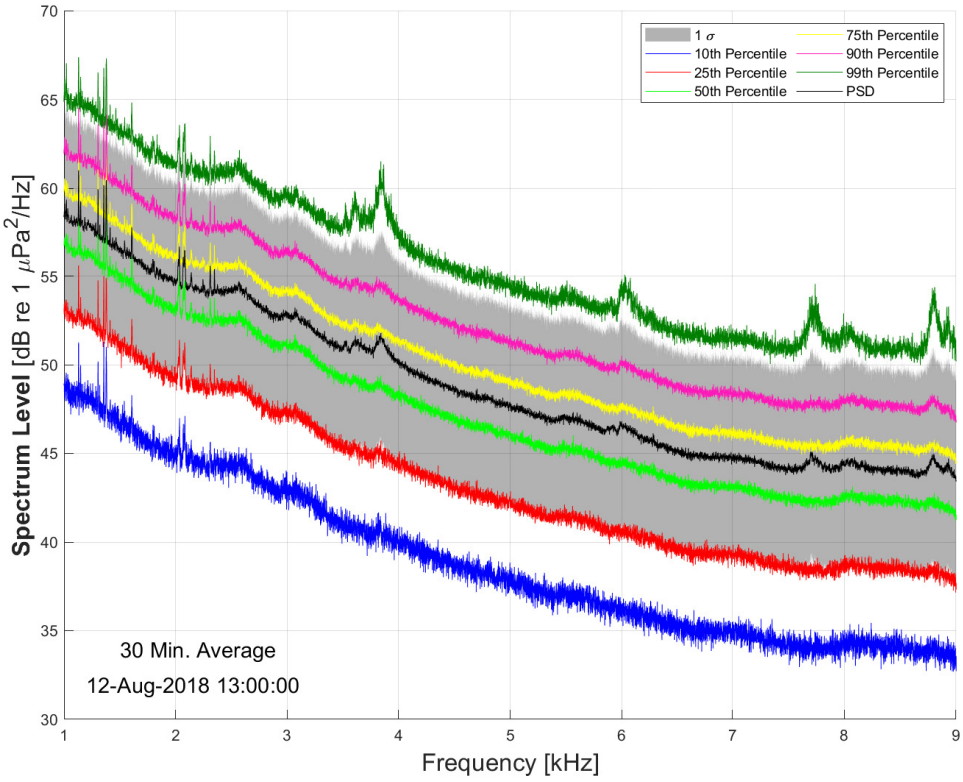

Figure A.52. Spectrum Level [dB re 1 μPa^2/Hz] versus frequency [kHz] using a 30 minute average. This data is taken from 1300Z on 12AUG2018. The statistics are described in Section 2.4.

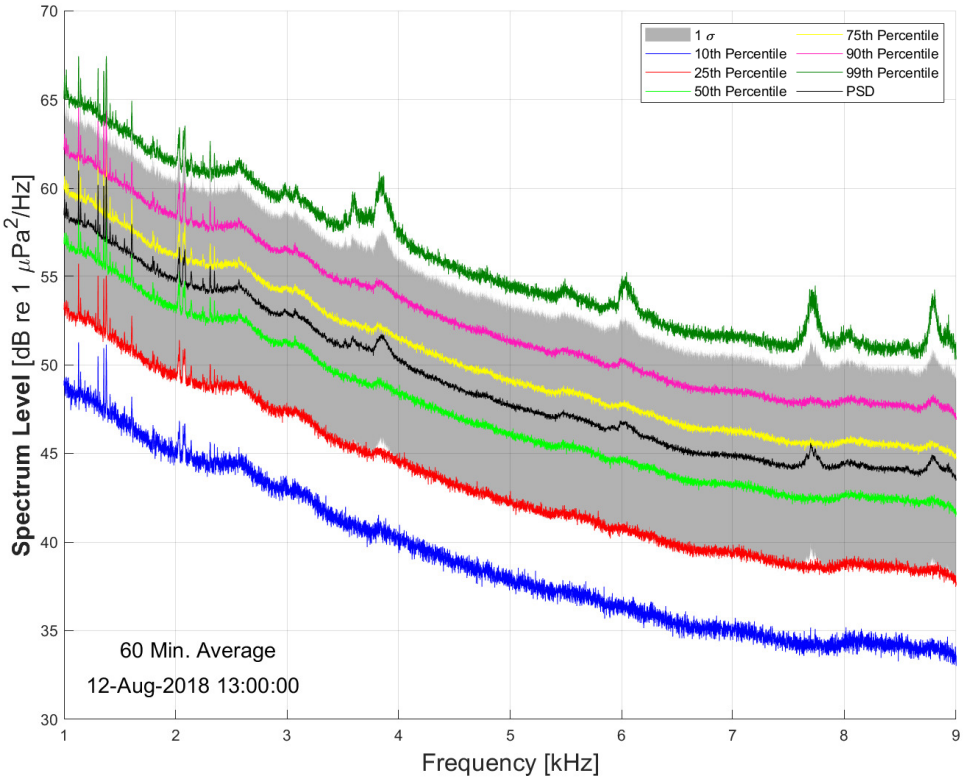

Figure A.53. Spectrum Level [dB re 1 μPa^2/Hz] versus frequency [kHz] using a 60 minute average. This data is taken from 1300Z on 12AUG2018. The statistics are described in Section 2.4.

A.3 Supplemental Model-Data Comparison Figures

A.3.1 Model-Data spectrum level comparison for second deployment

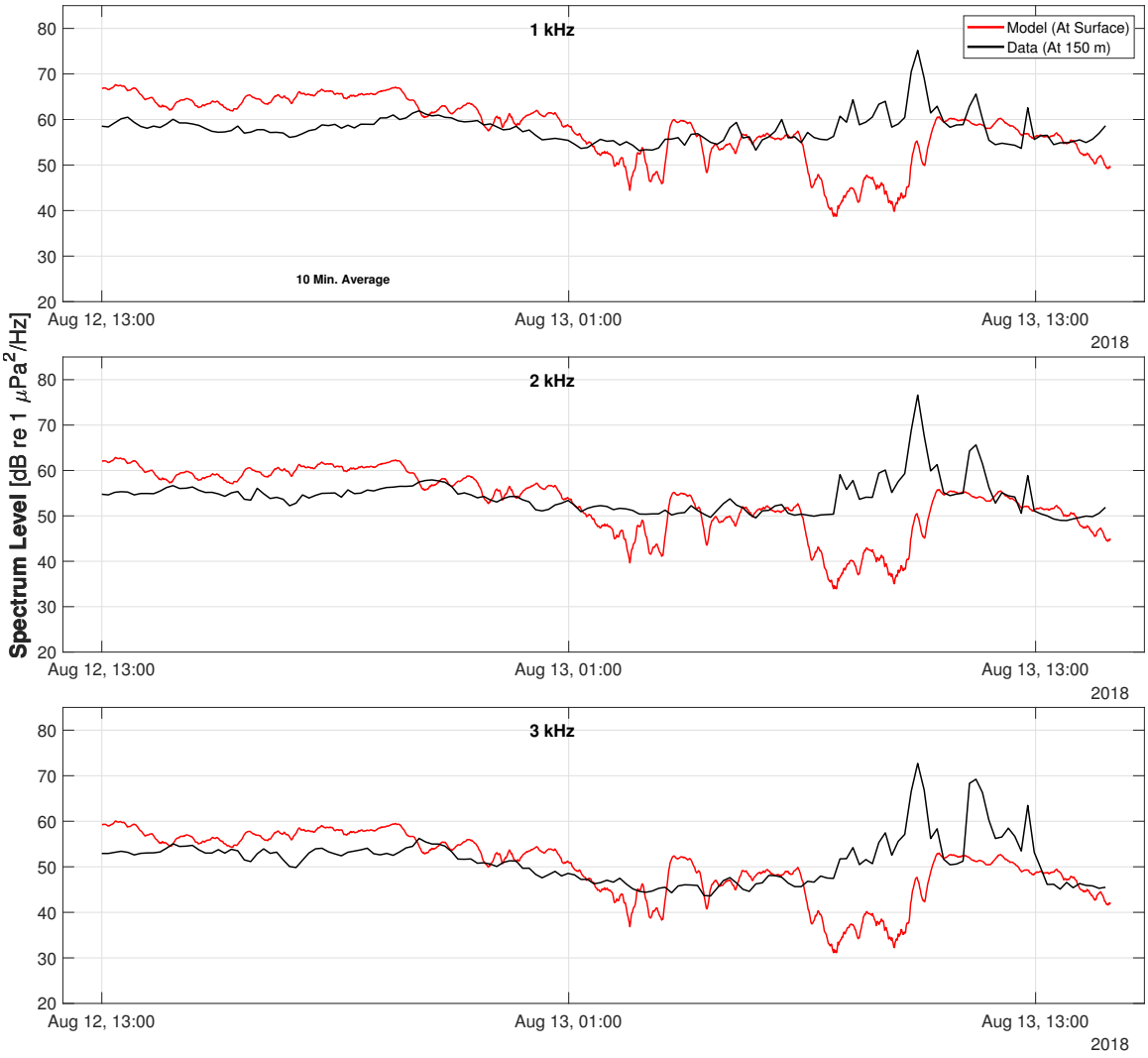

Figure A.54. Spectrum Level [dB re 1 μPa^2/Hz] for both the APL-UW model and data for frequencies 1, 2 and 3 kHz. Both data were collected from the second deployment using a 10 minute sliding average.

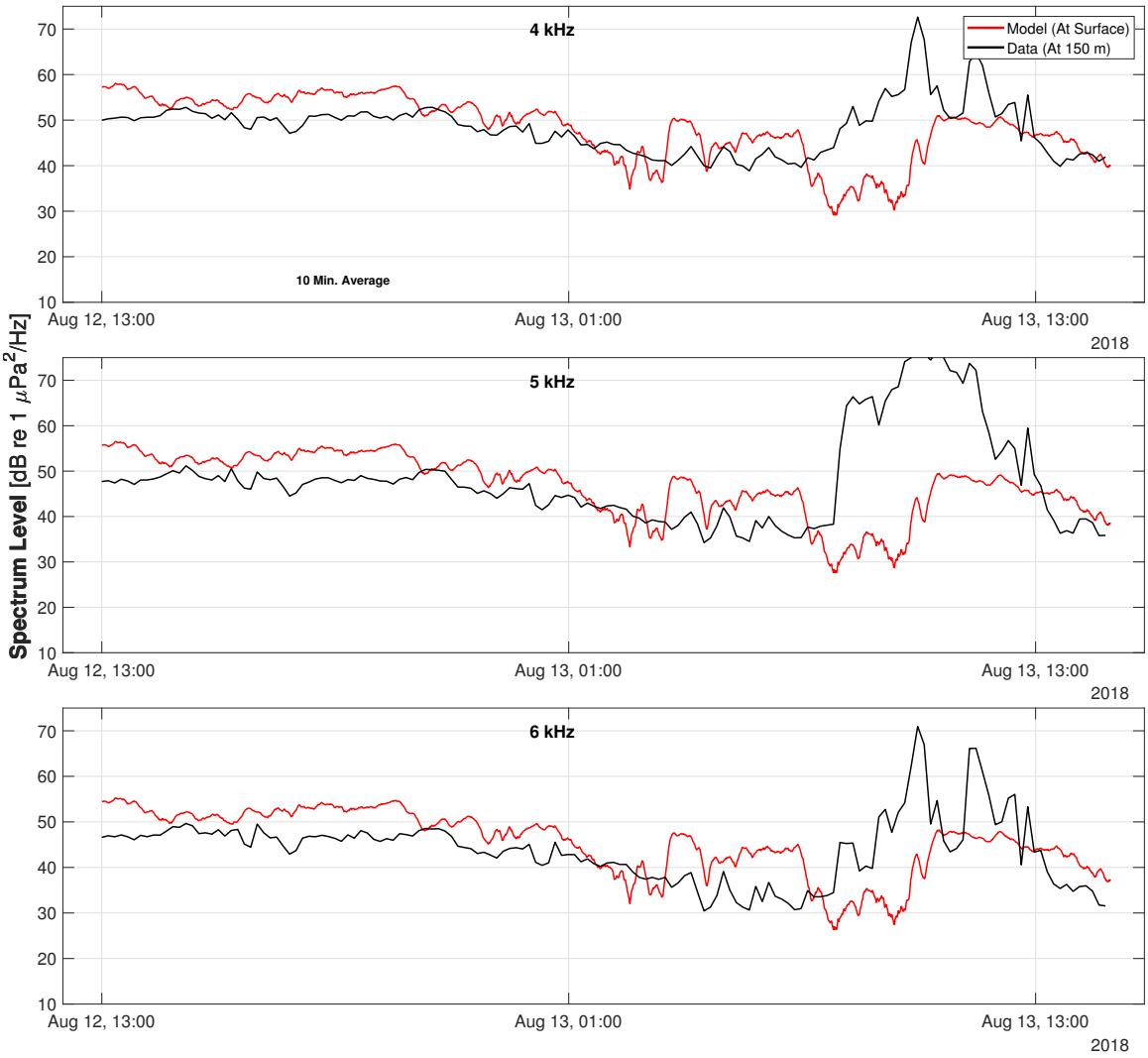

Figure A.55. Spectrum Level [dB re 1 μPa^2/Hz] for both the APL-UW model and data for frequencies 4, 5, and 6 kHz. Both data were collected from the second deployment using a 10 minute sliding average.

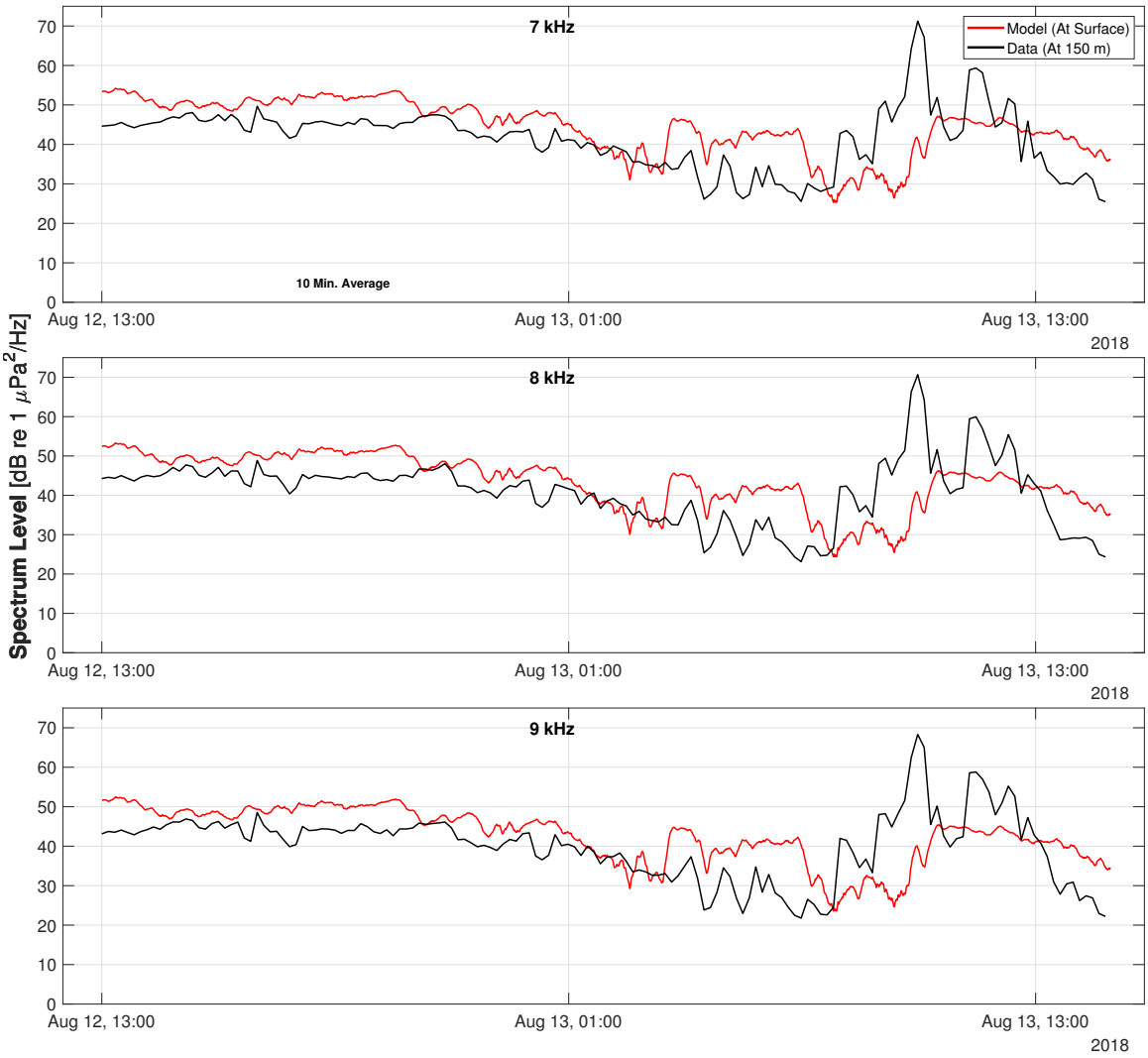

Figure A.56. Spectrum Level [dB re 1 μPa^2/Hz] for both the APL-UW model and data for frequencies 7, 8, and 9 kHz. Both data were collected from the second deployment using a 10 minute sliding average.

A.3.2 Additional frequencies for Figure 4.23

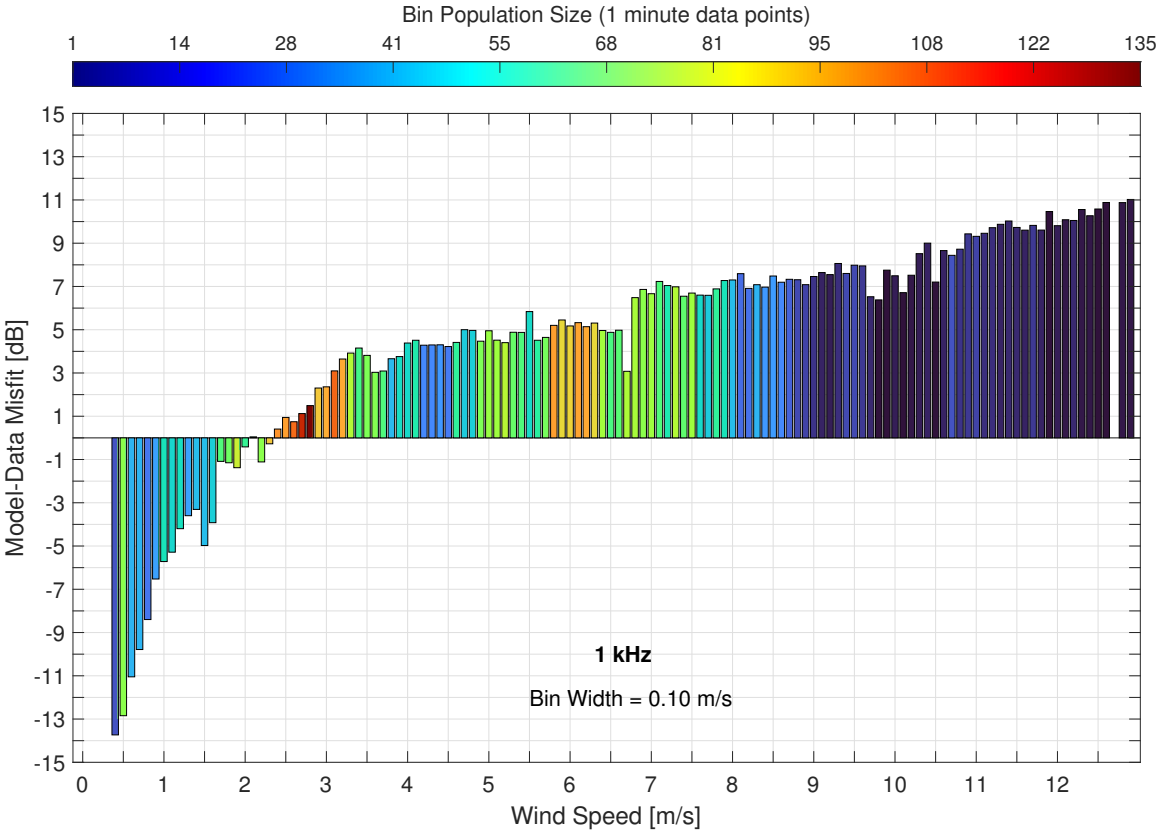

Figure A.57. Misfit between the APL-UW model and recorded data [dB] for 1 kHz based on bin width of 0.1 m/s wind speed with 1 minute sliding average.

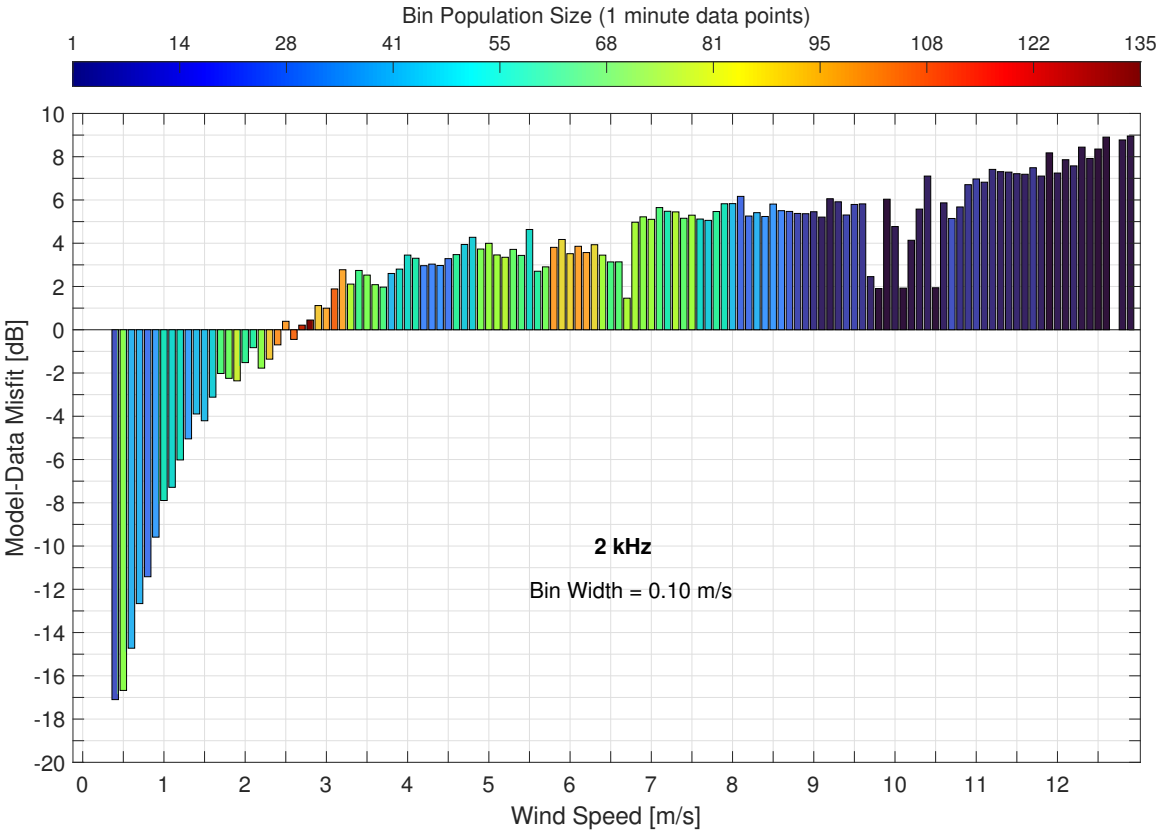

Figure A.58. Misfit between the APL-UW model and recorded data [dB] for 2 kHz based on bin width of 0.1 m/s wind speed with 1 minute sliding average.

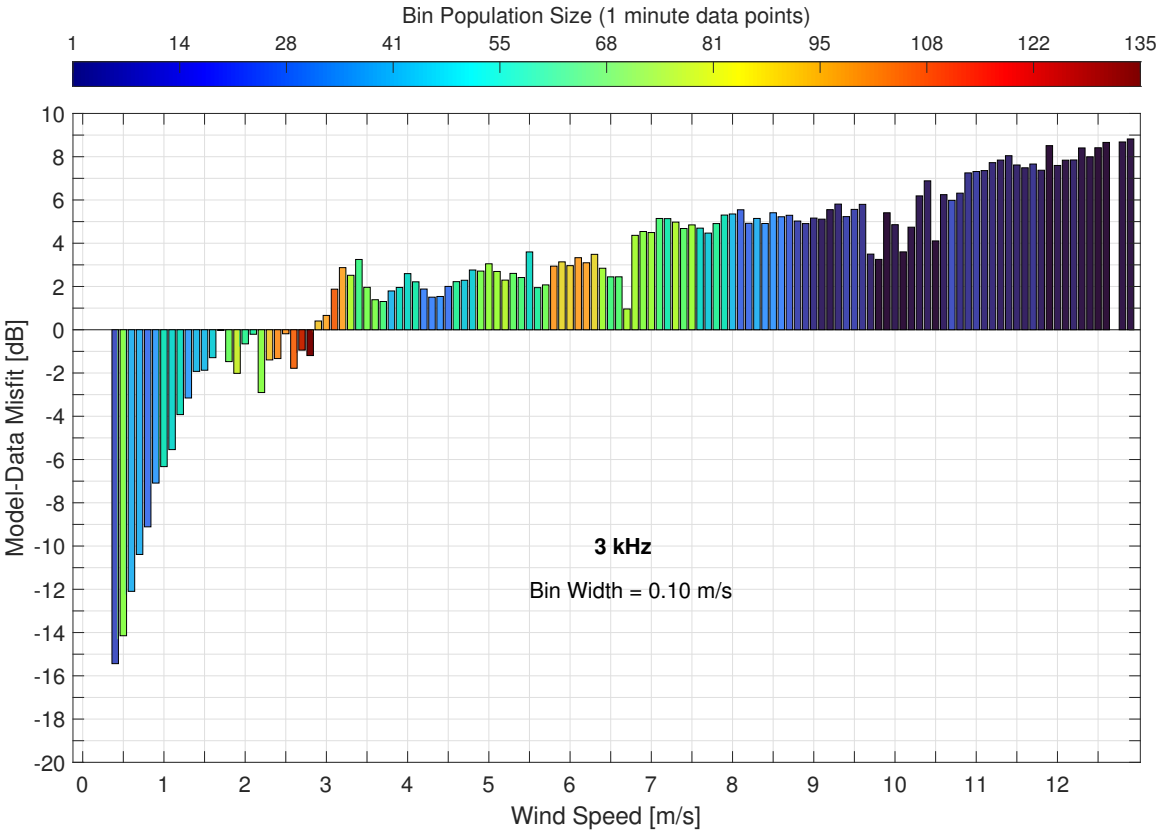

Figure A.59. Misfit between the APL-UW model and recorded data [dB] for 3 kHz based on bin width of 0.1 m/s wind speed with 1 minute sliding average.

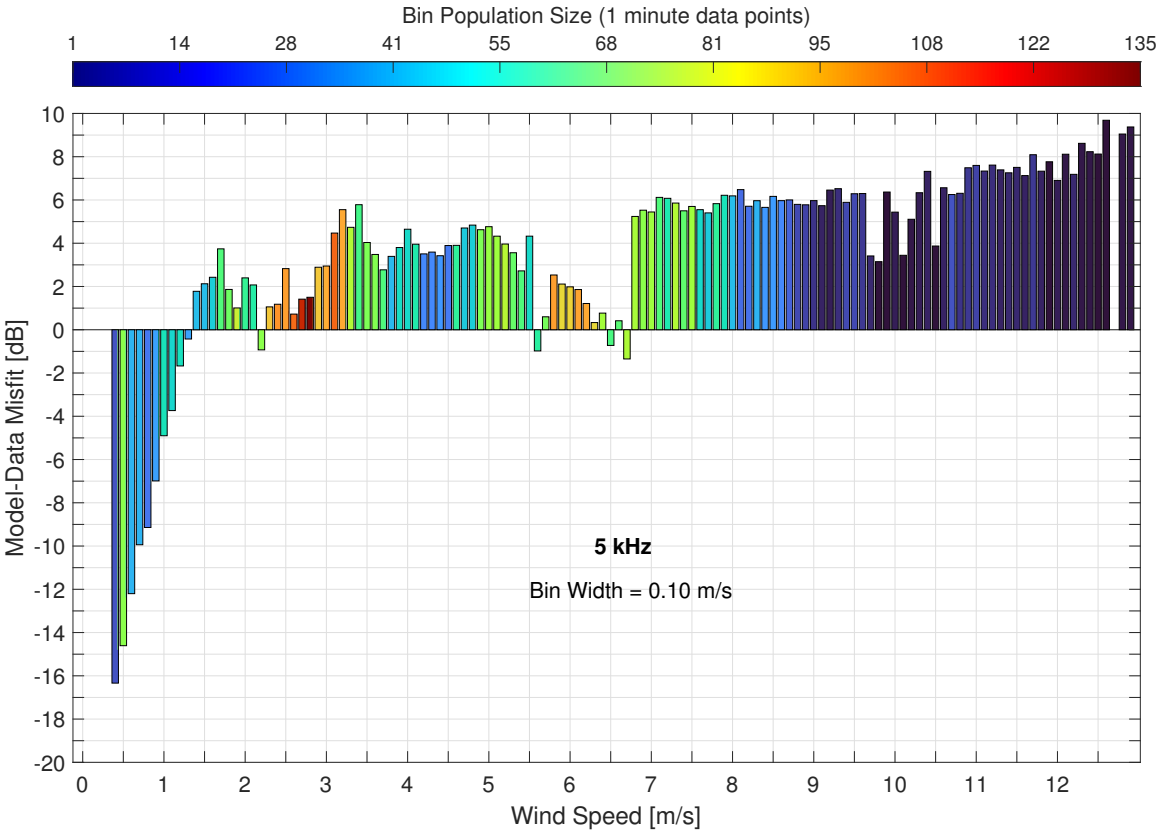

Figure A.60. Misfit between the APL-UW model and recorded data [dB] for 5 kHz based on bin width of 0.1 m/s wind speed with 1 minute sliding average.

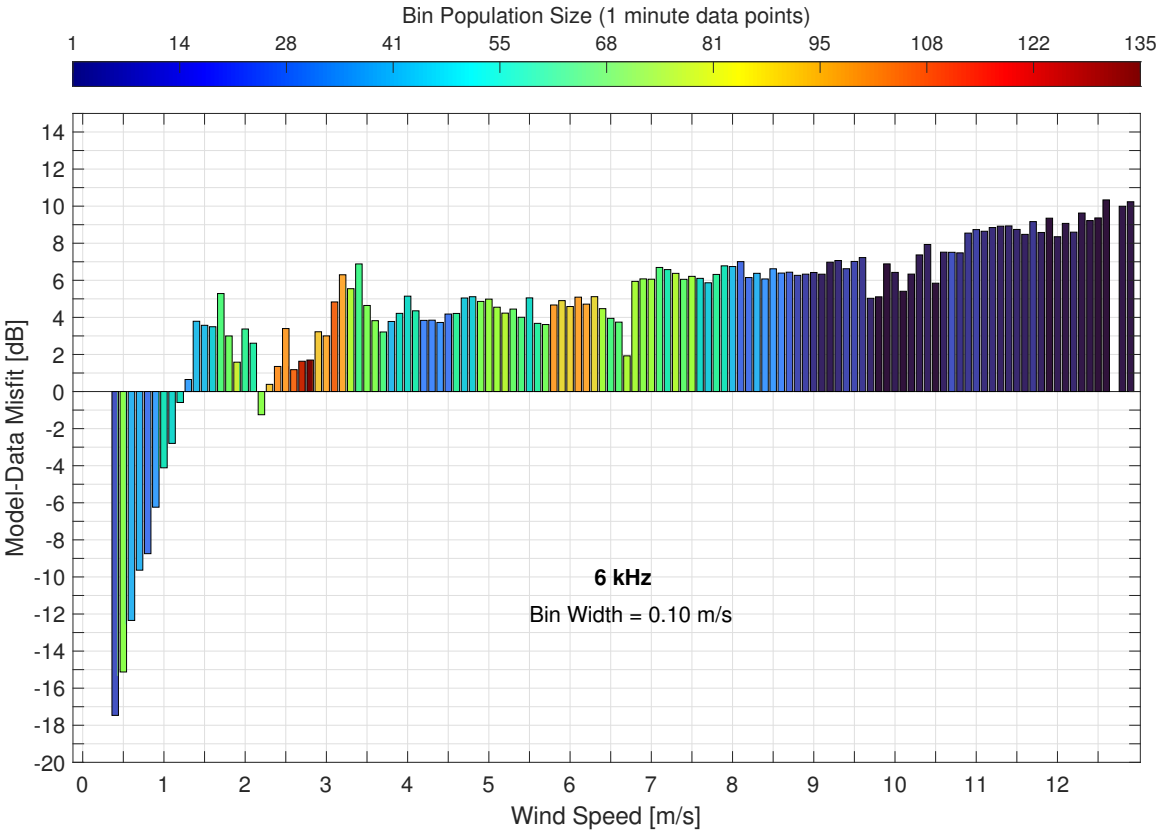

Figure A.61. Misfit between the APL-UW model and recorded data [dB] for 6 kHz based on bin width of 0.1 m/s wind speed with 1 minute sliding average.

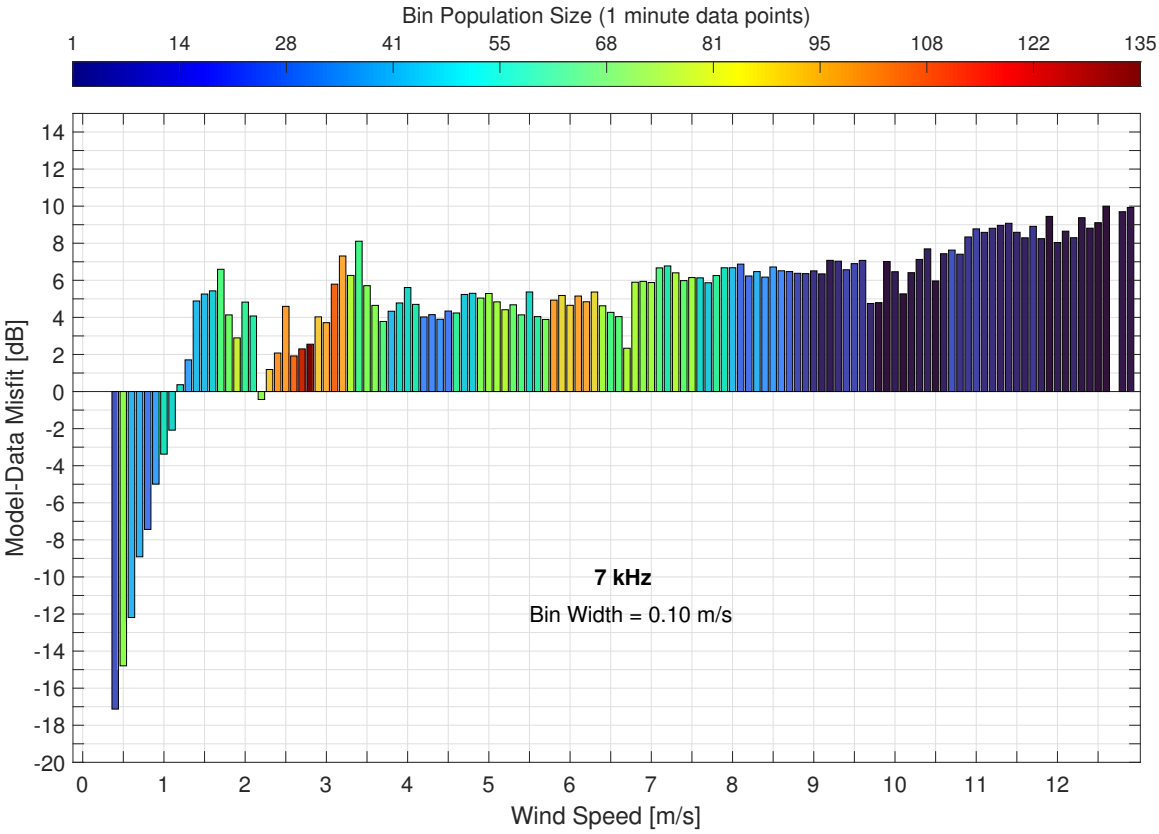

Figure A.62. Misfit between the APL-UW model and recorded data [dB] for 7 kHz based on bin width of 0.1 m/s wind speed with 1 minute sliding average.

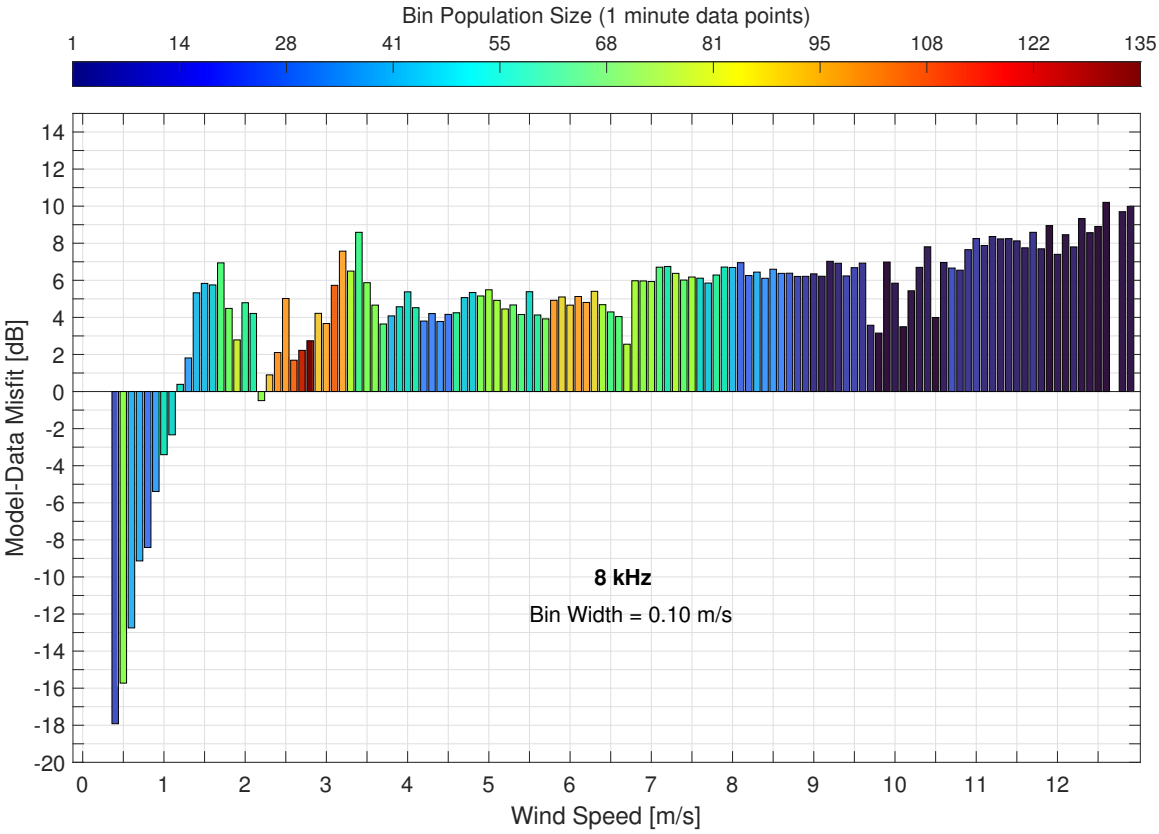

Figure A.63. Misfit between the APL-UW model and recorded data [dB] for 8 kHz based on bin width of 0.1 m/s wind speed with 1 minute sliding average.

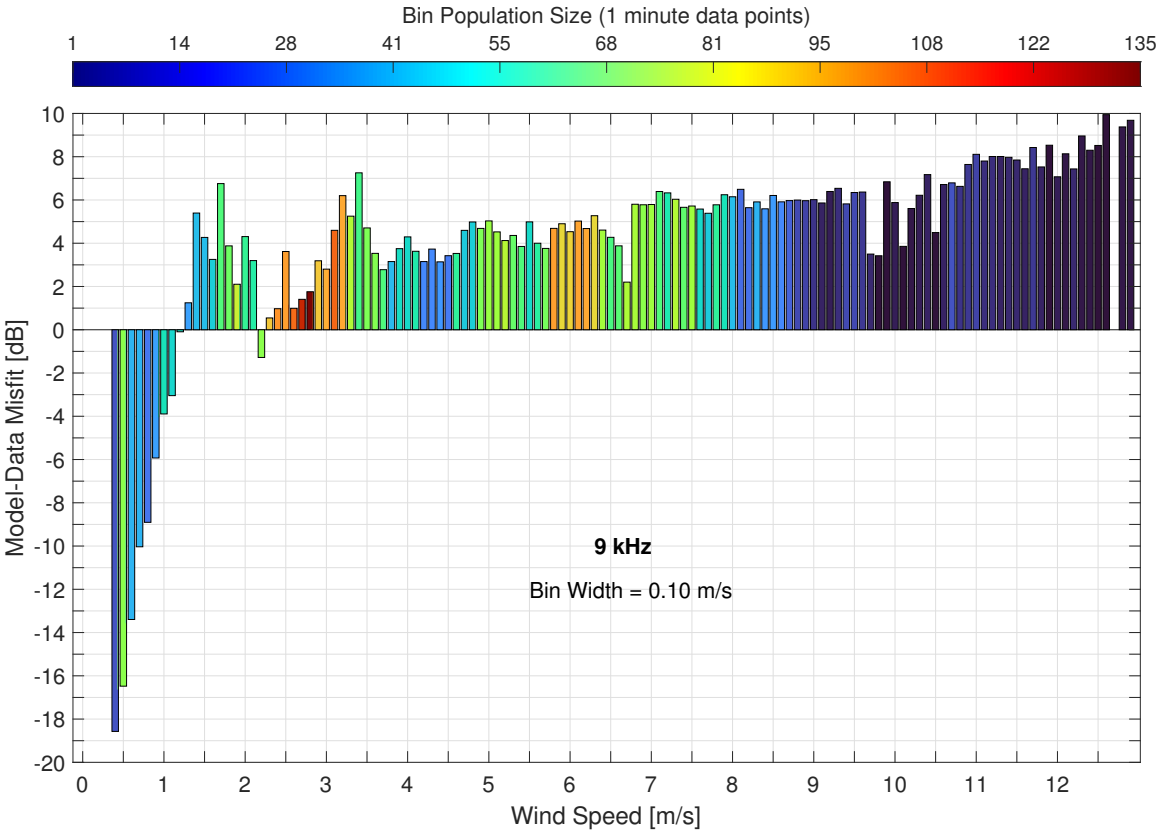

Figure A.64. Misfit between the APL-UW model and recorded data [dB] for 9 kHz based on bin width of 0.1 m/s wind speed with 1 minute sliding average.

THIS PAGE INTENTIONALLY LEFT BLANK

List of References

[1] L. Cohen, "The history of noise," *IEEE Signal Processing Magazine*, 2005.

[2] R. Urick, "Ambient noise in the sea," Undersea Warfare Technology Office, Naval Sea Systems Command, Department of the Navy, Tech. Rep., 1984.

[3] WS Hodgkiss and WA Kuperman, "Mid-frequency ambient noise observations with a 2D array in deep water. ONR Task Force Ocean Ambient Noise Innovation Forum," John C. Stennis Space Center. Mississippi, United States, Jan. 2023.

[4] S. Robinson, P. Lepper, and R. Hazelwood, "Good practice guide for underwater noise measurement," National Physical Laboratory, Tech. Rep., Mar. 2014.

[5] R. J. Urick, *Principles of Underwater Sound for Engineers*, 3rd ed. McGraw-Hill Book Company, 1967.

[6] R. Andrew, B. Howe, J. Mercer, and M. Dzieciuch. (2002, Apr.). Ocean ambient sound: Comparing the 1960s with the 1990s for a receiver off the California coast. *Acoustical Society of America*. [Online]. Available: https://asa.scitation.org/doi/pdf/10.1121/1.1461915

[7] UNCTAD. (2021, Jan.). UNCTAD Handbook of Statistics 2021. [Online]. Available: https://unctad.org/system/files/official-document/tdstat46_FS14_en.pdf

[8] D. Ross. (2005, Apr.). Ship Sources of Ambient Noise. *IEEE Journal of Oceanic Engineering*. [Online]. *30*(2). pp. 257–261. Available: https://ieeexplore.ieee.org/stamp/stamp.jsp?arnumber=1522502

[9] J. Hildebrand. (2009, Dec.). Anthropogenic and natural sources of ambient noise in the ocean. *Marine Ecology Progress Series*. [Online]. pp. 5–20. Available: https://www.jstor.org/stable/24874238

[10] V. Knudsen, R. Alford, and J. Emling. (1948). Underwater Ambient Noise. *Journal of Marine Research*. [Online]. pp. 410–429. Available: https://images.peabody.yale.edu/publications/jmr/jmr07-03-24.pdf

[11] G. M. Wenz. (1962, Dec.). Acoustic Ambient Noise in the Ocean: Spectra and Sources. *The Journal of the Acoustical Society of America*. [Online]. *34*(12). pp. 1936–1956. Available: https://asa.scitation.org/doi/pdf/10.1121/1.1909155

[12] J. L. Miksis-Olds, D. L. Bradley, and X. M. Niu. (2013). Decadal trends in Indian Ocean ambient sound. *The Journal of Acoustical Society of America*. [Online]. pp. 3464–3475. Available: https://asa.scitation.org/doi/pdf/10.1121/1.4821537

[13] J. Zhu, W. Guo, B. Zhang, Y. Ma, Y. Chen, and L. Lu. (2021, July). Spectrum Analysis of Deep Water Ambient Noise in the West Pacific. *IEEE/OES China Ocean Acoustics*. [Online]. pp. 512–515. Available: https://ieeexplore.ieee.org/stamp/stamp.jsp?tp=&arnumber=9519882

[14] J. Yang, J. A. Nyusten, S. C. Riser, and E. I. Thorsos. (2023, Mar.). Open ocean ambient noise data in the frequency bandof 100 Hz–50 kHz from the Pacific Ocean. *The Journal of the Acoustical Society of America*. Online *3*(3). Available: https://asa.scitation.org/doi/10.1121/10.0017349

[15] A. J. Perrone. (1969, Mar.). Deep-Ocean Ambient-Noise Spectra in the Northwest Atlantic. *The Journal of the Acoustical Society of America*. [Online]. pp. 762–770. Available: file:///C:/Users/c.griggs_local/Documents/MFN6ThesisGriggs/References/AmbientNoiseSpectraNWAtlantic.pdf

[16] W. D. Halliday, D. Barclay, A. N. Barkley, E. Cook, J. Dawson, R. C. Hilliard, N. E. Hussey, J. M. Jones, F. Juanes, M. Marcoux, A. Niemi, S. Nudds, M. K. Pine, C. Richards, K. Scharffenberg, K. Westdal, and S. J. Insley. (2021). Underwater sound levels in the Canadian Arctic, 2014–2019. *Marine Pollution Bulletin*. [Online]. p. 112437. Available: https://www.sciencedirect.com/science/article/pii/S0025326X21004719

[17] E. Dalberg, R. Lennartsson, M. Levonen, and L. Persson. (2005). Properties of Acoustic Ambient Noise in the Baltic Sea. Swedish Defence Research Agency. [Online]. Available: https://www.researchgate.net/publication/229051953_Properties_of_acoustic_ambient_noise_in_the_Baltic_sea

[18] M. Mustonen, A. Klauson, M. Andersson, D. Clorennec, T. Folegot, R. Koza, J. Pajala, L. Persson, J. Tegowski, J. Tougaard, M. Wahlberg,

and P. Sigray. (2019). Spatial and Temporal Variability of Ambient Underwater Sound in the Baltic Sea. *Scientific Reports*. [Online]. *9*(1). pp. 1–13. Available: https://www.proquest.com/docview/2290066256?parentSessionId=eawzAM4JZGlEMW1XfnVUgO9hTMfbPd0yoiYcZh95dec=&pq-origsite=primo&accountid=12702

[19] H. M. Walkinshaw. (2005, Apr.). Measurements of Ambient Noise Spectra in the South Norwegian Sea. *IEEE Journal of Ocean Engineering*. [Online]. *30*(2). pp. 262–266. Available: https://ieeexplore.ieee.org/stamp/stamp.jsp?tp=&arnumber=1522503

[20] L. Zedel, L. Gordon, and S. Osterhus. (1999, Aug.). Ocean Ambient Sound Instrument System: Acoustic Estimation of Wind Speed and Direction from a Subsurface Package. *Journal of Atmospheric and Oceanic Technology*. [Online]. pp. 1118–1126. Available: https://journals.ametsoc.org/view/journals/atot/16/8/1520-0426_1999_016_1118_oasisa_2_0_co_2.xml

[21] A. Codarin, L. E. Wysocki, F. Ladich, and M. Picciulin. (2009). Effects of ambient and boat noise on hearing and communication in three fish species living in a marine protected area (Miramare, Italy). *Marine Pollution Bulletin*. [Online]. pp. 1880–1887. Available: https://www-sciencedirect-com.libproxy.nps.edu/science/article/pii/S0025326X09003075?via=ihub

[22] E. C. Pettit, K. M. Lee, J. P. Brann, J. A. Nystuen, P. S. Wilson, and S. O'Neel. (2015). Unusually loud ambient noise in tidewater glacier fjords: A signal of ice melt. *Geophysical research letters*. [Online]. *42*(7). pp. 2309–2316. Available: https://agupubs.onlinelibrary.wiley.com/doi/pdf/10.1002/2014GL062950

[23] F. Harris, "On the use of windows for harmonic analysis with the discrete fourier transform," *Proceedings of the IEEE*, vol. 66, pp. 51–83, 1978.

[24] "APL-UW High-frequency ocean environmental acoustic models handbook," University of Washington Applied Physics Laboratory, Applied Physics Laboratory University of Washington; 1013 NE 40th St., Seattle, WA 98105, techreport, Oct. October 1994. Available: http://staff.washington.edu/dushaw/epubs/APLTM9407.pdf

[25] N. O. Office, "Fleet oceanographic and acoustic reference manual," Apr. 1999.

[26] GEBCO, "General bathymetric chart of the oceans (GEBCO)," Data Base, 2021. Available: https://www.gebco.net/data_and_products/gridded_bathymetry_data/gebco_2021/

[27] R. P. Hodges, *Underwater Acoustics: Analysis, Design and Performance of SONAR*, 1st ed., S. Schuller, Ed. John Wiley and Sons Ltd, The Atrium, Southern Gate, Chichester, West Sussex, PO19 8SQ, United Kingdom: John Wiley and Sons, Ltd., 2010.

[28] S. Saha, S. Moorthi, X. Wu, J. Wang, S. Nadiga, P. Tripp, D. Behringer, Y.-T. Hou, H. ya Chuang, M. Iredell, M. Ek, J. Meng, R. Yang, M. P. Mendez, H. van den Dool, Q. Zhang, W. Wang, M. Chen, and E. Becker. (2014, Mar.). The NCEP Climate Forecast System Version 2. *Journal of Climate*. [Online]. pp. 2185–2208. Available: https://journals.ametsoc.org/view/journals/clim/27/6/jcli-d-12-00823.1.xml

[29] B. B. Ma, J. A. Nyusten, and R.-C. Lien. (2005, Mar.). Prediction of underwater sound levels from rain and wind. *The Journal of Acoustical Society of America*. [Online]. pp. 3555–3565. Available: https://doi.org/10.1121/1.1910283

Initial Distribution List

1. Defense Technical Information Center
   Ft. Belvoir, Virginia
2. Dudley Knox Library
   Naval Postgraduate School
   Monterey, California